The Representative Particle Model

vorgelegt von
Diplom-Ingenieur
Nico Zobel
aus Berlin

von der Fakultät III - Prozesswissenschaften
der Technischen Universität Berlin
zur Erlangung des akademischen Grades

Doktor der Ingenieurwissenschaften
– Dr.-Ing. –

genehmigte Dissertation

Promotionsausschuss:

Vorsitzender: Prof. Dr.-Ing. Jörg Steinbach
Berichter: Prof. Dr. rer. nat. Frank Behrendt
Berichter: Prof. Dr.-Ing. Matthias Kraume

Tag der wissenschaftlichen Aussprache: 12. Juni 2007

Berlin 2007
D 83

Acknowledgement

I would like to express my gratitude to all those who gave me the possibility to complete this thesis.

I wish to thank ...

... Prof. Dr. rer. nat. habil. Frank Behrendt, the supervisor of this work, for making this work possible in the first place, for the experience of scientific freedom, for an always open door,

... Prof. Dr.-Ing. Matthias Kraume, the reviewer of this work, for accompanying my time at the TU Berlin for ten years and for numerous words of advice,

... PD Dr. rer. nat. habil. Karsten Reuter, my supervisor at the Fritz-Haber-Institute, for his generosity which also made this work possible at all, for letting an engineer work at a Max-Planck-Institute,

... Dipl.-Ing. Matija Bogdanic, Dr.-Ing. Michael Oevermann, Dipl.-Ing. Stephan Gerber, colleagues of mine at the TU Berlin, for working thouroughly through the most tedious parts of this work without complaining, for lots of very enlightening discussions,

... Dipl.-Ing. Birgit Wilmes, Dr.-Ing. Yunfei Kuo, former colleagues who shared an office with me, for being so great roommates, for helping me out so many times, for the things I learned from them,

... Dr.-Ing. York Neubauer, colleague of mine at the TU Berlin, for the GC/LAMS and biomass gasification success story, for his incredible patience,

... Horst Lochner, the soul of our institute at the TU, for everything he has done for all of us.

Dedicated to ...

... Pola and Djamal, my family. Thank you for your love!

... Roswitha and Klaus, my parents. Thank you for giving me freedom and safety!

Contents

List of Figures

List of Tables

Abstract

Several detailed single-particle models for thermal conversion of biomass have been established in recent years. With the Representative Particle Model (RPM) it is possible to integrate such a single-particle model into a packed-bed reactor model. In this work the concept of representative particles is further developed and evaluated.

The basic idea is that instead of modeling each individual particle in a packed-bed reactor, which would be computationally very expensive, only a limited number of particles are described in detail. These particular particles are considered as being representative for a finite volume element of the reactor. A detailed derivation of the governing differential balance equations is presented. Special emphasis is put on the boundary conditions of the single-particle model which have to be modified if they are to be integrated into a reactor model. The phenomenon of inter-particle heat transfer is modeled in a consistent manner for the first time. It is shown that the RPM hereby offers a way to improve the simulation of transient heat transfer in fluid-solid heterogeneous media by considering the history term.

Forthermore, the concept of the RPM is evaluated. Simulation results considering heating-up, drying and pyrolysis in a packed bed reactor are compared to experimental results. These evaluations demonstrate that the RPM is a promising method for multi-scale modeling.

Chapter 1

Introduction

The packed-bed reactor (PBR) is one of the "work horses" in the chemical industry, where it is mostly used for heterogeneous catalytic reactions. But there are also several PBR applications in other technical fields, such as: water cleansing by sand filters [1], combustion of waste [2], and gasification or pyrolysis of biomass [3].

Modeling the processes in a PBR is of major importance in order to optimize the reactor performance with respect to yield, safety, and long-term stability. For many decades reaction engineers have improved the modeling as well as the numerical schemes to solve these models. The evolution of PBR modeling has been documented in various review papers [4–6].

The variety of PBR models is probably almost as large as the number of applications. This is because there are numerous physical and chemical processes involved. It seems impossible to account for all of them in one comprehensive model. Actually, in most cases it is not necessary to describe the processes in the reactor in such detail. One task of the chemical engineer is always to decide which phenomena can be neglected and how to appropriately model the phenomena that should be included in the model.

In most cases it is totally sufficient to use a quasi-continuous and homogeneous model, where the two-(or more)-phase packed bed is treated as if it was just one fluid phase. Transient behaviour, however, is generally better described by a heterogeneous model, where distinguished phases are considered. For some applications, however, the quasi-continuous treatment of the phases is not appropriate. For instance, the processes in relatively large wood particles during pyrolysis, gasification, and combustion are rather complex. Discrete modeling of individual particles is, thus, advantageous, which raises the question:

How to integrate an intra-particle model into a PBR model?

This study will give one possible answer to this question which is the concept of representative particles. Instead of modeling each individual particle in a PBR, only a

limited number of particles are described in detail. These particular particles are considered as being representative for a finite volume element of the PBR. This basic idea is referred to as Representative Particle Model (RPM).

The major objectives of this work are to further develop the RPM approach and to demonstrate its usefulness in PBR modeling. This will be accomplished in consecutive steps. In Chapter 2 the RPM is characterized as opposed to other heterogeneous PBR models. In the subsequent Chapter 3 the basic model equations of the RPM will be derived. Inter-particle heat and mass transfer will be addressed and a new method will be introduced to describe this phenomenon within the RPM framework in a consistent manner. This method offers the opportunity to examine a prominent heat transfer problem: in Chapter 4 a somewhat extensive excursus will be presented dealing with transient heat transfer in packed beds with stagnant flow. The latter phenomenon is of special interest because it can still not be described satisfyingly accurate with quasi-continuous models despite of a lot of research activities. The higher complexity of the RPM as opposed to quasi-continuous models may be the key to a better understanding and description of that process. In the course of Chapter 4 it will be investigated if RPM can possibly solve that problem. An evaluation of the RPM is presented in Chapter 5. Results of the numerical simulation of heating-up of porous slate particles, drying, and pyrolysis of wood particles are presented, compared to experimental data, and discussed. In Chapter 6 a summary of the study and concluding remarks will be given. Finally, an outlook will be presented in Chapter 7.

Chapter 2

Heterogeneous models for packed bed reactors - a survey

As has been pointed out by Adler [4] in his review article, homogeneous quasi-continuous models are most commonly used. For steady states these models yield fairly good results since the temperature difference between the two (or more) phases is usually negligible (a few K). When it comes to transient processes, however, the temperature difference between fluid and solid can become significant (up to several 100 K [7–9]). In these and other cases summarized by Tsotsas [10] heterogeneous modeling is recommended in order to account for the differences between the phases.

In heterogeneous models the solid phase (i.e.: the particles) can be treated in basically three different ways: quasi-continuous, discrete or representative. The characteristics, advantages, and disadvantages of these three approaches will be outlined in the next sections. Special emphasis is put on how inter-particle heat transfer and shrinking bed height can be captured by these methods. For the sake of brevity a non-reactive, one-component flow will be considered. The respective energy balance for the fluid - which is treated quasi-continuously - is in all cases given by:

$$\varepsilon_f \, \varrho_f \, c_{p,f} \, \frac{\partial T_f}{\partial t} = -w \varrho_f c_{p,f} \frac{\partial T_f}{\partial z} + \frac{\partial}{\partial z}\left(\Lambda_z \frac{\partial T_f}{\partial z}\right) + \alpha \, s \, (T_s - T_f) \quad . \tag{2.1}$$

The terms on the right-hand side of Eq.(2.1) originate from heat convection, heat dispersion, and heat transfer between the phases, respectively.

2.1 Quasi-continuous models

Quasi-continuous heterogeneous models treat both phases as if they were distributed continuously over the whole spacial domain. At each point in space both phases exist with distinguished properties. A typical one-dimensional energy balance equation would be:

$$(1-\varepsilon_f)\,\varrho_s\,c_{p,s}\,\frac{\partial T_s}{\partial t} = \frac{\partial}{\partial z}\Big(\lambda_{\text{eff},s}\frac{\partial T_s}{\partial z}\Big) - \alpha\,s\,(T_s - T_f) \quad . \tag{2.2}$$

The description of the interphase heat transfer is consistent with Eq.(2.1). The inter-particle heat transfer is modeled by a Fourier-type term. The effective heat conductivity $\lambda_{\text{eff},s}$, however, is a problematic quantity. Usually semi-empirical relations for the heat conductivity of packed beds with stagnant flow [11–13] are applied here due to the lack of better relations. This is actually not consistent since these relations have been derived based on a homogeneous model, i.e. they include heat transfer through the (stagnant) fluid as well.

The quasi-continuous model is definitely the most widely used type of heterogeneous PBR models. However, it is very difficult to model shrinking bed height with these type of models.

2.2 Discrete particle models

Discrete particle models (DPM) are sometimes also referred to as "discrete-element models". In this approach an intra-particle model for each particle in the fixed bed is solved simultaneously with the fluid-phase balances. The size and the position of each particle has to be determined at every timestep. For the remainder of this study it will be postulated that the single-particle model is based on a one-dimensional spherical grid (radial coordinate r).

The DPMs are advantageous especially for processes where the size of the particles and hence the bed height changes with time. The heat transfer between neighbour particles can also be described right away by an appropriate boundary condition. In case of a non-reacting non-porous particle this boundary condition can, for instance, be written as:

$$-\,S\,\lambda_s''\left(\frac{\partial T_s}{\partial r}\right)'' = S\,\alpha\,(T_s - T_f) + \sum_j^{N_j}\dot{Q}_{sj} \quad , \tag{2.3}$$

where the last term on the right-hand side of Eq. (2.3) represents the heat transfer to or from the j neighbour particles.

The DPM can be considered as most complex and most accurate amongst the heterogeneous models. But the computational effort is enormous which is the major disadvantage. So far only very few applications have been modeled with DPM [14, 15].

2.3 Representative particle models (RPM)

In this approach of heterogeneous modeling a representative intra-particle model is solved for each finite volume element of the reactor. Representative means: all particles within the finite volume element are assumed to obey the same characteristics as the one for which the intra-particle model is solved. A schematic of this concept - which is sometimes also referred to as "1D+1D model" - is depicted in Fig. 2.1.

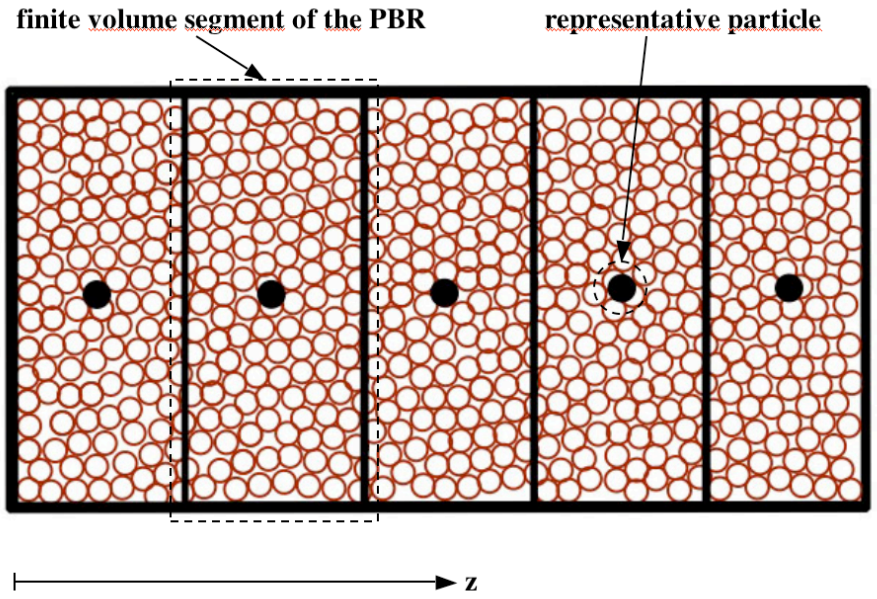

Figure 2.1: *Schematic of the RPM concept*

For the remainder of this study it will be postulated that a one-dimensional grid of finite volumes along the reactor axis (coordinate z) is used to describe a cylindrical PBR.

A typical boundary condition for the representative intra-particle model is basically the same as for the DPM (Eq. (2.3)). The only difference is that the inter-particle heat transfer can not be described as straight forward as for the DPM. Some additional modeling is required which will be outlined in Section 3.2.

The major advantages of the RPMs compared to DPMs are the significantly smaller computational effort and the easy integration into existing computer codes for simulation of PBRs. Hence, the RPM has been applied more often than the DPM but it is by far not as widely used as the quasi-homogeneous model.

In previous works inter-particle heat transfer was either neglected [16–18] or described by means of effective heat conductivities [19, 20], which is inconsistent since the RPM is a non-continuous model. In Chapter 3 a consistent formulation of inter-particle heat transfer within the RPM framework will be presented.

Modeling shrinking bed height is not possible with RPM right away. Some suggestions on how this could be achieved will be given in the outlook (Chapter 7).

2.4 Summary

The characteristics of the three categories of heterogeneous PBR models are visually summarized in Fig. 2.2.

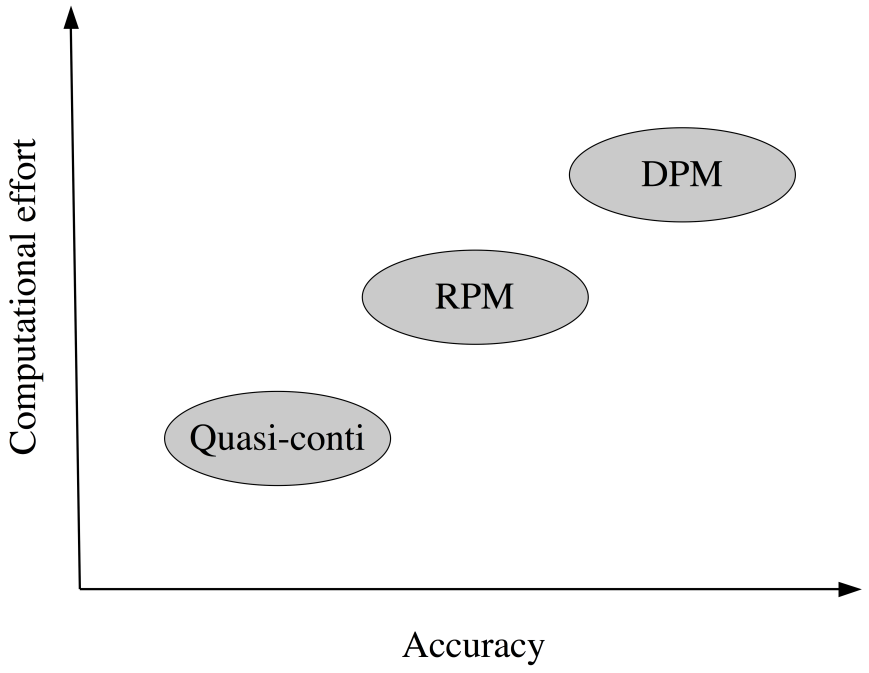

Figure 2.2: *Scheme of the characteristics of heterogeneous PBR models*

Clearly, it can in general not be stated which model is the best. It depends on the application and on the level of accuracy that has to be accomplished. For processes with fixed bed height and small particles (< 1 mm), such as heterogeneous catalysis, the quasi-continuous approach will most likely remain the predominant model of choice. However, processes where the particle size changes during operation (e.g.: combustion, gasification, and pyrolysis of biomass or waste) are probably better represented by RPM and DPM. It may be allowed to generalize that the larger the particles, the more appealing the RPM and DPM, respectively, and the less recommendable the quasi-continuous approach.

However, a recently emerging field of reaction engineering may lead to a very prominent role of RPM in the future: multi-scale modeling. This is a multi-disciplinary attempt to converge the models of different time and length-scales in order to describe the processes in chemical reactors from very first principles. The basic idea of multi-scale modeling is illustrated in Fig. 2.3.

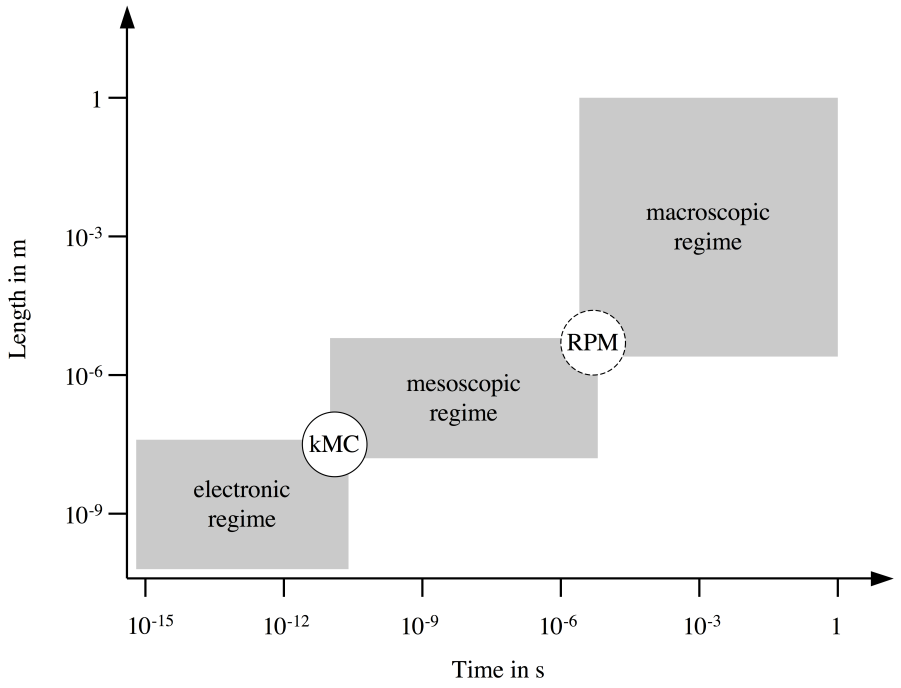

Figure 2.3: *Scales in chemical reaction engineering that have to be covered by multi-scale modeling*

The combination of electronic and mesoscopic regime has already been achieved by several techniques [21] (e.g. kinetic Monte-Carlo simulations [kMC]). The next step of coupling these methods to the macroscopic regime (i.e. to CFD simulations) will be developed in the near future. One promising method could be the RPM. If the multi-scale modeling approach is successful, then it will no longer be necessary to determine global kinetic parameters by experiments. These fitting-parameters do not only have a questionable physical or chemical meaning (if at all), they are also only valid for a rather limited intervall of conditions under which they have been experimentally evaluated. This shortcoming along with the substantial experimental effort can be overcome by use of multi-scale modeling. This method has, thus, the potential to revolutionize chemical engineering. RPM can be one part of this "revolution".

Chapter 3

RPM: The fundamental equations

The basic idea behind the concept of representative particles has already been introduced in Section 2.3. In this section the fundamental equations which represent this basic idea will be introduced.

It is, unfortunately, very common in the chemical reaction engineering and related scientific communities that the balance equations are commented rather briefly. In many cases not all underlying simplifying assumptions are mentioned (if any). In most cases the derivations of the balances are completely skipped for the sake of brevity, since instructive derivations are always somewhat lengthy.

The objective of this study is to establish and develop the Representative Particle Model as a method to model processes in fixed bed reactors. To do that, it is inevitable to motivate and derive the balance equations from a very fundamental and general starting point. This way, it can be motivated why certain simplifying assumptions are useful to make. The basic ideas behind the RPM concept can be illustrated more instructively.

A good simulation of a fixed bed reactor depends on different factors. How well are the properties of the species approximated? Do the mixing rules apply? How good are the correlations for the transport coefficients? Are the reaction kinetics close to reality? Are the numerical techniques appropriate to solve the system of equations? All these issues (and more) are important. But no matter how good these issues are addressed, if the balance equations are false, then the simulation will be poor. Therefore, the balances can be regarded as the basis of every model and every simulation. This basis has to be sound and comprehensible.

Deriving this basis for the RPM is the objective of this chapter.

In Section 3.1 the differential balance equations for the interstitial fluid will be derived.

The intra-particle model can be of (almost) any type. The only restrictions are: transient balances, spherical geometry, gradients occur only in radial direction. The vast

majority of the available intra-particle models obey these characteristics (for a survey of available intra-particle models the reader is referred to [22]). Any one of these sub-models can in principle be integrated into a RPM. However, two modifications have to be made, which are related to the phenomena of heat and mass transfer between neighbour particles (also referred to as inter-particle heat and mass transfer). This problem will be addressed in section 3.2.

3.1 The balance equations for the interstitial fluid

At first, the domain of the balances will be defined. After that, the different modes of transport in a fixed bed will be characterized. Finally, the species mass balances, the momentum balance, and the energy balance will be derived consecutively for the RPM framework.

3.1.1 The differential control volume

At the very beginning a differential control volume V_f has to be defined for which the balances are to be evaluated.

Let us consider a cylindrical fixed bed consisting of solid porous particles. In the interstitial region between the particles there shall be only one fluid phase. All processes within the particles (i.e.: at and beneath the external particle surface) are described by the intra-particle model which is assumed to be one-dimensional and spherical. What remains to be described is the interstitial fluid phase outside the external surface of the porous particles. This means that the fluid phase(s) in the pores of the particles are not part of the control volume since they are considered to be part of the particle's domain.

In order to reduce the complexity of the following derivations it will be postulated that there are neither radial nor azimuthal fluxes (of mass, momentum, and energy, respectively) in the interstitial regions at any time. This is a very strong postulation but it is a quite good approximation in many fixed bed applications. Of course, taking all three spatial dimensions into account would lead to a model which is by far more general. But the addition of the two other dimensions does not have any benefit as far as the understanding of the RPM concept is concerned. Actually, it would be detrimental for that purpose. The gain in ease of comprehension is payed for by loss of generality of the model.

Based on these considerations it is useful to define the differential control volume as follows: If the cylindrical fixed bed reactor was cut at two positions (z and $z + \Delta z$)

perpendicular to the reactor axis (as depicted in Fig. 3.1), then the volume V of this plate would be $A_R \cdot \Delta z$, with A_R being the inner cross section of the reactor. However, only the interstitial fluid phase in this plate is what will be referred to as differential control volume V_f in the following. V_f has, therefore, the shape of a porous cylindric plate of thickness Δz.

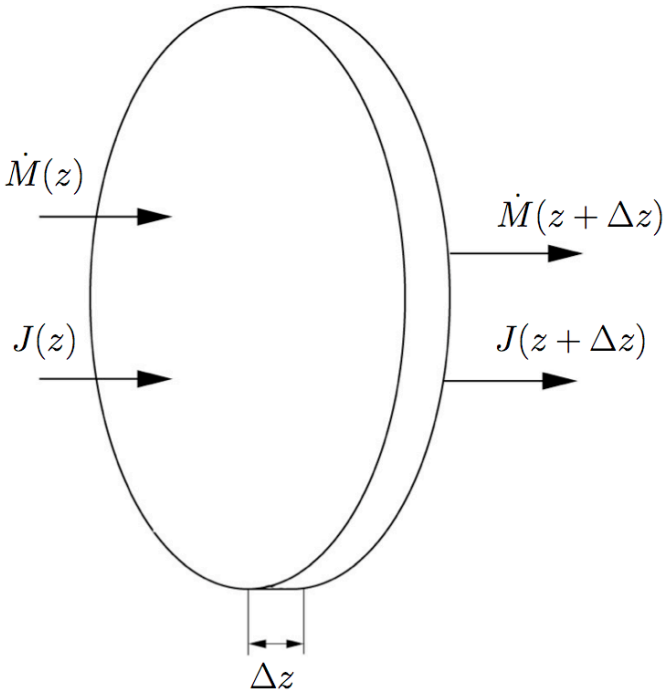

Figure 3.1: *Cylindric reactor volume element V with length Δz*

The boundary ∂V_f of the control volume can be devided into four parts: inlet boundary $A_f(z) = \varepsilon_f A_R$ (with ε_f being the volume fraction of the interstitial fluid in the fixed bed) , outlet boundary $A_f(z+\Delta z) = A_f(z)$, the interface between interstitial fluid and reactor wall A_W, and the interfaces between particles and interstitial fluid A_{sf}.

For this differential control volume the balances for species mass, total mass, momentum, and energy will be derived in the remainder of the chapter.

3.1.2 Transport phenomena in the fluid phase of fixed beds

Mass transfer in fixed beds occurs in three different ways: convection, dispersion, and diffusion.

(a) Convection

Actually, every component i of a gaseous mixture has its own velocity $\underline{w}_i$. Unfortunately, it is practically impossible to measure these different velocities in a mixture. What can be measured, however, is the mean velocity (i.e.: the velocity of the center of mass). The latter is defined as follows:

$$\underline{w} \equiv \frac{\sum_{i=1}^{N_i} \varrho_{f,i}\, \underline{w}_i}{\sum_{i=1}^{N_i} \varrho_{f,i}} = \sum_{i=1}^{N_i} Y_{f,i}\, \underline{w}_i \quad . \tag{3.1}$$

The convective mass flux $\underline{\dot{m}}_f$ is given by:

$$\underline{\dot{m}}_f = \sum_{i=1}^{N_i} \varrho_{f,i}\, \underline{w} = \varrho_f\, \underline{w} = \varrho_f \sum_{i=1}^{N_i} Y_{f,i}\, \underline{w}_i = \sum_{i=1}^{N_i} \varrho_{f,i}\, \underline{w}_i \quad . \tag{3.2}$$

Obviously, for the total mass flux it does not matter if the mean velocity $\underline{w}$ is used for every component or if the component velocity $\underline{w}_i$ is used, the sum over all components leads to the same quantity.

The convective flux of inner energy $\underline{\dot{u}}_{w,f}$ (enthalpy $\underline{\dot{h}}_{w,f}$) is nothing but the flux of inner energy (enthalpy) that is associated with the mean velocity. Therefore:

$$\underline{\dot{u}}_{w,f} = \sum_{i=1}^{N_i} \varrho_{f,i}\, u_{f,i}\, \underline{w} \quad , \tag{3.3}$$

and

$$\underline{\dot{h}}_{w,f} = \sum_{i=1}^{N_i} \varrho_{f,i}\, h_{f,i}\, \underline{w} \quad . \tag{3.4}$$

It is worth noting that

$$\sum_{i=1}^{N_i} \varrho_{f,i}\, u_{f,i}\, \underline{w}_i \quad \neq \quad \sum_{i=1}^{N_i} \varrho_{f,i}\, u_{f,i}\, \underline{w} \quad , \tag{3.5}$$

and

$$\sum_{i=1}^{N_i} \varrho_{f,i}\, h_{f,i}\, \underline{w}_i \quad \neq \quad \sum_{i=1}^{N_i} \varrho_{f,i}\, h_{f,i}\, \underline{w} \quad . \tag{3.6}$$

This inequality can also be expressed as: the convective flux of inner energy (enthalpy) is in general not equal to the total flux of inner energy (enthalpy). It will be outlined later what the difference is between the two.

(b) Dispersion

This phenomenon can be briefly illustrated by a thought experiment: Let us assume two particles in a fluid plug flow in axial direction (no diffusion). If they start at the same axial position z both particles will cover the same distance in a certain time intervall Δt. Their paths of motion will be parallel. Now assume that these particles enter a fixed bed at the same time. Their paths will not be parallel any more. In other words: the two fluid particles will move in lateral direction with respect to one another. This lateral movement is the cause for what is referred to as lateral dispersion. This phenomenon is illustrated in Fig. 3.2.

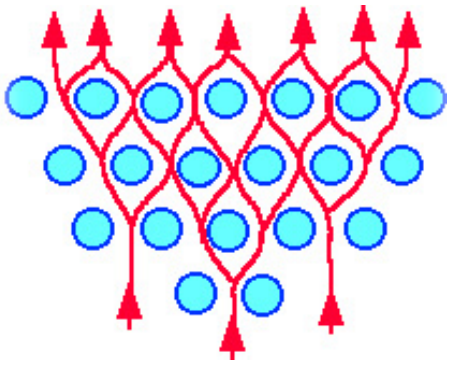

Figure 3.2: *Illustration of lateral dispersion*

Additionaly, after a certain time intervall Δt both particles will most probably not be at the same axial position. That is: they will have moved in axial direction relative to each other. This relative movement in axial direction is referred to as axial dispersion. Both lateral and axial dispersion lead to a decrease in concentration gradients as illustrated in Fig. 3.3 for the axial direction.

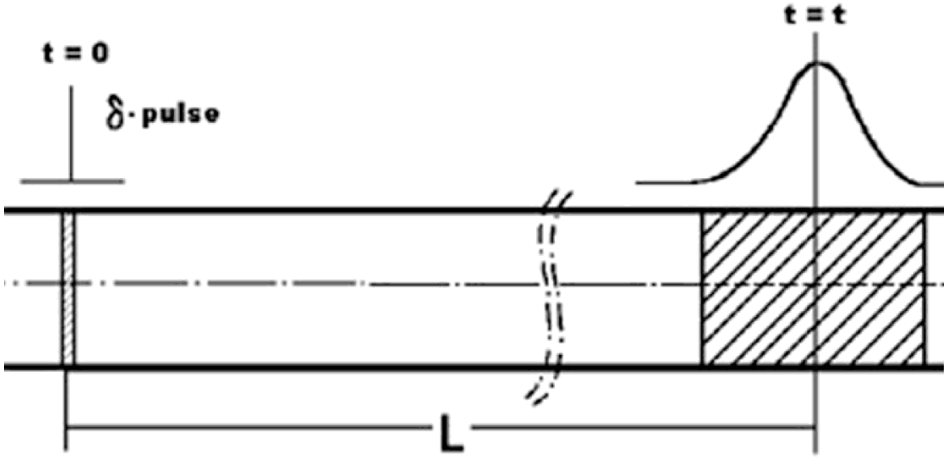

Figure 3.3: *Illustration of axial dispersion*

This is a clear similarity between dispersion and diffusion. Therefore, the axial dispersion flux $j_{f,i}$ is usually described by a Fick's law (which is also true for lateral dispersion):

$$j_{f,i} = -\varrho_f \, D_z \left(\frac{\partial Y_{f,i}}{\partial z} \right) \quad . \tag{3.7}$$

Here, D_z is the axial dispersion coefficient.

The heat dispersion flux $\underline{\dot{u}}_{j,f}$ ($\underline{\dot{h}}_{j,f}$) is the inner energy (enthalpy) that is associated with the mass dispersion flux, i.e.:

$$\underline{\dot{u}}_{j,f} = \sum_{i=1}^{N_i} \underline{j}_{f,i} u_{f,i} \quad , \tag{3.8}$$

$$\underline{\dot{h}}_{j,f} = \sum_{i=1}^{N_i} \underline{j}_{f,i} h_{f,i} \quad . \tag{3.9}$$

The total heat transfer by convection and dispersion can be obtained by adding Eq. (3.3) and Eq. (3.8), resulting in:

$$\underline{\dot{u}}_f = \underline{\dot{u}}_{w,f} + \underline{\dot{u}}_{j,f} = \sum_{i=1}^{N_i} \varrho_{f,i} \, \underline{w} \, u_{f,i} + \sum_{i=1}^{N_i} \underline{j}_{f,i} \, u_{f,i} = \sum_{i=1}^{N_i} (\varrho_{f,i} \, \underline{w} + \underline{j}_{f,i}) \, u_{f,i} \quad . \tag{3.10}$$

The same holds for the enthalpy flux:

$$\underline{\dot{h}}_f = \underline{\dot{h}}_{w,f} + \underline{\dot{h}}_{j,f} = \sum_{i=1}^{N_i} \varrho_{f,i} \, \underline{w} \, h_{f,i} + \sum_{i=1}^{N_i} \underline{j}_{f,i} \, h_{f,i} = \sum_{i=1}^{N_i} (\varrho_{f,i} \, \underline{w} + \underline{j}_{f,i}) \, h_{f,i} \quad . \tag{3.11}$$

These quantities must be equal to the sum of energy fluxes of all components, i.e.:

$$\underline{\dot{u}}_f = \sum_{i=1}^{N_i} \varrho_{f,i} \, \underline{w}_i \, u_{f,i} \qquad \text{and} \qquad \underline{\dot{h}}_f = \sum_{i=1}^{N_i} \varrho_{f,i} \, \underline{w}_i \, h_{f,i} \quad . \tag{3.12}$$

Comparing the coefficients in Eqs. (3.10 - 3.12) shows that:

$$\varrho_{f,i} \, \underline{w}_i = \varrho_{f,i} \, \underline{w} + \underline{j}_{f,i} \quad . \tag{3.13}$$

Taken the sum over all components of a mixture yields:

$$\sum_{i=1}^{N_i} \varrho_{f,i} \, \underline{w}_i = \sum_{i=1}^{N_i} \varrho_{f,i} \, \underline{w} + \sum_{i=1}^{N_i} \underline{j}_{f,i} \quad . \tag{3.14}$$

The definition of the mean velocity in Eq. (3.1) leads to:

$$\sum_{i=1}^{N_i} \underline{j}_{f,i} = 0 \quad . \tag{3.15}$$

This is consistent with Eq. (3.7). However, although the sum of the mass dispersion fluxes over the components vanishes in any case, the sum of the heat dispersion fluxes does not vanish in general, which can be observed from Eqs. (3.8) and (3.9).

From Eq. (3.7) it follows that in case of pure fluids and homogeneous mixtures $\underline{j}_{f,i} = 0$ holds. But this only means that dispersion has no effect on the mass balance. It still occurs. Or in other words: the phenomenon of dispersion occurs also in pure fluids and homogeneous mixtures, but it can not be observed due to the fact that molecules of one species are not distinguishable from one another.

Equations (3.8) and (3.9) are a consequence of the fact that dispersion is related to exactly the same phenomenon as dispersion of mass. It is very important to note that this is only true for heterogeneous models. In homogeneous models the heat transfer between neighbour particles as well as between particle and fluid also contribute to a better mixing. Therefore, in homogeneous models these two phenomena have to be included in the dispersion model. But in heterogeneous models the latter two effects have to be modeled explicitely.

However, Eqs. (3.8) and (3.9) fail to predict heat dispersion in pure fluids and in perfectly mixed multi-component flows, since in these cases $\underline{j}_{f,i} = 0$. Hence, an alternative model for heat dispersion is required. Since dispersion of heat leads to a decrease of temperature gradients it is in most cases modeled by Fourier's law using a heat dispersion coefficient Λ_z (or to be more precise: an enthalpy dispersion coefficient).

$$\underline{\dot{h}}_{j,f} = \sum_{i=1}^{N_i} \underline{j}_{f,i}\, h_{f,i} = -\Lambda_z \left(\frac{\partial T_f}{\partial z} \right) \quad . \tag{3.16}$$

The equivalence of heat and mass dispersion (in case of heterogeneous modeling) is represented by the fact that the Lewis number for axial (and lateral) dispersion is unity:

$$\mathrm{Le} \equiv \frac{a}{D} = \frac{\Lambda_z}{\varrho_f c_{p,f} D_z} = \frac{\varrho_f c_{p,f} D_z}{\varrho_f c_{p,f} D_z} = 1 \quad . \tag{3.17}$$

(c) Diffusion

Convection and dispersion can be regarded as macroscopic and mesoscopic transport, respectively. Diffusion is transport on microscopic level due to concentration gradients. The diffusion flux can be determined as in Eq. (3.7), except that the transport coefficient is the diffusivity D_i rather than the dispersion coefficient D_z. The order of magnitude of diffusivity in a gas mixture is 10^{-5} m^2/s. Dispersion coefficients can be estimated by $D_z \sim w_z d_s$. In the experiments that will be considered in this work particle sizes are of the order of 10^{-2} m and velocities are in the 0.1 m/s range. This means that $D_z \approx 10^{-3}$ m^2/s. Hence, diffusion can be neglected as compared to dispersion.

Similarly, heat dispersion is also two orders of magnitude higher than heat conduction, which is why the latter can be neglected compared to the former.

3.1.3 Derivation of the species and total mass balances

A general mass balance of species i reads [23]:

$$\int_{V_f} \frac{\partial \varrho_{f,i}}{\partial t} \mathrm{d}V = -\int_{\partial V_f} \varrho_{f,i}\, \underline{w}_i \cdot \underline{n}\, \mathrm{d}A + \int_{V_f} \dot{r}_{f,i}\, \mathrm{d}V \quad . \tag{3.18}$$

The terms on the right-hand side of Eq. (3.18) refer to mass transfer across the entire boundary of the control volume and homogeneous chemical reactions occuring within V_f, respectively. The following postulations are made:

1. All quantities are distributed homogeneously over the cross section $A_f(z)$.
2. The radial and azimuthal velocities are zero, i.e.: $\underline{w}_i = \begin{pmatrix} 0 \\ 0 \\ w_i \end{pmatrix}$.
3. $\Delta z \to 0$.

With these postulations the mass balance of species i can be rewritten as:

$$\frac{\partial \varrho_{f,i}}{\partial t} V_f = -\int_{\partial V_f} \varrho_{f,i}\, \underline{w}_i \cdot \underline{n}\, \mathrm{d}A + \dot{r}_{f,i}\, V_f \quad . \tag{3.19}$$

The surface integral is evaluated at the four abovementioned subdomains (inlet, outlet, wall-fluid interface, particle-fluid interface). At the inlet all quantities are homogeneously distributed and the normal vector of that surface is exactly opposite to the z-direction, which means: $\underline{w}_i \cdot \underline{n} = -w_i$. Hence:

$$-\int_{A_f(z)} \varrho_{f,i}\, \underline{w}_i \cdot \underline{n}\, \mathrm{d}A = \left(\varrho_{f,i}\, w + j_{f,i}\right)_z A_f \quad . \tag{3.20}$$

The same applies to the outlet boundary $A_f(z + \Delta z)$, with the exception that here $\underline{w}_i \cdot \underline{n} = w_i$ since the normal vector of the boundary is in the same direction as the velocity. Thus:

$$-\int_{A_f(z+\Delta z)} \varrho_{f,i}\, \underline{w} \cdot \underline{n}\, \mathrm{d}A = -\left(\varrho_{f,i}\, w + j_{f,i}\right)_{z+\Delta z} A_f \quad . \tag{3.21}$$

At the reactor wall the normal vector of the boundary is perpendicular to the velocity. Thus, with the postulations listed above, no mass can be transferred through this boundary.

The mass transfer between the particles and the fluid (may it be convective or non-convective) can be readily described by the particle model. Every mass that crosses the external surface S of the particle also crosses the boundary A_{sf} of the control volume V_f. It has to be taken into account that the sign of the integral changes since a mass flux that leaves a particle is negative within the particle model framework while it is positive in the case of the interstitial fluid in the reactor. If N_s is the number of solid particles in the control volume, then:

$$-\int_{A_{sf}} \varrho_{f,i}\, \underline{w}_i \cdot \underline{n}\, \mathrm{d}A = N_s \int_S \varrho''_{f,i}\, \underline{v}''_i \cdot \underline{n}\, \mathrm{d}A \quad . \tag{3.22}$$

Due to the one-dimensional nature of the particle model it can be concluded that all quantities are distributed homogeneously over the particle surface. Thus, the integral can be transformed into a product. Furthermore, at the particle surface $\underline{v}_i \cdot \underline{n} = v_i$ holds. Also $N_s\, S = A_{sf}$ (N_s can be a real number). Therefore, the surface integral can be evaluated by:

$$-\int_{A_{sf}} \varrho_{f,i}\, \underline{w}_i \cdot \underline{n}\, \mathrm{d}A = \left(\varrho''_{f,i}\, v''_i\right) A_{sf} \quad . \tag{3.23}$$

Use of the mean intra-particle velocity v which is defined analogously to Eq. (3.1) gives:

$$-\int_{A_{sf}} \varrho_{f,i}\, \underline{w}_i \cdot \underline{n}\, \mathrm{d}A = \left(\varrho''_{f,i}\, v'' + j''_{f,i}\right) A_{sf} \quad . \tag{3.24}$$

The diffusion flux $j''_{f,i}$ normal to the particle surface can be described by means of a mass transfer coefficient β''_i. The Stefan correction ζ_i has to be considered in this case [24] since the convection changes the concentration gradient and, hence, also β''_i. Thus:

$$-\int_{A_{sf}} \varrho_{f,i}\, \underline{w}_i \cdot \underline{n}\, \mathrm{d}A = \left(\varrho''_{f,i}\, v'' + \zeta_i \beta''_i [\varrho''_{f,i} - \varrho_{f,i}]\right) A_{sf} \quad . \tag{3.25}$$

According to the film theory the Stefan correction is given by:

$$\zeta_i = \frac{v''/\beta''_i}{\exp(v''/\beta''_i) - 1} \quad . \tag{3.26}$$

Based on the aforementioned assumptions and considerations the mass balance of species i in the interstitial fluid can be written as:

$$\begin{aligned} \frac{\partial \varrho_{f,i}}{\partial t} V_f =& \left(\varrho_{f,i}\, w + j_{f,i}\right)_z A_f - \left(\varrho_{f,i}\, w + j_{f,i}\right)_{z+\Delta z} A_f + \\ &+ \left(\varrho''_{f,i}\, v'' + \zeta_i \beta''_i [\varrho''_{f,i} - \varrho_{f,i}]\right) A_{sf} + \dot{r}_{f,i}\, V_f \quad . \end{aligned} \tag{3.27}$$

Using the first-order Taylor expansion yields:

$$\begin{aligned} \frac{\partial \varrho_{f,i}}{\partial t} V_f =& - \frac{\partial \left(\varrho_{f,i}\, w\right)}{\partial z} A_f \Delta z - \frac{\partial j_{f,i}}{\partial z} A_f \Delta z + \\ &+ \left(\varrho''_{f,i}\, v'' + \zeta_i \beta''_i [\varrho''_{f,i} - \varrho_{f,i}]\right) A_{sf} + \dot{r}_{f,i}\, V_f \quad . \end{aligned} \tag{3.28}$$

Dividing by V_f results in:

$$\frac{\partial \varrho_{f,i}}{\partial t} = -\frac{\partial\left(\varrho_{f,i}\, w\right)}{\partial z} - \frac{\partial j_{f,i}}{\partial z} + \frac{A_{sf}}{V_f}\left(\varrho''_{f,i} v + \zeta_i \beta''_i [\varrho''_{f,i} - \varrho_{f,i}]\right) + \dot{r}_{f,i} \quad . \tag{3.29}$$

Furthermore, A_{sf} (the area of the solid-fluid interface in V) can be expressed in terms of the specific surface s of the particles as follows:

$$\frac{A_{sf}}{V_f} = \frac{s\, V_s}{\varepsilon_f V} = \frac{s\,(1-\varepsilon_f)V}{\varepsilon_f V} = s\,\frac{(1-\varepsilon_f)}{\varepsilon_f} \quad . \tag{3.30}$$

This leads - together with Eq. (3.7) - to the mass balance of species i:

$$\frac{\partial \varrho_{f,i}}{\partial t} = -\frac{\partial(\varrho_{f,i} w)}{\partial z} + \frac{\partial}{\partial z}\left(\varrho_f\, D_z\, \frac{\partial(\varrho_{f,i}/\varrho_f)}{\partial z}\right) + s\,\frac{1-\varepsilon_f}{\varepsilon_f}\left(\varrho''_{f,i}\, v'' + \zeta_i \beta''_i [\varrho''_{f,i} - \varrho_{f,i}]\right) + \dot{r}_{f,i} \quad . \tag{3.31}$$

For the derivation of the energy balance (see subsection 3.1.5) it is advantageous to use the species velocity v_i:

$$\frac{\partial \varrho_{f,i}}{\partial t} = -\frac{\partial(\varrho_{f,i} w)}{\partial z} - \frac{\partial j_{f,i}}{\partial z} + s\,\frac{1-\varepsilon_f}{\varepsilon_f}\left(\varrho''_{f,i}\, v''_i\right) + \dot{r}_{f,i} \quad . \tag{3.32}$$

The total mass balance (continuity equation) is equivalent to the sum over all species mass balances. The dispersion terms as well as the homogeneous reaction term vanish by taking that sum. Hence, the continuity equation reads:

$$\frac{\partial \varrho_f}{\partial t} = -\frac{\partial(w \varrho_f)}{\partial z} + s\,\frac{1-\varepsilon_f}{\varepsilon_f}\left(\varrho''_f\, v''\right) \quad . \tag{3.33}$$

Both the third term on the right-hand side of Eq. (3.32) as well as the second term on the right-hand side of Eq. (3.33) represent the major difference between RPM and quasi-continuous heterogeneous models. These terms are the connection between single-particle model and interstitial gas in the reactor domain. Hence, they are of central importance in the RPM approach.

3.1.4 Derivation of the momentum balance

The general momentum balance in vector notation reads [23]:

$$\int_{V_f} \frac{\partial}{\partial t}\left(\varrho_f \, \underline{w}\right) \mathrm{d}V = -\int_{\partial V_f} \varrho_f \, (\underline{w}\,\underline{w}) \cdot \underline{n} \, \mathrm{d}A + \int_{\partial V_f} \underline{\underline{\tau}} \cdot \underline{n} \, \mathrm{d}A + \int_{V_f} \varrho_f \, \underline{\phi} \, \mathrm{d}V \quad . \tag{3.34}$$

The terms on the right-hand side of Eq.(3.34) refer to convective transport of momentum across the boundaries (∂V_f) of the control volume and momentum generation (or consumption) by surface and volume forces, respectively. The mean velocity as defined in Eq.(3.1) is used here. The heterogeneous mass transfer between solid and fluid phase is not an additional source of momentum because it has zero velocity (due to the rotational symmetry of the particle model).

The following assumptions are made:

1. All intensive quantities are distributed homogeneously over the cross-sectional area in the fluid.
2. The radial and azimuthal velocities are zero, i.e.: $\underline{w} = \begin{pmatrix} 0 \\ 0 \\ w \end{pmatrix}$.
3. $\Delta z \to 0$.
4. No relevant volumetric forces.

With these assumptions the momentum balance can be rewritten as:

$$\frac{\partial(\varrho_f \, \underline{w})}{\partial t} V_f = -\int_{\partial V_f} \left[\varrho_f \, (\underline{w}\,\underline{w}) - \underline{\underline{\tau}} \right] \cdot \underline{n} \, \mathrm{d}A \quad . \tag{3.35}$$

In analogy to subsection 3.1.3, the integral over the boundary ∂V_f of the control volume is devided into the four subdomains $A_f(z)$, $A_f(z+\Delta z)$, A_W, and A_{sf}.

At the inlet boundary the velocity field within the fluid phase is postulated to be homogeneous (as for every other axial position). Hence, no tangential stresses occur, only normal stresses. That is why the stress tensor reads:

$$\underline{\underline{\tau}} = -p \, \underline{\underline{\delta}} \quad . \tag{3.36}$$

Hence:

$$\begin{aligned} \dot{Q}_{A_f(z)} &\equiv -\int_{A_f(z)} \left[\varrho_f (\underline{w}\,\underline{w}) - \underline{\underline{\tau}} \right] \cdot \underline{n} \, \mathrm{d}A \\ \dot{Q}_{A_f(z)} &= -\left[\varrho_f \begin{pmatrix} 0 & 0 & 0 \\ 0 & 0 & 0 \\ 0 & 0 & w^2 \end{pmatrix} + \begin{pmatrix} p & 0 & 0 \\ 0 & p & 0 \\ 0 & 0 & p \end{pmatrix} \right]_z \cdot \begin{pmatrix} 0 \\ 0 \\ -1 \end{pmatrix} A_f \quad . \end{aligned} \tag{3.37}$$

Here, only the axial momentum balance is relevant, i.e.:

$$\dot{Q}_{A_f(z)} = \Big[\varrho_f w^2 + p\Big]_z \, A_f \quad . \tag{3.38}$$

The same is true for the outlet boundary, except for the direction of the normal vector. Hence, the sign changes:

$$\dot{Q}_{A_f(z+\Delta z)} = -\Big[\varrho_f w^2 + p\Big]_{z+\Delta z} \, A_f \quad . \tag{3.39}$$

At the reactor wall as well as at the particles surfaces the momentum is diminished by friction (due to lateral velocity gradients). The latter is accounted for by a semi-empirical relation. For now, the momentum sink due to interphase friction will be referred to as F_{sf}. Based on these considerations the momentum balance in axial direction can be written as:

$$\frac{\partial(\varrho_f \, w)}{\partial t} V_f = \Big[\varrho_f w^2 + p\Big]_z \, A_f - \Big[\varrho_f w^2 + p\Big]_{z+\Delta z} \, A_f - F_{sf} \quad . \tag{3.40}$$

Application of the first-order Taylor expansion and dividing by V_f yields:

$$\frac{\partial(\varrho_f \, w)}{\partial t} = -\frac{\partial(\varrho_f \, w^2)}{\partial z} - \frac{\partial p}{\partial z} - \frac{F_{sf}}{V_f} \quad . \tag{3.41}$$

For the third term on the right-hand side of Eq.(3.41) Ergun's equation [25] is applied. The latter relation is valid for homogeneous models (i.e.: it is written in terms of superficial velocity). Therefore it can not be applied right away. Ergun's equation reads:

$$\frac{F_{sf}}{V} = f_1 \frac{\dot{V}_f}{A_R} + f_2 \Big(\frac{\dot{V}_f}{A_R}\Big)^2 \quad , \tag{3.42}$$

with

$$f_1 \equiv 150 \, \frac{(1-\varepsilon_f)^2}{\varepsilon_f^3} \, \frac{\eta_f}{d_s^2} \quad \text{and} \quad f_2 \equiv 1.75 \, \frac{(1-\varepsilon_f)}{\varepsilon_f^3} \, \frac{\varrho_f}{d_s} \quad . \tag{3.43}$$

This is equivalent to:

$$\varepsilon_f \frac{F_{sf}}{V_f} = f_1 \varepsilon_f w + f_2 (\varepsilon_f w)^2 \quad . \tag{3.44}$$

Now, the third term on the right-hand side of Eq.(3.41) can be replaced to give:

$$\frac{\partial(\varrho_f \, w)}{\partial t} = -\frac{\partial(\varrho_f \, w^2)}{\partial z} - \frac{\partial p}{\partial z} - f_1 w - \varepsilon_f f_2 w^2 \quad . \tag{3.45}$$

This is the form of the momentum balance that has to be solved.

3.1.5 Derivation of the energy balance

The energy balance of a mixture with N_i components reads [23]:

$$\begin{aligned} \sum_{i=1}^{N_i} \int_{V_f} \frac{\partial}{\partial t} \big(\varrho_{f,i} \, e_{f,i}\big) \mathrm{d}V = &- \sum_{i=1}^{N_i} \int_{\partial V_f} \varrho_{f,i} \, e_{f,i} \, \underline{w}_i \cdot \underline{n} \, \mathrm{d}A + \sum_{i=1}^{N_i} \int_{\partial V_f} \big(\underline{\underline{\tau}}_i \cdot \underline{w}_i\big) \cdot \underline{n} \, \mathrm{d}A + \\ &- \int_{\partial V_f} \underline{\dot{q}}_{f,\lambda} \cdot \underline{n} \, \mathrm{d}A + \int_{V_f} \varrho_f \, \underline{\phi} \cdot \underline{w} \, \mathrm{d}V + \int_{V_f} \varrho_f \, \rho \, \mathrm{d}V \quad . \end{aligned} \tag{3.46}$$

The mass specific energy

$$e \equiv u + e_{kin} = u + \frac{1}{2}|\underline{w}|^2 \tag{3.47}$$

is composed of inner and kinetic energy. The terms on the right-hand side of Eq.(3.46) refer to energy transfer associated to mass transfer across the entire boundary (∂V_f) of the control volume, work by forces that act on the boundary, heat conduction through ∂V_f, work by volumetric forces, and absorption of radiation by the fluid, respectively.

The following assumptions are made:

1. All intensive quantities are distributed homogeneously over the cross-sectional area in the fluid.
2. The radial and azimuthal velocities are zero, i.e.: $\underline{w}_i = \begin{pmatrix} 0 \\ 0 \\ w_i \end{pmatrix}$.
3. $\Delta z \to 0$.
4. No absorption of radiation by the fluid, i.e.: $\rho = 0$.
5. Specific kinetic energy is negligible compared to specific inner energy, i.e.: $u \gg e_{kin}$.
6. The contribution of the volumetric forces can be neglected in case of fluids, i.e.: $\underline{\phi} = \underline{0}$.
7. Heat conduction is negligible as compared to heat dispersion and convection.
8. The fluid is a mixture of ideal gases.

With these assumptions the energy balance can be rewritten as:

$$\sum_{i=1}^{N_i} \frac{\partial(\varrho_{f,i}\, u_{f,i})}{\partial t} V_f = -\int\limits_{\partial V_f} \Big[\sum_{i=1}^{N_i} \big(\varrho_{f,i}\, u_{f,i}\, \underline{w}_i - \underline{\underline{\tau}}_i \cdot \underline{w}_i\big) + \underline{\dot{q}}_{f,\lambda}\Big] \cdot \underline{n}\, \mathrm{d}A \quad . \tag{3.48}$$

In analogy to subsection 3.1.3, the integral over the boundary ∂V_f of the control volume is devided into the four subdomains $A_f(z)$, $A_f(z+\Delta z)$, A_W, and A_{sf}.

All intensive quantities are homogeneously distributed over the inlet boundary, which means that Eq.(3.36) holds. Heat conduction can be neglected compared to convection. Hence:

$$\begin{aligned}
\dot{Q}_{A_f(z)} &\equiv -\sum_{i=1}^{N_i} \int\limits_{A_f(z)} \Big[\varrho_{f,i}\, u_{f,i}\, \underline{w}_i - \underline{\underline{\tau}}_i \cdot \underline{w}_i\Big] \cdot \underline{n}\, \mathrm{d}A \\
&= -\sum_{i=1}^{N_i} \Big[\varrho_{f,i}\, u_{f,i}\, \underline{w}_i - \underline{\underline{\tau}}_i \cdot \underline{w}_i\Big]_z \cdot \underline{n}\, A_f \\
&= -\sum_{i=1}^{N_i} \left[\varrho_{f,i}\, u_{f,i} \begin{pmatrix} 0 \\ 0 \\ w_i \end{pmatrix} - \begin{pmatrix} -p_i & 0 & 0 \\ 0 & -p_i & 0 \\ 0 & 0 & -p_i \end{pmatrix} \cdot \begin{pmatrix} 0 \\ 0 \\ w_i \end{pmatrix}\right]_z \cdot \begin{pmatrix} 0 \\ 0 \\ -1 \end{pmatrix} A_f \\
&= \sum_{i=1}^{N_i} \Big[\varrho_{f,i}\, u_{f,i} w_i + p_i w_i\Big]_z A_f \\
&= \sum_{i=1}^{N_i} \Big[\varrho_{f,i} \left(u_{f,i} + \frac{p_i}{\varrho_{f,i}}\right) w_i\Big]_z A_f \\
&= \sum_{i=1}^{N_i} \Big[\varrho_{f,i}\, h_{f,i}\, w_i\Big]_z A_f \quad .
\end{aligned} \tag{3.49}$$

The same applies to the outlet boundary $A_f(z+\Delta z)$, with the exception that here the normal vector of the boundary is in positive z-direction. Thus:

$$\dot{Q}_{A_f(z+\Delta z)} = -\Big[\sum_{i=1}^{N_i} \varrho_{f,i}\, h_{f,i}\, w_i\Big]_{z+\Delta z} A_f \quad . \tag{3.50}$$

At the reactor wall the normal vector of the boundary surface is perpendicular to the velocity. There is also no temperature gradient in radial direction due to the first of the postulations listed above. Thus, no energy can be transferred through this boundary, neither by convection nor by conduction. To still be able to describe a non-adiabatic reactor wall the concept of the heat transfer coefficient (α_W) is applied here as shown in Eq.(3.51). It has to be noted that this is, actually, an inconsistency of the model. But there is no other way to describe wall-to-fluid heat transfer in a model with one dimension in space.

$$\dot{Q}_{A_W} \equiv -\int\limits_{A_W} \Big[\sum_{i=1}^{N_i} \big(\varrho_{f,i}\, u_{f,i}\, \underline{w}_i - \underline{\underline{\tau}}_i \cdot \underline{w}_i\big) + \underline{\dot{q}}_{f,\lambda}\Big] \cdot \underline{n}\, \mathrm{d}A = -\alpha_W A_W \big(T_f - T_W\big) \quad . \tag{3.51}$$

For the heat transfer between particles and fluid the same arguments hold as outlined in subsection 3.1.3. Thus:

$$-\int\limits_{A_{sf}} \Big[\sum_{i=1}^{N_i} \big(\varrho_{f,i}\, u_{f,i}\, \underline{w}_i - \underline{\underline{\tau}}_i \cdot \underline{w}_i\big) + \underline{\dot{q}}_{f,\lambda}\Big] \cdot \underline{n}\, \mathrm{d}A = \Big[\sum_{i=1}^{N_i} \varrho''_{f,i}\, h''_{f,i}\, v''_i + \dot{q}''_{s,\lambda}\Big] A_{sf} \quad . \tag{3.52}$$

Based on the aforementioned assumptions and considerations the energy balance of the fluid in the control volume can be written as:

$$\begin{aligned}\sum_{i=1}^{N_i} \frac{\partial(\varrho_{f,i}\, u_{f,i})}{\partial t} V_f = &\Big[\sum_{i=1}^{N_i} \varrho_{f,i}\, h_{f,i}\, w_i\Big]_z A_f - \Big[\sum_{i=1}^{N_i} \varrho_{f,i}\, h_{f,i}\, w_i\Big]_{z+\Delta z} A_f + \\ &- \alpha_W A_W \big(T_f - T_W\big) + \Big[\sum_{i=1}^{N_i} \varrho''_{f,i}\, h''_{f,i}\, v''_i + \dot{q}''_{s,\lambda}\Big] A_{sf} \quad .\end{aligned} \tag{3.53}$$

Using the first-order Taylor expansion yields:

$$\begin{aligned}\sum_{i=1}^{N_i} \frac{\partial(\varrho_{f,i}\, u_{f,i})}{\partial t} V_f = &-\sum_{i=1}^{N_i} \frac{\partial}{\partial z}\big(\varrho_{f,i}\, h_{f,i}\, w_i\big) A_f \Delta z - \alpha_W A_W \big(T_f - T_W\big) + \\ &+ \Big[\sum_{i=1}^{N_i} \varrho''_{f,i}\, h''_{f,i}\, v''_i + \dot{q}''_{s,\lambda}\Big] A_{sf} \quad .\end{aligned} \tag{3.54}$$

Dividing by V_f results in:

$$\begin{aligned}\sum_{i=1}^{N_i} \frac{\partial(\varrho_{f,i}\, u_{f,i})}{\partial t} = &-\sum_{i=1}^{N_i} \frac{\partial}{\partial z}\big(\varrho_{f,i}\, h_{f,i}\, w_i\big) - \alpha_W \frac{A_W}{V_f}\big(T_f - T_W\big) + \\ &+ \frac{A_{sf}}{V_f}\Big[\sum_{i=1}^{N_i} \varrho''_{f,i}\, h''_{f,i}\, v''_i + \dot{q}''_{s,\lambda}\Big] \quad .\end{aligned} \tag{3.55}$$

Furthermore:

$$\frac{A_W}{V_f} = \frac{2\pi R\, \Delta z}{\varepsilon_f \pi R^2\, \Delta z} = \frac{2}{\varepsilon_f\, R} \tag{3.56}$$

With Eqs.(3.30) and (3.56) the energy balance reads:

$$\begin{aligned}\sum_{i=1}^{N_i} \frac{\partial(\varrho_{f,i}\, u_{f,i})}{\partial t} = &-\sum_{i=1}^{N_i} \frac{\partial}{\partial z}\big(\varrho_{f,i}\, h_{f,i}\, w_i\big) - \alpha_W \frac{2}{\varepsilon_f\, R}\big(T_f - T_W\big) + \\ &+ s\, \frac{1-\varepsilon_f}{\varepsilon_f}\Big[\sum_{i=1}^{N_i} \varrho''_{f,i}\, h''_{f,i}\, v''_i + \dot{q}''_{s,\lambda}\Big] \quad .\end{aligned} \tag{3.57}$$

To obtain a differential equation for the temperature some further modifications are necessary. For this purpose the mass specific inner energy $u_{f,i}$ is expressed by means of the mass specific enthalpy $h_{f,i} = c_{p,i} T_f + h_{ref,i}$ as follows:

$$\begin{aligned}\frac{\partial}{\partial t}\big(\varrho_{f,i} u_{f,i}\big) &= \frac{\partial}{\partial t}\Big(\varrho_{f,i}\big(h_{f,i} - \frac{p_i}{\varrho_{f,i}}\big)\Big) \\ &= \frac{\partial}{\partial t}\big(\varrho_{f,i} h_{f,i} - p_i\big) \\ &= \varrho_{f,i}\, \frac{\partial h_{f,i}}{\partial t} + h_{f,i}\, \frac{\partial \varrho_{f,i}}{\partial t} - \frac{\partial p_i}{\partial t} \, .\end{aligned} \tag{3.58}$$

Together with application of the product rule to the convection term in Eq.(3.57) and after some rearranging this yields:

$$\sum_{i=1}^{N_i} \varrho_{f,i} \frac{\partial h_{f,i}}{\partial t} - \frac{\partial p}{\partial t} = -\sum_{i=1}^{N_i} h_{f,i} \left(\frac{\partial \varrho_{f,i}}{\partial t} + \frac{\partial (\varrho_{f,i} w_i)}{\partial z} \right) - \sum_{i=1}^{N_i} \varrho_{f,i} w_i \frac{\partial h_{f,i}}{\partial z} + \\ - \alpha_W \frac{2}{\varepsilon_f R} (T_f - T_W) + s \frac{1-\varepsilon_f}{\varepsilon_f} \left(\sum_{i=1}^{N_i} \varrho''_{f,i} h''_{f,i} v''_i + \dot{q}''_{s,\lambda} \right) \quad . \tag{3.59}$$

By use of Eq.(3.13) this equation can be modified to give:

$$\sum_{i=1}^{N_i} \varrho_{f,i} \frac{\partial h_{f,i}}{\partial t} - \frac{\partial p}{\partial t} = -\sum_{i=1}^{N_i} h_{f,i} \left(\frac{\partial \varrho_{f,i}}{\partial t} + \frac{\partial (\varrho_{f,i} w_i)}{\partial z} \right) - \sum_{i=1}^{N_i} (\varrho_{f,i} w + j_{f,i}) \frac{\partial h_{f,i}}{\partial z} + \\ - \alpha_W \frac{2}{\varepsilon_f R} (T_f - T_W) + s \frac{1-\varepsilon_f}{\varepsilon_f} \left(\sum_{i=1}^{N_i} \varrho''_{f,i} h''_{f,i} v''_i + \dot{q}''_{s,\lambda} \right) \quad . \tag{3.60}$$

The species mass balance (Eq.(3.32)) - slightly rearranged - reads:

$$\frac{\partial \varrho_{f,i}}{\partial t} + \frac{\partial (\varrho_{f,i} w_i)}{\partial z} = s \frac{1-\varepsilon_f}{\varepsilon_f} (\varrho''_{f,i} v''_i) + \dot{r}_{f,i} \quad . \tag{3.61}$$

Substituting the term in big parenthesis in Eq.(3.60) by the right-hand side of Eq.(3.61) gives:

$$\sum_{i=1}^{N_i} \varrho_{f,i} \frac{\partial h_{f,i}}{\partial t} - \frac{\partial p}{\partial t} = -\sum_{i=1}^{N_i} h_{f,i} \left(s \frac{1-\varepsilon_f}{\varepsilon_f} (\varrho''_{f,i} v''_i) + \dot{r}_{f,i} \right) - \sum_{i=1}^{N_i} (\varrho_{f,i} w + j_{f,i}) \frac{\partial h_{f,i}}{\partial z} + \\ - \alpha_W \frac{2}{\varepsilon_f R} (T_f - T_W) + s \frac{1-\varepsilon_f}{\varepsilon_f} \left(\sum_{i=1}^{N_i} \varrho''_{f,i} h''_{f,i} v''_i + \dot{q}''_{s,\lambda} \right) \quad . \tag{3.62}$$

At this stage it is helpful to make a short excursion. The specific enthalpy is a variable of state (Zustandsvariable), i.e.:

$$\frac{\partial h_{f,i}}{\partial t} = \left[\frac{\partial h_{f,i}}{\partial p} \right]_T \frac{\partial p}{\partial t} + \left[\frac{\partial h_{f,i}}{\partial T} \right]_p \frac{\partial T}{\partial t} \quad . \tag{3.63}$$

For ideal gases we have:

$$\left[\frac{\partial h_{f,i}}{\partial p} \right]_T = 0 \qquad \text{and} \qquad \left[\frac{\partial h_{f,i}}{\partial T} \right]_p \equiv c_{p,i} \quad . \tag{3.64}$$

Therefore:

$$\frac{\partial h_{f,i}}{\partial t} = c_{p,i} \frac{\partial T_f}{\partial t} \qquad \text{and analogously} \qquad \frac{\partial h_{f,i}}{\partial z} = c_{p,i} \frac{\partial T_f}{\partial z} \quad . \tag{3.65}$$

Using $\varrho_f\, c_{p,f} \equiv \sum_{i=1}^{N_i} \varrho_{f,i}\, c_{p,i}$, inserting Eq.(3.65) in Eq.(3.62) and rearrangement yields:

$$\begin{aligned}\varrho_f\, c_{p,f}\, \frac{\partial T_f}{\partial t} - \frac{\partial p}{\partial t} = &- \varrho_f\, c_{p,f}\, w \frac{\partial T_f}{\partial z} - \sum_{i=1}^{N_i} j_{f,i}\, c_{p,i} \frac{\partial T_f}{\partial z} + \\ &- \alpha_W \frac{2}{\varepsilon_f\, R}\left(T_f - T_W\right) - \sum_{i=1}^{N_i} h_{f,i}\, \dot{r}_{f,i} + \\ &- s\, \frac{1-\varepsilon_f}{\varepsilon_f} \left[\sum_{i=1}^{N_i} \varrho''_{f,i}\, v''_i\, (h_{f,i} - h''_{f,i}) - \dot{q}_{s,\lambda}\right]_{r_s} \quad .\end{aligned} \tag{3.66}$$

This is the desired differential equation for the temperature. Some modifications are useful. First of all $\varrho_f c_{p,f}(\partial T_f/\partial t) \gg (\partial p/\partial t)$. Therefore the latter term is neglected. The second term on the right-hand side of Eq.(3.66) is related to the heat transfer by dispersion. How it is related will be shown in the following.

$$\frac{\partial \underline{\dot{h}}_{j,f}}{\partial z} = \sum_{i=1}^{N_i} j_{f,i} \frac{\partial h_{f,i}}{\partial z} + \sum_{i=1}^{N_i} h_{f,i} \frac{\partial j_{f,i}}{\partial z} \quad . \tag{3.67}$$

In analogy to Eq. (3.65) and with Eq. (3.16) this means:

$$\frac{\partial}{\partial z}\left(-\Lambda_z \frac{\partial T_f}{\partial z}\right) = \sum_{i=1}^{N_i} j_{f,i}\, c_{p,i} \frac{\partial T_f}{\partial z} + \sum_{i=1}^{N_i} h_{f,i} \frac{\partial j_{f,i}}{\partial z} \quad . \tag{3.68}$$

From Eq. (3.16) it follows:

$$\sum_{i=1}^{N_i} j_{f,i}\, c_{p,i} \frac{\partial T_f}{\partial z} = \frac{\partial}{\partial z}\left(-\Lambda_z \frac{\partial T_f}{\partial z}\right) - \sum_{i=1}^{N_i} h_{f,i} \frac{\partial j_{f,i}}{\partial z} \quad . \tag{3.69}$$

The very last term is usually neglected, which will also be done here. In fact, it seems worth investigating, under which conditions this term may have significant influence. However, this is not in the scope of this study.

The forth term on the right-hand side of Eq.(3.66) represents the enthalpy change due to homogeneous reactions. In order to use the reaction enthalpy $\Delta_R \tilde{H}_k$ of reaction k some further transformations are required. If N_r homogeneous reactions do occur, then:

$$\begin{aligned}\sum_{i=1}^{N_i} h_{f,i}\, \dot{r}_{f,i} &= \sum_{i=1}^{N_i} \tilde{h}_{f,i}\, \tilde{\dot{r}}_{f,i} = \sum_{i=1}^{N_i} \tilde{h}_{f,i} \left[\sum_{k=1}^{N_r} \nu_{i,k}\, \tilde{\dot{r}}_k\right] \\ &= \sum_{k=1}^{N_r} \left(\sum_{i=1}^{N_i} \nu_{i,k}\, \tilde{h}_{f,i}\right) \tilde{\dot{r}}_k = \sum_{k=1}^{N_r} \left(\Delta_R \tilde{H}_k\right) \tilde{\dot{r}}_k \quad .\end{aligned} \tag{3.70}$$

Hence, the differential equation for the temperature reads:

$$\begin{aligned}\varrho_f\, c_{p,f}\frac{\partial T_f}{\partial t} =& -\varrho_f\, c_{p,f}\, w\frac{\partial T_f}{\partial z} + \frac{\partial}{\partial z}\left(\Lambda_z\frac{\partial T_f}{\partial z}\right) + \\ & - \alpha_W\frac{2}{\varepsilon_f\, R}\left(T_f - T_W\right) - \sum_{k=1}^{N_r}\left(\Delta_R\tilde{H}_k\right)\tilde{\dot{r}}_k + \\ & - s\,\frac{1-\varepsilon_f}{\varepsilon_f}\left[\sum_{i=1}^{N_i}\varrho''_{f,i}\, c''_{p,i}\, v''_i\,(T_f - T''_s) - \dot{q}''_{s,\lambda}\right] \quad .\end{aligned} \tag{3.71}$$

Diffusion can be neglected For the sake of brevity the following quantity is introduced:

$$\dot{c}''_{p,s} \equiv \sum_{i=1}^{N_i}\varrho''_{f,i}\, c''_{p,i}\, v''_i \quad . \tag{3.72}$$

Heterogeneous heat transfer by conduction can be described by means of a heat transfer coefficient α''. In analogy to the mass transfer also α'' has to be corrected if not only conduction but also convection occurs simultaneously. In case of heat transfer the correction factor ζ_h can be estimated by [24]:

$$\zeta_h = \frac{\dot{c}_{p,s}/\alpha''}{\exp(\dot{c}_{p,s}/\alpha'') - 1} \quad . \tag{3.73}$$

This leads to the final form of the energy balance as it is used in this study:

$$\begin{aligned}\varrho_f\, c_{p,f}\frac{\partial T_f}{\partial t} =& -\varrho_f\, c_{p,f}\, w\frac{\partial T_f}{\partial z} + \frac{\partial}{\partial z}\left(\Lambda_z\frac{\partial T_f}{\partial z}\right) + \\ & - \alpha_W\frac{2}{\varepsilon_f\, R}\left(T_f - T_W\right) - \sum_{k=1}^{N_r}\left(\Delta_R\tilde{H}_k\right)\tilde{\dot{r}}_k + \\ & - s\,\frac{1-\varepsilon_f}{\varepsilon_f}\left[\left(\dot{c}''_{p,s} + \zeta_h\,\alpha''\right)\left(T_f - T''_s\right)\right] \quad .\end{aligned} \tag{3.74}$$

The major difference between RPM and quasi-continuous heterogeneous models is the quantity denoted with $\dot{c}''_{p,s}$ (Eq. (3.72)). Another difference is the necessity to consider the Stefan-correction (as in the species mass balance, Eq. (3.32)).

3.2 Inter-particle heat and mass transfer

As has already been mentioned at the beginning of this chapter, the integration of an intra-particle model into a RPM requires - in principle - modifications of the sub-model in two respects: inter-particle heat and mass transfer. In the available single-particle models these phenomena are not included since only a single particle is modeled which is surrounded by a fluid. In a fixed bed, however, the particles do not only interact with the interstitial fluid but also with neighbour particles. The latter interactions have to be modeled as well, if the intra-particle model is to be integrated into a RPM.

In Subsection 3.2.1 it will be outlined how inter-particle heat transfer within RPM framework has been modeled in previous studies. The shortcomings of these attempts lead to the new method which will be suggested in Subsection 3.2.2.

3.2.1 Previous solutions

Modeling heat transfer between neighbour particles within the RPM framework has been done in different ways:

Wurzenberger et al. [19] as well as Bauer [20] introduced Fourier-type terms to describe heat transfer between neighbour particles. In both cases effective conductivities were used. The effective conductivity not only implies radiation and conduction through the contact areas but also conduction within the solid particle (please refer to [11] or [13] for detailed description). The latter is already accounted for by the intra-particle model. In general, the concept of effective conductivities is applicable only to quasi-continuous models and, hence, not to DPM and RPM, respectively.

Chejne et al. [26] presented a model that treats the solid phase as both continuous and discrete, i.e.: a transient one-dimensional heat balance of the quasi-continuous solid along the reactor axis is solved along with transient one-dimensional heat balances of representative particles at each node. While radiation is neglected, conduction between neighbour particles is considered in the quasi-continuous heat balance of the solid phase only, but not in the intraparticle model. It is doubtful that this model is a realistic representation of reality since it is questionable to deal with two temperature fields for one phase.

Sheikholeslami and Watkinson [16], Handley and Heggs [18] as well as Steele et al. [17] did not consider interparticle heat transfer at all in their RPM approaches.

This short review illustrates that the inter-particle heat transfer within the representative particle approach has not been described in a consistent manner so far.

The reason for applying a Fourier-type term (as in [19] and [20]) might be a misleading understanding of the process that has to be described: If $\dot{Q}_{sj}$ is interpreted as (a)

the heat transfer between two representative particles on neighbour gridpoints of the grid representing the reactor, one might come up with the idea to apply the effective conductivity approach. But $\dot{Q}_{sj}$ can only be interpreted as (b) the heat transfer between a representative particle and its (contacting) neighbour particle. The consequence of these different interpretations is that in case (b) only the heat transfer between the surfaces of two contacting particles is relevant, while in case (a) also intra-particle conduction is included. The latter would be inconsistent, since the conduction within a particle is already described by the inter-particle model.

3.2.2 The new method

The inter-particle heat transfer appears in the outer boundary condition of the intra-particle model, which reads:

$$-S\,\lambda_s''\left(\frac{\partial T_s}{\partial r}\right)'' = S\,\alpha''\left(T_s'' - T_f\right) + \sum_j^{N_j} \dot{Q}_{sj} \quad . \tag{3.75}$$

This means that all energy coming from the inside of the particle to the external surface is either transferred to the surrounding fluid or to neighbour particles (or vice versa).

According to Slavin et al. [11] there are four distinct modes of heat transfer between the surfaces of two contacting particles: radiation ($\dot{Q}_r$), gaseous conduction in an inner ($\dot{Q}_i$) and an outer ($\dot{Q}_o$) region, and solid conduction through the contact ($\dot{Q}_c$). Expressing the heat transfer between two contacting hemispheres with surface temperatures T_s and T_j, respectively, in terms of conductances (G) yields:

$$\dot{Q}_{sj} = \dot{Q}_r + \dot{Q}_i + \dot{Q}_o + \dot{Q}_c \quad , \tag{3.76}$$

$$\dot{Q}_{sj} = \Big(G_r + G_i + G_o + G_c\Big)\Big(T_s'' - T_j''\Big) \quad . \tag{3.77}$$

For determination of the different conductances the reader is referred to [11].

The representative particle at axial position k in a one-dimensional reactor is in contact with neighour particles in upstream (u) and downstream (d) directions, i.e.:

$$-S\,\lambda_{s,k}''\left(\frac{\partial T_{s,k}}{\partial r}\right)'' = S\,\alpha''\left(T_k'' - T_{f,k}\right) + G_u\left(T_k'' - T_u''\right) + G_d\left(T_k'' - T_d''\right) \quad . \tag{3.78}$$

It is worth noting that T_u'' (T_d'') is not the surface temperature of the next representative particle in upstream (downstream) direction, which would be T_{k-1}'' (T_{k+1}''). Instead, T_u'' (T_d'') is the surface temperature of a representative neighbour particle in upstream (downstream) direction which can be determined by interpolation between two axial gridpoints (i.e. between two representative particles).

For comparison the method as suggested by Wurzenberger et al. [19] and Bauer [20]) is shown below:

$$
\begin{aligned}
-S\,\lambda''_{s,k}\left(\frac{\partial T_{s,k}}{\partial r}\right)'' = \quad & S\,\alpha''\left(T''_k - T_{f,k}\right) + \\
& + \left(\frac{\pi}{4}d_s^2\right)\lambda_{\text{eff}}\,\frac{T''_k - T''_{k-1}}{\Delta z} + \left(\frac{\pi}{4}d_s^2\right)\lambda_{\text{eff}}\,\frac{T''_k - T''_{k+1}}{\Delta z} \quad .
\end{aligned}
\tag{3.79}
$$

The difference of the two methods can be made clear if one assumes that the cylindrical finite volume elements have a length which is equal to the diameter of the representative particle. In this case $T''_{k+1} = T''_d$ and $T''_{k-1} = T''_u$, i.e. two representative particles in neighbouring finite cells are also representative neighbour particles because they are in contact with each other. In this case it is necessary to determine the heat transfer between two contacting spheres. The heat transfer within the spheres is irrelevant. But by applying the effective conductivity one also considers intra-particle heat transfer. This is already accounted for by the intra-particle model.

Thus, for the heat transfer between contacting particles the relation in Eq. (3.78) will be applied in this study. This relation offers a possibility to improve the mathematical description of transient heat transfer in heterogeneous media (such as a fixed bed with stagnant flow). This problem will be investigated in the next chapter.

For the analogue phenomenon of inter-particle mass transfer between neighbour particles no model has been proposed so far. This is most probably due to the negligible impact of this phenomenon. It will, thus, neither be considered in this work.

Chapter 4

Transient heat transfer in packed beds - relevance of the history term

4.1 Introduction

A remarkable fact is that transient heat transfer in heterogeneous media (and, thus, also in packed beds with stagnant flow) can not be described reliably by existing models. All of these models, which will be described in Section 4.2, have in common that they are based on the quasi-continuous approach. Neither the DPM nor the RPM has been applied to investigate that phenomenon.

In several previous studies the transient heat transfer from (or to) a rigid sphere situated in a fluid of infinite extension has been examined [27–31]. It was shown by different derivations that a history term has to be considered in the transient energy balance of the particle. So far no study has been conducted examining the significance of the history term in case of transient heat transfer in packed beds with stagnant flow. If the history term plays a role, then the RPM will be the appropriate way to model that phenomenon because it is much more difficult to integrate the history term into quasi-continuous models than into a RPM.

Therefore, the objective of this section is to examine if the neglection of the history term is the reason for the shortcomings in current models for transient heat transfer in heterogeneous media. To do that, the history term has to be derived for particles in packed beds, which will be done in Section 4.3. In the subsequent Section 4.4 it will be examined if the result is consistent with previous derivations of the history term. After that the significance of the history term for heat transfer in packed beds is investigated (Section 4.5), followed by a short discussion and conclusion.

4.2 Models for transient heat transfer in heterogeneous media

The parabolic heat conduction equation (Eq. (4.1)) in conjunction with an effective heat conductivity (λ_{eff}) is most commonly used for heat transfer in packed beds.

$$\vec{q}\,(\vec{r},t) = -\lambda_{\text{eff}}\,\nabla T(\vec{r},t) \quad . \tag{4.1}$$

Several semi-empirical relations for λ_{eff} exist [11, 12] and have been applied successfully to steady-state processes. However, it was observed in various experiments [32–36] that this model fails to describe transient heat transfer in heterogeneous media. A prerequisite for the validity of the parabolic equation is local thermal equilibrium, i.e. the temperatures of the fluid and solid phase are equal in every differential volume element. To account for local thermal non-equilibrium in transient heat transfer, the dual phase lag (DPL) model was proposed [37]. It was suggested that Eq. (4.1) needs to be modified as follows:

$$\vec{q}\,(\vec{r},t+\tau_q) = -\lambda_{\text{eff}}\,\nabla T(\vec{r},t+\tau_T) \quad . \tag{4.2}$$

τ_q and τ_T are referred to as lag times for heat flux and temperature gradient, respectively. Expanding $\vec{q}$ and ∇T in Taylor series, where the terms of higher than first order are neglected, yields:

$$\vec{q}\,(\vec{r},t) + \tau_q \frac{\partial \vec{q}\,(\vec{r},t)}{\partial t} = -\lambda_{\text{eff}} \left(\nabla T(\vec{r},t) + \tau_T \frac{\partial \nabla T(\vec{r},t)}{\partial t} \right) \quad . \tag{4.3}$$

Experimental studies [32,34] demonstrated that the heat transfer equation according to the DPL model (Eq. (4.3)) is better suited for transient heat transfer in heterogeneous media than Fourier's law (Eq. (4.1)). But the evaluation of the lag times is still a matter of discussion. In a very recent study [38] it was theoretically predicted that $\tau_T > \tau_q$. According to Eq. (4.2) this means that the heat flux depends on a temperature gradient of the future. This raises the question if the principle of causality is violated if $\tau_T > \tau_q$ holds. Fitting of experimental data resulted in the opposite conclusion [34, 39]. Furthermore it has been found by experiment [32] and by theory [38] that the lag times can be of the order of several 100 seconds. These large values indicate that the neglection of the higher order terms of the Taylor series expansion that was used in the derivation of Eq. (4.3) is not justified, meaning that the DPL model is not adequate. Hence, it is to be expected that at large values of the lag times τ_q or τ_T Eq. (4.3) does not hold.

In many studies $\tau_T = 0$ is adopted, resulting in the hyperbolic heat transfer equation:

$$\vec{q}\,(\vec{r},t) + \tau_q\, \frac{\partial \vec{q}\,(\vec{r},t)}{\partial t} = -\lambda_{\text{eff}}\,\nabla T(\vec{r},t) \quad . \tag{4.4}$$

Equation (4.4) is often referred to as Cattaneo-Vernotte [40, 41] equation. It has also been successfully applied to various transient heat transfer processes in heterogeneous

media [33,35,36]. But the experimental data to which the Cattaneo-Vernotte equation were applied, have been questioned seriously [42, 43]. The order of magnitude of the lag time τ_q (also often referred to as relaxation time) is also a matter of controversy, as has been pointed out by Roetzel et al. [33].

In light of these considerations it can be concluded that the parabolic equation (Eq. (4.1)) can not be applied universally for transient heat transfer in heterogeneous media, but the establishment of a model that reliably predicts transient heat transfer remains a task for the scientific community. Both the hyperbolic (4.4) and the DPL model (Eq. (4.3)) can not be applied reliably.

One major shortcoming of the parabolic heat transfer equation (Eq. (4.1)) is that the commonly used relations for the effective thermal conductivity λ_{eff} only apply to steady state heat transfer in heterogeneous media [24]. Most empirical and theoretical correlations for heat transfer coefficients are also only valid for steady state. If they are applied to transient heat transfer, an error will be introduced. It will be shown in this study that the history term is a means to correct this error. An analog error is introduced by applying λ_{eff} to transient heat transfer in heterogeneous media. Thus, it seems possible that this error can be corrected by a history term as well. If the history term has a significant impact, then the fact that the parabolic equation (Eq. (4.1)) fails to describe transient heat transfer in heterogeneous media may be due to the neglection of the correction/history term.

4.3 Derivation of the history term for a particle in a packed bed

So far the history term was only derived for a dilute suspension of particles. That is: the distances between neighbour particles are so large that interaction between them can be neglected. In a monodisperse packed bed a spherical particle is in contact with an average of six neighbour particles [44]. The zone between two contacting spherical particles is depicted in Fig. 4.1.

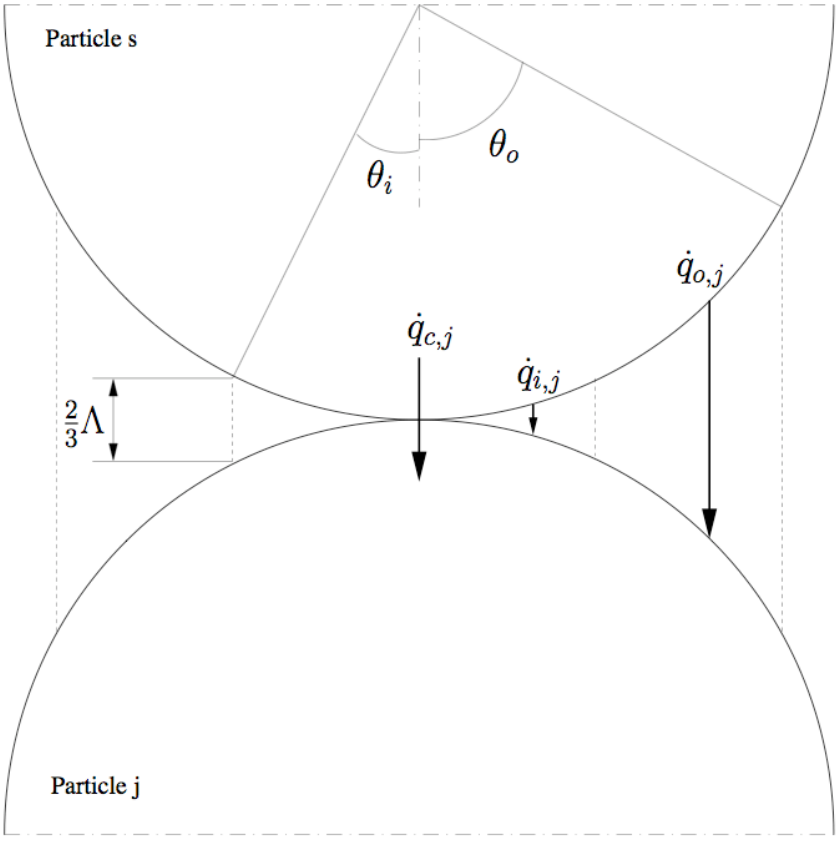

Figure 4.1: *Zone between two contacting spheres*

The fluid in the interstitial region is assumed to be stagnant. It is furthermore assumed that the temperature in the solid particles is homogeneous (but not constant in time). This assumption is justified by the fact that the heat conductivities of solids are several orders of magnitude larger than those of gases. For metals this assumption also holds in combination with liquids.

There are in principle three different ways of heat transfer between the surfaces of two contacting particles in a stagnant fluid: radiation ($\dot{q}_r$), conduction through the fluid, and conduction through the contact area ($\dot{q}_c$). Slavin et al. [11] pointed out that the conduction through the fluid can be further categorized: In a region where the gap between the two spheres is less than two third of the molecular mean free path (Ω) it is more likely for a molecule to collide with the surface than with another molecule. The heat transfer within this inner region is referred to as $\dot{q}_i$. In an outer region, where the gap is $> (2/3)\,\Omega$, heat transfer occurs by "usual" conduction ($\dot{q}_o$).

Thus, the energy balance of a particle with homogeneous temperature in a packed bed without heat source/sink reads:

$$\varrho_s c_{p,s} V_s \frac{\mathrm{d}T_s}{\mathrm{d}t} = -\sum_{j=1}^{6} \left(\int\limits_{A_{c,j}} \vec{\dot{q}}_{c,j} \, \mathrm{d}\vec{A} + \int\limits_{A_{i,j}} \vec{\dot{q}}_{i,j} \, \mathrm{d}\vec{A} + \int\limits_{A_{o,j}} \vec{\dot{q}}_{o,j} \, \mathrm{d}\vec{A} + \int\limits_{A_{r,j}} \vec{\dot{q}}_{r,j} \, \mathrm{d}\vec{A} \right) \quad . \tag{4.5}$$

Here j is the index for one of the six neighbour particles. $A_{c,j}$, $A_{i,j}$, $A_{o,j}$, and $A_{r,j}$ are the areas of the particle surface through which $\dot{q}_{c,j}$, $\dot{q}_{i,j}$, $\dot{q}_{o,j}$, and $\dot{q}_{r,j}$ are transferred, respectively. The boundary of the inner contact region $A_{i,j}$ is given by θ_i (see Fig. 4.1). According to Slavin et al. [11]:

$$\begin{aligned} \theta_i &= \frac{(2/3)\,\Omega - 2h}{r_s^2} \qquad \text{if} \qquad \frac{2}{3}\,\Omega > 2h \quad , \\ \theta_i &= 0 \qquad\qquad \text{if} \qquad \frac{2}{3}\,\Omega \leqslant 2h \quad . \end{aligned} \tag{4.6}$$

Here, h is the roughness of the particle surface. Angle θ_o, the outer boundary for $A_{o,j}$, can only be roughly estimated to be 60°.

In a first study Slavin et al. [45] concluded that the conductance across the particle-particle contact was negligible except under conditions of low gas pressures. In a second study [11] they also showed that at gas pressures above 0.048 bar and at temperatures between 300 and 900 K the heat conduction in the outer fluid region $\dot{q}_o$ dominates all other modes of heat transfer between contacting spheres. Thus, if no heat sink/source is present, then the energy balance of the particle reduces to:

$$\varrho_s c_{p,s} V_s \frac{\mathrm{d}T_s}{\mathrm{d}t} = -\sum_{j=1}^{6} \int\limits_{A_{o,j}} \vec{\dot{q}}_{o,j} \, \mathrm{d}\vec{A} = \sum_{j=1}^{6} \int\limits_{A_{o,j}} \left(\lambda_{f,j} \nabla T_{f,j}\right) \mathrm{d}A \quad . \tag{4.7}$$

That is: the energy of the particle is altered only by heat conduction through the fluid (under the conditions stated above). In general $\dot{q}_{o,j}$ is not distributed homogeneously over $A_{o,j}$. Therefore the integrals in Eq. (4.7) can not be determined analytically. The latter can be made possible if the geometry of the contact region depicted in Fig. 4.1 is modeled as shown in Fig. 4.2.

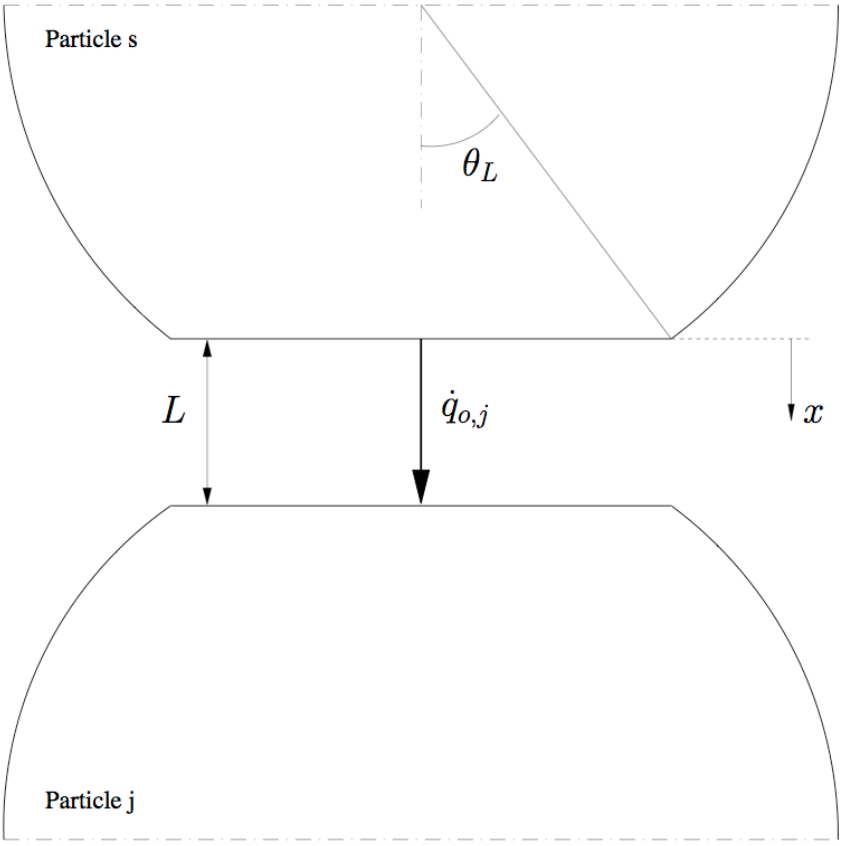

Figure 4.2: *Model for the zone between two contacting spheres*

According to this model the heat transfer between two contacting spheres is represented by one-dimensional heat conduction between two parallel planes. Under the assumption that the fluid temperature between these two parallel planes is only dependent on time and coordinate x (see Fig. 4.2) the energy balance of the particle can be simplified to:

$$\varrho_s c_{p,s} V_s \frac{\mathrm{d}T_s}{\mathrm{d}t} = \sum_{j=1}^{6} \lambda_{f,j} \left(\frac{\partial T_{f,j}(0,t)}{\partial x} \right) A_{o,j} \quad . \tag{4.8}$$

The gradient $(\partial T_{f,j}/\partial x)$ can now be determined analytically which will be outlined in the following.

If the dimensionless responses $y_k^*(t)$ of an output variable $y(t)$ to step changes of various input variables $u_k(t)$ are known, then Duhamel's theorem reads [46]:

$$y(t) = \sum_{k=1}^{n} \left(u_k(0)\; y_k^*(t) + \int_0^t y_k^*(t-\tau) \frac{\mathrm{d}u_k(\tau)}{\mathrm{d}\tau} \mathrm{d}\tau \right) \quad . \tag{4.9}$$

This superposition of several input variables $u_k(t)$ is only possible if the dimensionless responses $y_k^*(t)$ do not depend on the values of $u_{l \neq k}(t)$. It will be demonstrated in the course of this study, that this condition is valid in our case.

The two time-dependent input quantities in our case are the temperatures of the two parallel planes (i.e. the temperatures of two neighbour particles, $T_s(t)$ and $T_j(t)$, respectively). The output quantity of interest here is the temperature field of the fluid $T_{f,j}(x,t)$ between particle s and particle j. If the initial temperature field is homogeneous, i.e. $T_{f,j}(x,0) = T_0$, then Duhamel's theorem reads:

$$T_{f,j}(x,t) - T_0 = \int_0^t T^*_{\Delta s}(x, t-\tau)\frac{\mathrm{d}T_s(\tau)}{\mathrm{d}\tau}\mathrm{d}\tau + \int_0^t T^*_{\Delta j}(x, t-\tau)\frac{\mathrm{d}T_j(\tau)}{\mathrm{d}\tau}\mathrm{d}\tau \quad . \tag{4.10}$$

$T^*_{\Delta s}$ and $T^*_{\Delta j}$ are the dimensionless transient responses of the fluid temperature field to step changes of the temperatures T_s and T_j, respectively. These responses will be analytically derived in the next paragraphs. Equation (4.10) can be further simplified by taking the derivative with respect to x, since we are actually interested in the gradient at the surface of the particle (i.e. at $x = 0$):

$$\frac{\partial T_{f,j}(0,t)}{\partial x} = \int_0^t \left[\left(\frac{\partial T^*_{\Delta s}(0, t-\tau)}{\partial x} \right) \frac{\mathrm{d}T_s(\tau)}{\mathrm{d}\tau} + \left(\frac{\partial T^*_{\Delta j}(0, t-\tau)}{\partial x} \right) \frac{\mathrm{d}T_j(\tau)}{\mathrm{d}\tau} \right] \mathrm{d}\tau \quad . \tag{4.11}$$

Equation (4.11) shows that we have to determine the time-dependent gradients of the dimensionless fluid temperature at $x = 0$ for step changes of T_s and T_j, respectively. This will be done in the following.

The analytical solution for the one-dimensional transient temperature field $T_{f,j}(x,t)$ in a stagnant fluid bounded by two parallel planes is given in [47]. If the temperatures at the two boundaries are kept fixed at $T_{f,j}(0, t > 0) = T_s$ and $T_{f,j}(L, t > 0) = T_j$, respectively, then:

$$\begin{aligned} T_{f,j}(x,t) = {} & T_s + (T_j - T_s)\frac{x}{L} + \dots \\ & + \frac{2}{\pi}\sum_{n=1}^{\infty} \frac{(-1)^n\, T_j - T_s}{n} \sin\frac{n\pi x}{L} \exp\left[-\frac{a_{f,j} n^2 \pi^2 t}{L^2} \right] + \dots \\ & + \frac{2}{L}\sum_{n=1}^{\infty} \sin\frac{n\pi x}{L} \exp\left[-\frac{a_{f,j} n^2 \pi^2 t}{L^2} \right] \int_0^L T(y,0) \sin\frac{n\pi y}{L}\mathrm{d}y \quad . \end{aligned} \tag{4.12}$$

For a homogeneous initial temperature field, i.e.: $T_{f,j}(x,0) = T_0$, the integral on the right-hand side can be evaluated as follows:

$$\int_0^L T_0 \sin\frac{n\pi y}{L}\mathrm{d}y = -\frac{LT_0}{n\pi}\left[\cos\frac{n\pi y}{L} \right]_0^L = -\frac{LT_0}{n\pi}\left[(-1)^n - 1 \right] \quad . \tag{4.13}$$

Hence, the transient temperature field can be rewritten as:

$$\begin{aligned} T_{f,j}(x,t) = {} & T_s + (T_j - T_s)\frac{x}{L} + \dots \\ & + \frac{2}{\pi}\sum_{n=1}^{\infty} \frac{(-1)^n\,(T_j - T_0) - (T_s - T_0)}{n} \sin\frac{n\pi x}{L} \exp\left[-\frac{a_{f,j} n^2 \pi^2 t}{L^2} \right] \quad . \end{aligned} \tag{4.14}$$

A temperature step change at $x = L$ is equivalent to setting $T_s(t > 0) = T_0$. The influence of a change of T_s on the fluid temperature gradient at $x = 0$ will be evaluated seperately (see Eq. (4.18)). The resulting transient temperature at is therefore:

$$T_{\Delta j}(x,t) = T_0 + (T_j - T_0)\left(\frac{x}{L} + \frac{2}{\pi}\sum_{n=1}^{\infty}\frac{(-1)^n}{n}\sin\frac{n\pi x}{L}\exp\left[-\frac{a_{f,j}n^2\pi^2 t}{L^2}\right]\right) \quad . \tag{4.15}$$

The derivative with respect to x is:

$$\frac{\partial T_{\Delta j}(x,t)}{\partial x} = \frac{T_j - T_0}{L}\left(1 + 2\sum_{n=1}^{\infty}(-1)^n\cos\frac{n\pi x}{L}\exp\left[-\frac{a_{f,j}n^2\pi^2 t}{L^2}\right]\right) \quad . \tag{4.16}$$

For the gradient of the dimensionless temperature at $x = 0$ we get:

$$\frac{\partial T^*_{\Delta j}(0,t)}{\partial x} = \frac{1}{T_j - T_0}\frac{\partial T_{\Delta j}(0,t)}{\partial x} = \frac{1}{L}\left(1 + 2\sum_{n=1}^{\infty}(-1)^n\exp\left[-\frac{a_{f,j}n^2\pi^2 t}{L^2}\right]\right) \quad . \tag{4.17}$$

Hence, the second gradient in the integral of Eq. (4.11) is known. The first gradient in that equation can be determined analogously, yielding:

$$\frac{\partial T^*_{\Delta s}(0,t)}{\partial x} = \frac{1}{T_s - T_0}\frac{\partial T_{\Delta s}(0,t)}{\partial x} = -\frac{1}{L}\left(1 + 2\sum_{n=1}^{\infty}\exp\left[-\frac{a_{f,j}n^2\pi^2 t}{L^2}\right]\right) \quad . \tag{4.18}$$

The analytical solutions for the two gradients (Eqs. (4.17) and (4.18)) show that these responses do not depend on either one of the two input parameters T_j and T_s. Therefore Duhamel's theorem - as written in equations (4.10) and (4.11) - can be applied in our case. Substituting the gradients in the integral of Eq. (4.11) with equations (4.17) and (4.18) yields:

$$\begin{aligned}\frac{\partial T_{f,j}(0,t)}{\partial x} = &-\frac{1}{L}\int_0^t\left(1 + 2\sum_{n=1}^{\infty}\exp\left[-\frac{a_{f,j}n^2\pi^2(t-\tau)}{L^2}\right]\right)\frac{\mathrm{d}T_s}{\mathrm{d}\tau}\,\mathrm{d}\tau + \dots \\ &+\frac{1}{L}\int_0^t\left(1 + 2\sum_{n=1}^{\infty}(-1)^n\exp\left[-\frac{a_{f,j}n^2\pi^2(t-\tau)}{L^2}\right]\right)\frac{\mathrm{d}T_j}{\mathrm{d}\tau}\,\mathrm{d}\tau \quad .\end{aligned} \tag{4.19}$$

$$\begin{aligned}\Rightarrow \frac{\partial T_{f,j}(0,t)}{\partial x} = &\frac{T_j - T_s}{L} \\ &+\frac{2}{L}\int_0^t\sum_{n=1}^{\infty}\exp\left[-\frac{a_{f,j}n^2\pi^2(t-\tau)}{L^2}\right]\left((-1)^n\frac{\mathrm{d}T_j}{\mathrm{d}\tau} - \frac{\mathrm{d}T_s}{\mathrm{d}\tau}\right)\mathrm{d}\tau.\end{aligned} \tag{4.20}$$

This result can now be applied to the energy balance of the particle, Eq. (4.8), resulting in:

$$\varrho_s c_{p,s} V_s \frac{\mathrm{d}T_s}{\mathrm{d}t} = \sum_{j=1}^{6} A_{o,j} \lambda_{f,j} \frac{T_j - T_s}{L} + \ldots + \sum_{j=1}^{6} A_{o,j} \frac{2\lambda_{f,j}}{L} \int_0^t \sum_{n=1}^{\infty} \exp\left[-\frac{a_{f,j} n^2 \pi^2 (t-\tau)}{L^2} \right] \left((-1)^n \frac{\mathrm{d}T_j}{\mathrm{d}\tau} - \frac{\mathrm{d}T_s}{\mathrm{d}\tau} \right) \mathrm{d}\tau. \tag{4.21}$$

For the sake of brevity the second term on the right-hand side of Eq. (4.21) will be referred to as f_{HT} in the following. It is, again, to be noted that this equation only holds for a particle in a packed bed with stagnant fluid with $\lambda_s \gg \lambda_f$ and negligible radiation.

For a physical interpretation of the history term let us at first focus on the first term on the right-hand side of Eq. (4.21). This term describes the heat flow through $A_{o,j}$ if the fluid temperature fields are at steady state. The ratio $\lambda_{f,j}/L$ is equal to the heat transfer coefficient. If this relation for steady state heat transfer between two parallel planes is applied to transient heat transfer as well, then an error will be introduced. This error is corrected by means of the history term. Therefore, f_{HT} can be regarded as a correction term.

4.4 The case of a dilute suspension

The major difference between the derivation presented in this study and the derivations in previous studies [28, 30, 31] is that the latter considered infinite geometry. In other words: the fluid surrounding the particle was of infinite dimension ($r \to \infty$). The history term as derived in those studies included the time derivative of the temperature which the fluid would have if the particle was not present. This is an artificial quantity and, thus, not measurable. In the derivation presented in Section 4.3 a fluid of finite dimension (length L in Fig. 4.2) was considered. No artificial quantities are included in the relation for the history term, only measurable ones (see Eq. (4.21)).

The history term derived for finite dimension should comply with the relation derived in [28, 30, 31]. In order to investigate this, a geometry as depicted in Fig. 4.3 will be considered in the following. A spherical particle is surrounded by a stagnant fluid, which has the shape of a hollow sphere with inner radius r_s and outer radius r_h.

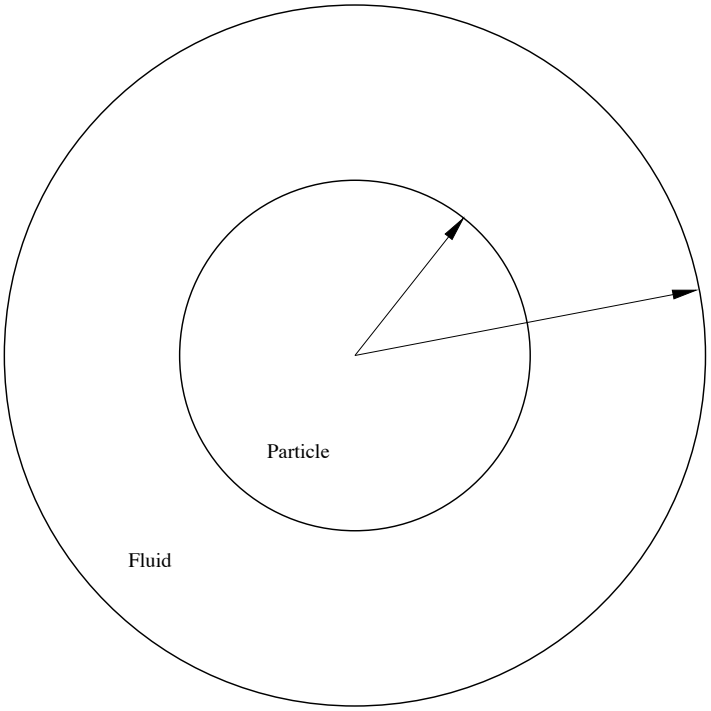

Figure 4.3: *Geometry of a hollow sphere with outer radius r_h and inner radius r_s*

If the same procedure as in section 4.3 is applied, the following form of the particle's energy balance can be derived:

$$\begin{aligned}\varrho_s c_{p,s} V_s \frac{dT_s}{dt} &= \frac{A_s \lambda_f (T_h - T_s)}{r_s (1 - r_s/r_h)} + \dots \\ &+ \frac{2A_s \lambda_f}{r_h - r_s} \int_0^t \sum_{n=1}^{\infty} \exp\left[-\frac{a_f n^2 \pi^2 (t-\tau)}{(r_h - r_s)^2} \right] \left((-1)^n \frac{r_h}{r_s} \frac{dT_h}{d\tau} - \frac{dT_s}{d\tau} \right) d\tau \quad .\end{aligned} \tag{4.22}$$

The second term on the right-hand side of Eq. (4.22) is the history term derived for finite geometry. Infinite geometry corresponds to $r_h \gg r_s$. In this case T_h is equivalent to the fluid's temperature at large distance from the particle ($T_{f,\infty}$). Hence, for infinite geometry Eq. (4.22) can be written as:

$$\begin{aligned}\varrho_s c_{p,s} V_s \frac{\mathrm{d}T_s}{\mathrm{d}t} &= A_s \frac{\lambda_f}{r_s} (T_{f,\infty} - T_s) + \dots \\ &+ \frac{2A_s \lambda_f}{r_h} \int_0^t \sum_{n=1}^{\infty} \exp\left[-\frac{a_{f,j} n^2 \pi^2 (t-\tau)}{r_h^2} \right] \left((-1)^n \frac{r_h}{r_s} \frac{\mathrm{d}T_{f,\infty}}{\mathrm{d}\tau} - \frac{\mathrm{d}T_s}{\mathrm{d}\tau} \right) \mathrm{d}\tau \quad .\end{aligned} \tag{4.23}$$

Let us now focus on the history term in Eq. (4.23) , which will be referred to as f_{HT} in the following. It is:

$$f_{HT} = \frac{2A_s \lambda_f}{r_h} \left[\frac{r_h}{r_s} \int_0^t \sum_{n=1}^{\infty} (-1)^n \exp\left[-C^2 n^2\right] \frac{\mathrm{d}T_{f,\infty}}{\mathrm{d}\tau} \mathrm{d}\tau - \int_0^t \sum_{n=1}^{\infty} \exp\left[-C^2 n^2\right] \frac{\mathrm{d}T_s}{\mathrm{d}\tau} \mathrm{d}\tau \right], \tag{4.24}$$

with

$$C \equiv \frac{\pi\sqrt{a_f(t-\tau)}}{r_h} \quad . \tag{4.25}$$

For $r_h \gg r_s$ (i.e. very small C) the second sum in (4.24) can be approximated as an integral:

$$\sum_{n=1}^{\infty} \exp\left[-C^2 n^2\right] = \int_0^{\infty} \exp\left[-C^2 x^2\right] \mathrm{d}x = \frac{\sqrt{\pi}}{2\,C} = \frac{r_h}{2\sqrt{\pi a_f(t-\tau)}} \quad . \tag{4.26}$$

The first sum in (4.24) can be transformed as follows:

$$\sum_{n=1}^{\infty} (-1)^n \exp\left[-C^2 n^2\right] = \sum_{n=1}^{\infty} \Big(\exp\left[-C^2 (2n)^2\right] - \exp\left[-C^2 (2n-1)^2\right] \Big) \quad . \tag{4.27}$$

Again, for $r_h \gg r_s$ these sums can be approximated as integrals, thus:

$$\begin{aligned} \sum_{n=1}^{\infty} (-1)^n \exp\left[-C^2 n^2\right] &= \int_0^{\infty} \exp\left[-(2C)^2 x^2\right] \mathrm{d}x - \int_0^{\infty} \exp\left[-(2C)^2 (x-\frac{1}{2})^2\right] \mathrm{d}x \\ &= \int_0^{\infty} \exp\left[-(2C)^2 x^2\right] \mathrm{d}x - \int_{-1/2}^{\infty} \exp\left[-(2C)^2 x^2\right] \mathrm{d}x \\ &= -\int_{-1/2}^{0} \exp\left[-(2C)^2 x^2\right] \mathrm{d}x \quad = \quad \frac{1}{2} \quad . \end{aligned} \tag{4.28}$$

Substituting the two sums in the history term (4.24) with the relations (4.26) and (4.28) yields:

$$f_{HT} = A_s \lambda_f \int_0^t \left[\frac{1}{r_s} \frac{\mathrm{d}T_{f,\infty}}{\mathrm{d}\tau} - \frac{1}{\sqrt{\pi a_f}} \frac{1}{\sqrt{t-\tau}} \frac{\mathrm{d}T_s}{\mathrm{d}\tau} \right] \mathrm{d}\tau \quad . \tag{4.29}$$

Hence, the energy balance of the particle (4.23) can be modified to give:

$$\varrho_s c_{p,s} V_s \frac{\mathrm{d}T_s}{\mathrm{d}t} = A_s \frac{2\lambda_f}{d_s} (T_{f,\infty} - T_s) + \frac{A_s \lambda_f}{\sqrt{\pi a_f}} \int_0^t \left[\frac{\sqrt{\pi a_f}}{r_s} \frac{\mathrm{d}T_{f,\infty}}{\mathrm{d}\tau} - \frac{1}{\sqrt{t-\tau}} \frac{\mathrm{d}T_s}{\mathrm{d}\tau} \right] \mathrm{d}\tau. \tag{4.30}$$

This form of the particle's energy balance should be compared to the energy balance as derived by Coimbra and Rangel [28]. The latter is printed below:

$$\varrho_s c_{p,s} V_s \frac{\mathrm{d}T_s}{\mathrm{d}t} = A_s \frac{2\lambda_f}{d_s} (\tilde{T}_f - T_s) + \frac{A_s \lambda_f}{\sqrt{\pi a_f}} \int_0^t \left[\frac{1}{\sqrt{t-\tau}} \left(\frac{\mathrm{d}\tilde{T}_f}{\mathrm{d}\tau} - \frac{\mathrm{d}T_s}{\mathrm{d}\tau} \right) \right] \mathrm{d}\tau + \varrho_f c_{p,f} V_s \frac{\mathrm{d}\tilde{T}_f}{\mathrm{d}t}. \tag{4.31}$$

The terms containing the particle temperature T_s are equal in both (4.30) and (4.31). The temperature $\tilde{T}_f$ in Eq. (4.31) is the (artificial) homogeneous temperature that

the fluid would have if the particle was not present, while temperature $T_{f,\infty}$ is the (measurable) fluid temperature at r_h ($\gg r_s$). In other words: $\tilde{T}_f$ has a different physical meaning than $T_{f,\infty}$. Therefore it is clear that the terms containing these temperatures are different in the two energy balances.

Thus, it can be concluded that the results of the two derivations are consistent.

4.5 Significance of the history term for a particle in a packed bed

In order to examine the significance of the history term of a particle in a packed bed let us consider a thought experiment with a setup as depicted in Fig. 4.4.

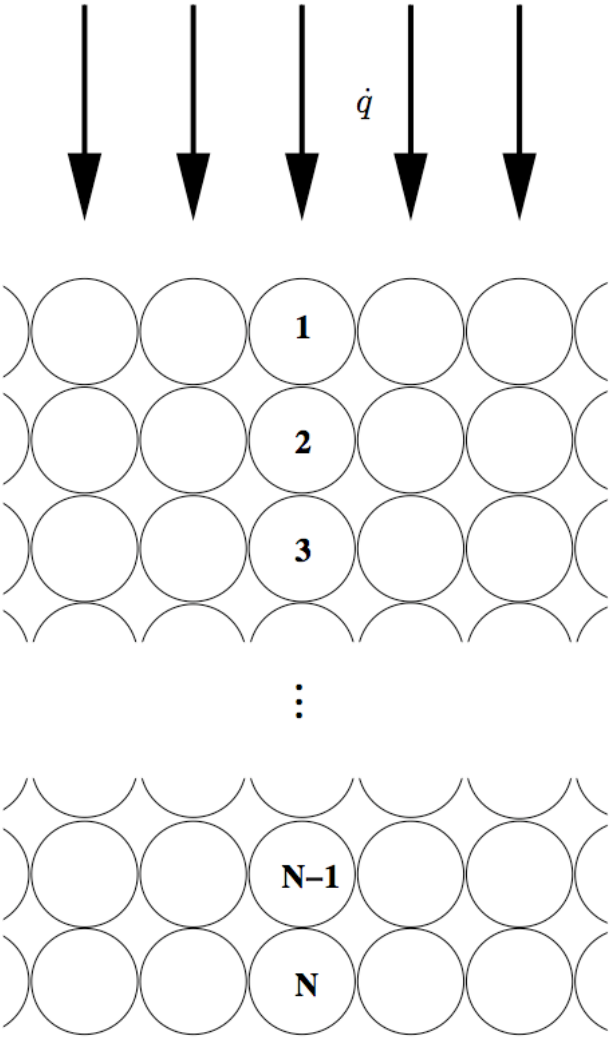

Figure 4.4: *Setup of the thought experiment*

A cluster containing N particle layers and with homogeneous initial temperature T_0 is subjected to a constant heat flux $\dot{q}$. The heat transfer occurs one-dimensionally,

i.e. perpendicular to the cluster surface. In this case only two of the six neighbours of a particle in the bulk are relevant. The temperature of the N-th particle layer at the bottom is held constant at T_0. The properties (ϱ, c_p, λ) of both fluid and solid are assumed to be constant. As stated above, the temperature of each particle is homogeneous, which is equivalent to the assumtion that $\lambda_s \to \infty$.

Under these conditions and by use of dimensionless variables defined by:

$$t^* \equiv \frac{a_f t}{d_s^2} \tag{4.32}$$

and

$$T^* \equiv \frac{(T_{1,\infty} - T)}{(T_{1,\infty} - T_0)} \tag{4.33}$$

the energy balance of a particle i (Eq. 4.21) having two neighbours can be transformed into:

$$\begin{aligned} \frac{2}{3\chi(2-\gamma)} \frac{\mathrm{d}T_i^*}{\mathrm{d}t^*} = \; & (T_{i-1}^* - T_i^*) + (T_{i+1}^* - T_i^*) + \ldots \\ & + 2 \int_0^{t^*} \sum_{n=1}^{\infty} \exp\left[-\left(\frac{n\pi}{\gamma}\right)^2 (t^* - \tau^*) \right] \left((-1)^n \frac{\mathrm{d}T_{i-1}^*}{\mathrm{d}\tau^*} - \frac{\mathrm{d}T_i^*}{\mathrm{d}\tau^*} \right) \mathrm{d}\tau^* \\ & + 2 \int_0^{t^*} \sum_{n=1}^{\infty} \exp\left[-\left(\frac{n\pi}{\gamma}\right)^2 (t^* - \tau^*) \right] \left((-1)^n \frac{\mathrm{d}T_{i+1}^*}{\mathrm{d}\tau^*} - \frac{\mathrm{d}T_i^*}{\mathrm{d}\tau^*} \right) \mathrm{d}\tau^*, \end{aligned} \tag{4.34}$$

with $\chi \equiv c_{p,f}/c_{p,s}$, $V_s = \pi d_s^3/6$, $\gamma \equiv L/d_s$, and thus $A_o = \gamma(2-\gamma)\pi d_s^2/4$.

The dimensionless energy balance of a particle in the topmost layer reads:

$$\begin{aligned} \frac{2}{3\chi(2-\gamma)} \frac{\mathrm{d}T_1^*}{\mathrm{d}t^*} = \; & (T_2^* - T_1^*) + \frac{1}{N-1} + \ldots \\ & + 2 \int_0^{t^*} \sum_{n=1}^{\infty} \exp\left[-\left(\frac{n\pi}{\gamma}\right)^2 (t^* - \tau^*) \right] \left((-1)^n \frac{\mathrm{d}T_2^*}{\mathrm{d}\tau^*} - \frac{\mathrm{d}T_1^*}{\mathrm{d}\tau^*} \right) \mathrm{d}\tau^*, \end{aligned} \tag{4.35}$$

whereas the temperature of the particles at the bottom is held constant, i.e.:

$$\frac{dT_N^*}{dt^*} = 0 \quad . \tag{4.36}$$

For the derivation of the second term on the right-hand side of Eq. (4.35) the reader is referred to Appendix A.

The system of N differential equations (Eqs. (4.34)-(4.36)) can now be solved numerically. For this purpose the integrals are approximated by the trapez rule. The LIMEX solver [48–50] is used to integrate the system of differential equations.

It is to be noted that the dimensionless transient temperature field in the cluster does neither depend on $\dot{q}$ nor d_s. Only the impacts of three parameters are to be investigated: γ and N are geometrical parameters of the model whereas the ratio of the volumetric heat capacities χ is the only physical parameter and therefore of special interest.

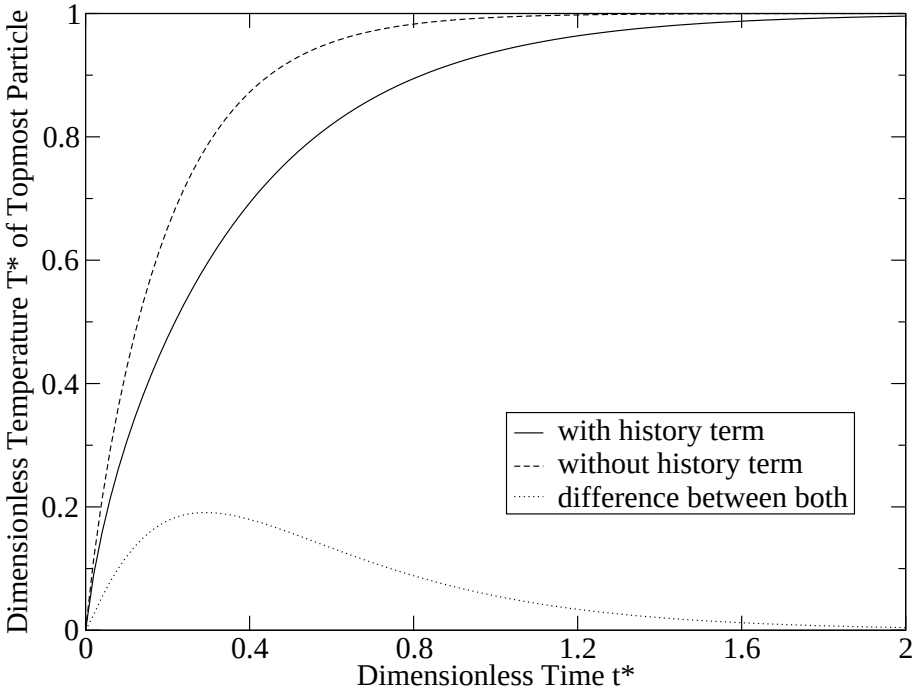

Figure 4.5: *Dimensionless temperature of the topmost particle layer with and without consideration of the history term (N=3 , γ = 0.2 , χ = 1.0)*

In Fig. 4.5 a typical result of the numerical integration is shown. Depicted is the time dependent dimensionless temperature of the particles in the topmost layer of the cluster (see Fig. 4.4). As is to be expected, the history term does not affect the steady-state temperature field. Neglection of the history term leads to an overestimation of the transient temperature. This is due to the fact that the transient heat transfer from particle to fluid is larger than the steady-state heat transfer. The difference in the dimensionless temperature that results from neglection of the history term is also depicted in Fig. 4.5. The impact of the three aforementioned parameters on the dimensionless temperature field can be quantified by the maximum of this difference, which will be referred to as ϑ^* in the following.

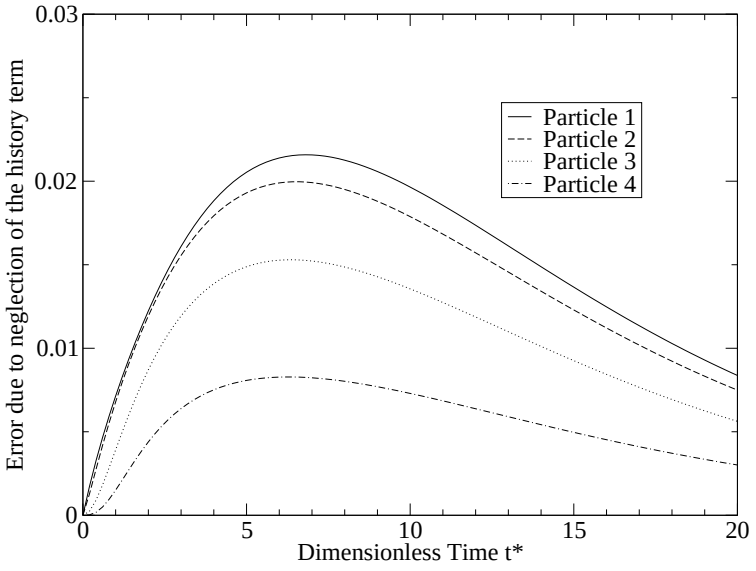

Figure 4.6: *Error in dimensionless temperature due to neglection of the history term for different particles (enumeration according to Fig. 4.4, N=5 , γ = 0.2 , χ = 1.0)*

In Fig. 4.6 the error in dimensionless temperature due to neglection of the history term is plotted as a function of time for several particles (or particle layers) in the cluster. Clearly, ϑ^* (the maximum of this error) of the topmost particle layer is larger than for all subsurface layers. This is due to the way the dimensionless temperature is defined. In the subsequent diagrams, where the impact of the three parameters will be investigated, the maximum value of ϑ^* for the topmost particle layer will be used as a means to quantify the significance of the history term.

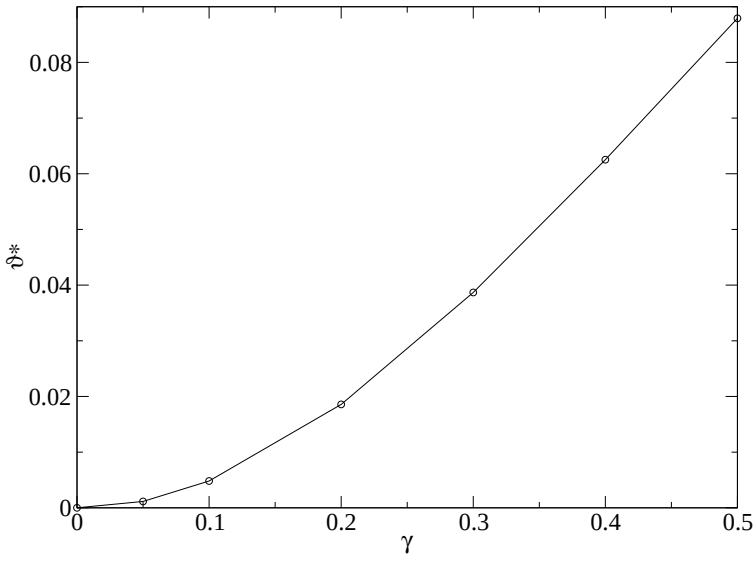

Figure 4.7: *Maximum dimensionless error due to neglection of the history term in dependence of the geometrical parameter γ (N=3 , χ = 1.0)*

The geometric parameter γ represents the ratio L/d_s . This quantity has to be estimated by considering at which distance L the real heat transfer geometry as depicted

in Fig. 4.1 is represented best by the parallel planes model (Fig. 4.2). There are two boundary cases: For $\gamma \to 0$ the temperature field between the almost touching parallel planes will reach steady state quasi instantaneously, which is why the impact of the history term should vanish ($\vartheta^* \to 0$). The largest geometrically meaningful value of γ is 1. In this case ϑ^* should be the largest since it takes the longest time to reach the steady-state temperature field. The numerical results depicted in Fig. 4.7 are in agreement with these considerations. The graph also shows that for $0.1 < \gamma < 0.5$ the order of magnitude of ϑ^* does not change. For examining the significance of the history term it is sufficient to estimate the order of magnitude of ϑ^*. Therefore γ will be set arbitrarily to 0.2 in the following.

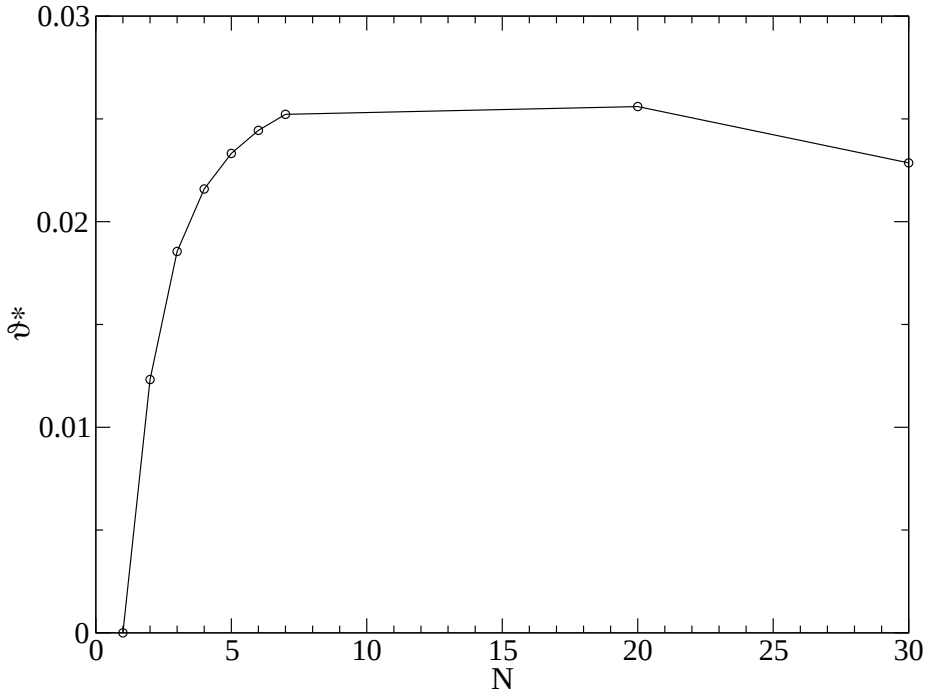

Figure 4.8: *Maximum dimensionless error due to neglection of the history term in dependence of the number of particle layers (γ = 0.2 , χ = 1.0)*

The dependence of ϑ^* on the number of particle layers N is illustrated in Fig. 4.8. For an understanding it is again useful to consider the two border cases: If $N = 1$ then the history term has no impact because the temperature of the particle layer is held constant. Thus $\vartheta^* = 0$. For $N \to \infty$ the denominator in the definition of the dimensionless temperature (Eq. (4.33)) is infinite. The temperature difference due to neglection of the history term is finite. Therefore, $\vartheta^* \to 0$. In light of these considerations it is clear why a vulcano-type behaviour as depicted in Fig. 4.8 can be observed. The main conclusion that can be drawn is that for $1 < N < 30$ the order of magnitude of ϑ^* is independend from N. Therefore N will be set arbitrarily to 3 in the following.

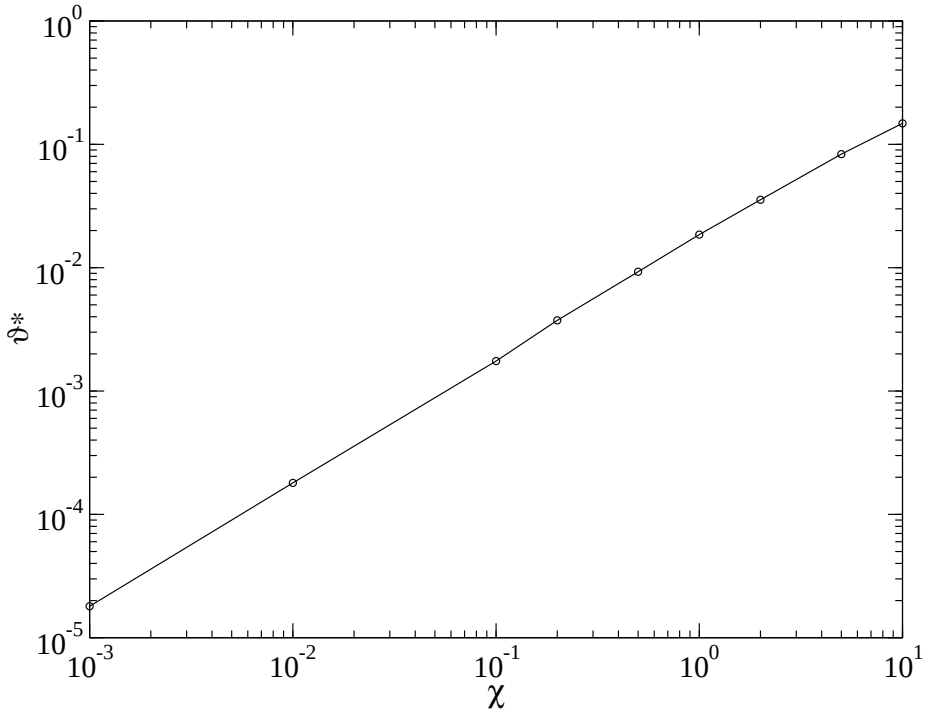

Figure 4.9: *Maximum dimensionless error due to neglection of the history term in dependence of the volumetric heat capacity ratio χ (N=3 , γ = 0.2)*

Having demonstrated that the geometrical parameters γ and N do not change the order of magnitude of ϑ^* it turns out that the physical parameter χ is of fundamental importance as far as the significance of the history term is concernced. The major result of this chapter is depicted in Fig. 4.9. For illustrative purposes heat capacity ratios $\chi \equiv (\varrho c_p)_f/(\varrho c_p)_s$ for several materials are listed in Tab. 4.1

Table 4.1: *Heat capacity ratios*

	water	octane	air (20 $°C$,1bar)
aluminium	1.7	0.65	0.0005
CrNi steel	1.0	0.4	0.0003
cast iron	0.95	0.37	0.0003
glass	2.5	0.96	0.0007
PVC	3.0	1.2	0.0009
concrete	2.2	0.84	0.0006
wood	3.5	1.4	0.0011

It can be concluded that the history term is significant for transient heat transfer in liquid-solid systems ($\chi \approx 10^0$). For gas-solid systems ($\chi \approx 10^{-3}$) the history term can be neglected.

If the fluid in the interstitial region between two neighbouring solid particles has a significantly lower volumetric heat capacity compared to the solid (as is the case for

gas-solid systems), then the temperature of the solid changes much slowlier than the temperature of the fluid. In other words: The temperature field in the fluid reaches steady state quasi instantaneously. Therefore, the error that is introduced by using steady-state relationships for the heat transfer coefficient is very small. The history term (which corrects this error) can, thus, be neglected, except for very high heating rates which will be discussed in Section 4.6.

However, if the fluid has a volumetric heat capacity which is in the same order of magnitude as the one of the solid, then the time required for the temperature field in the fluid to reach steady state is significantly long. Therefore, it is not justified to use steady-state relationships for the heat transfer coefficient (or effective heat conductivities) unless they are corrected by the history term.

4.6 Discussion

It is to be expected that the larger the heat flux $\dot{q}$ the more significant the history term, since the change of temperature with time increases and, thus, the deviation from steady state in the transient regime. This expectation may be regarded as contradictory to the fact that ϑ^* does not depend on $\dot{q}$. But the dependence is "hidden" in the definition of the dimensionless temperature (Eq. (4.33)), since in case of our thought experiment:

$$\dot{q} = \lambda_{\text{eff}} \frac{(T_{1,\infty} - T_0)}{(N-1)\, d_s} \quad . \tag{4.37}$$

Let ΔT be the absolute error due to neglection of the history term. Then it follows from Eq. (4.33) and Eq. (4.37):

$$\Delta T = \vartheta^* (T_{1,\infty} - T_0) = \vartheta^* \frac{(N-1)\, d_s}{\lambda_{\text{eff}}}\, \dot{q} \quad . \tag{4.38}$$

Therefore, it can be concluded that the absolute error (in K) due to neglection of the history term is proportional to the heat flux.

Let us now estimate this error for the experimental setup that was used by Polesek-Karczeweska [51]. In that study a packed bed of glass spheres in air ($\chi \approx 7.4 \cdot 10^{-4}$) with a height of 0.041 m was heated by a lamp ($\dot{q} = 880$ W/m^2). Figure 4.9 shows that in this case $\vartheta^* \approx 10^{-5}$. With $\lambda_{\text{eff}} = 0.35$ W/(m K), as determined in that study, it follows that $(T_{1,\infty} - T_0) \approx 100$ K. Therefore, neglection of the history term leads to an error of approximately 10^{-3} K, which is insignificant. However, if the heat flux is three or more orders of magnitude larger, then the error becomes relevant. But heat fluxes of these magnitudes (10^6 - 10^7 W/m^2) are usually not encountered in chemical engineering.

Jiang et al. [34] carried out experiments with laser pulse heating of $\dot{q} = 2.27 \cdot 10^9$ W/m^2. If this heat flux would have been imposed on the packed bed used by Polesek, then the error would be of the order of 10^3 K. This group was able to show that the larger $\dot{q}$ the stronger the non-Fourier heat conduction behaviour. This experimental finding is in line with the argumentation outlined in this section.

4.7 Conclusion

It has been shown in previous studies that the history term in the transient energy balance of a spherical particle surrounded by a fluid of infinite dimension has a significant effect on the particle's temperature. In this study it has been shown that the history term can be interpreted as a correction term. It corrects the error of applying steady-state heat transfer coefficients (as well as effective thermal conductivites) to transient processes. These quantities must be corrected if they are applied to transient processes. The latter can be done by considering the history term. The RPM is a very useful method to include the history term.

For the first time a derivation of the history term based on a geometry of finite dimension has been presented resulting in a relation where no artificial quantities exist (as opposed to previous studies). Only measurable quantities are contained.

The history term can be neglected in most cases of transient heat transfer in gas-solid packed beds. It can not be neglected if the heat flux is very large ($\dot{q} > 10^6$ W/m^2), as is the case in laser pulse heatings. In liquid-solid packed beds the history term is always significant.

The fact that transient heat transfer in heterogeneous media can sometimes not be described by Fourier's law is in part, but not primarily due to the fact that the effective thermal conductivity is only applicable to steady state processes.

Chapter 5

Evaluation of the RPM concept

The processes with which the RPM shall be evaluated will be heating-up of slate particles, as well as drying and pyrolysis of wood, mainly because of two reasons. Firstly: an intra-particle model including these processes has recently been established and successfully evaluated by Wilmes [22] who also developed a FORTRAN code for numerical simulations of a single porous particle. Secondly: the experimental data base for these processes is sound. At the Research Center Karlsruhe systematic experiments have been conducted [52–55] that cover all processes.

The intra-particle model as developed by Wilmes [22] will be introduced in Section 5.1. Special attention is put on the boundary conditions. In the subsequent Section 5.2 the reactor model is outlined. After the numerical algorithm to solve the system of differential-algebraic equations is introduced briefly in Section 5.3, the test facility is described with which the experimental data have been observed in Section 5.4. Results of numerical simulations are compared to experiments in Sections 5.5 to 5.7. Heating-up, drying and pyrolysis are considered and discussed subsequently. The chapter ends with a conclusion in Section 5.8.

5.1 The intra-particle model

In her PhD thesis Wilmes [22] developed and successfully evaluated a single-particle model where heating-up, drying, pyrolysis, gasification as well as homogeneous gas phase reactions in the pores are included. For a comprehensive description of the model (derivation of partial differential equations from balances as well as initial and boundary conditions) and the numerical algorithms that have been implemented for numerical simulation, the reader is referred to [22]. Here, only the governing partial differential equations (PDEs) will be presented along with major assumptions.

The one-dimensional single-particle model is formulated in spherical coordinates. The three phases (gaseous [subscript f], liquid [subscript liq], and solid [subscript sol]) are treated quasi-continuously. Thermal equilibrium is postulated between the three phases. The internal surface can be considered as much bigger than the external surface of the porous particle.

5.1.1 Balance equations

In the following equations the prime ($'$) refers to quantities inside a particle in order to distinguish between quantities inside and outside the particles (the latter are unprimed). Quantities at the external particle surface are referred to by a double prime ($''$).

Mass balances

The mass balance of the gas phase reads:

$$\frac{\partial(\varepsilon'_f \, \varrho'_f)}{\partial t} = -\nabla \cdot (\varrho'_f \underline{v}'_f) + \varepsilon'_{sol} \, \dot{r}'_{sol|f} + \varepsilon'_{liq} \, \dot{r}'_{liq|f} \quad , \tag{5.1}$$

where $\dot{r}'_{sol|f}$ and $\dot{r}'_{liq|f}$ represent the solid-gas and liquid-gas mass transfer, respectively, while ε'_f stands for the volume fraction occupied by the gas phase. The liquid phase consists only of water which is assumed to be stagnant. It is not distinguished between bound (i.e. adsorbed) and free water. The liquid mass balance is given by:

$$\frac{\partial(\varepsilon'_{liq} \, \varrho'_{liq})}{\partial t} = -\varepsilon'_{liq} \, \dot{r}'_{liq|f} \quad . \tag{5.2}$$

The mass of the solid phase is changed only by heterogeneous reactions, i.e.:

$$\frac{\partial(\varepsilon'_{sol} \, \varrho'_{sol})}{\partial t} = -\varepsilon'_{sol} \, \dot{r}'_{sol|f} \quad . \tag{5.3}$$

Species mass balances

Since it is assumed that the liquid exclusively consists of water, the species mass balances are written for the i-th gas phase component only. There appear three source (sink) terms due to homogeneous reactions, water evaporation (or condensation), and heterogeneous reactions, respectively:

$$\frac{\partial(\varepsilon'_f \varrho'_f Y'_{f,i})}{\partial t} = -\nabla \cdot (\varrho'_f Y'_{f,i} \underline{v}'_f + \underline{j}'_{f,i}) + \varepsilon'_f \dot{r}'_{f|f,i} + \varepsilon'_{sol} \dot{r}'_{sol|f,i} + \varepsilon'_{liq} \dot{r}'_{liq|f,i} \quad . \tag{5.4}$$

The mass fractions of the solid components (wood and char) are determined as outlined in Subsection 5.1.4.

Momentum balance

Solid and liquid phase are not moving. The gas obeys laminar flow. Instead of solving a transient PDE for the momentum, a stationary form of the momentum balance is solved which is known as Darcy's law:

$$\underline{v}'_f = -\frac{K_f}{\eta'_f} \nabla p' \quad , \tag{5.5}$$

where K_f represents the permeability of the gas phase. The pressure p' inside the particle is determined by application of the equation of state for ideal gases.

Energy balance

As mentioned earlier, it is assumed that all three phases are in thermal equilibrium, i.e.: they have the same temperature. The partial differential equation for that temperature as derived from the energy balance reads:

$$\begin{aligned} \left(\varepsilon'_f \, \varrho'_f \, c'_{p,f} + \varepsilon'_{liq} \, \varrho'_{liq} \, c'_{p,liq} + \varepsilon'_{sol} \, \varrho'_{sol} \, c'_{p,sol}\right) \frac{\partial T'_s}{\partial t} = \\ - \left(\varrho'_f \, c'_{p,f} \, \underline{v}'_f + + \sum_i c'_{p,f,i} \, \underline{j}'_{f,i} \right) \nabla T'_s \; + \nabla\left(\lambda'_{eff} \nabla T'_s\right) \\ - \sum_i h'_{f,i} \left(\varepsilon'_f \, \dot{r}'_{f|f,i} + \varepsilon'_{sol} \, \dot{r}'_{sol|f,i}\right) - \Delta h_{liq|f} \, \varepsilon'_{liq} \, \dot{r}'_{liq|f} \quad . \end{aligned} \tag{5.6}$$

5.1.2 Boundary conditions

Since the momentum balance is an algebraic equation, no boundary condition is required in this case. For the PDEs the Neumann boundary condition applies at the center of the particle, i.e.:

$$\left(\frac{\partial y}{\partial r}\right)_{r=0} = 0 \quad . \tag{5.7}$$

The interplay between representative particle and interstitial gas phase of the reactor is described by the boundary conditions of the PDEs at the surface of the particle. Therefore these boundary conditions are of special interest.

The mass flux of species i delivered from the inside of the particle to the external surface ($\dot{m}''_{i,r-}$) must be equal to the mass flux that is leaving the external particle surface ($\dot{m}''_{i,r+}$), or vice versa. This mass flux comprises convection and diffusion. Therefore it can be written:

$$\begin{aligned} \dot{m}''_{i,r-} &= \dot{m}''_{i,r+} \\ \Rightarrow \quad (\varrho''_{f,i} v''_f + j''_{f,i})_{r-} &= (\varrho''_{f,i} v''_f + j''_{f,i})_{r+} \quad . \end{aligned} \tag{5.8}$$

The convective fluxes on both sides of Eq. (5.8) cancel each other. The diffusive fluxes are described by Fick's law. The mass fraction gradient at the inner side ($r-$) is given by the intra-particle field of the mass fraction. The counterpart at the outer side ($r+$) can be estimated by use of the mass transfer coefficient (which has to be corrected due to the convective flux). Thus, the boundary condition for the species mass balance at the particle surface reads:

$$-D''_{i,eff}\ \varrho''_f \left(\frac{\partial Y'_{f,i}}{\partial r}\right)_{r-} = \zeta_i \beta''_i \left[\varrho''_{f,i} - \varrho_{f,i}\right] \quad . \tag{5.9}$$

An analog motivation holds for the boundary condition of the energy balance. But there is one difference. Heat transfer at the outer side of the particle surface does not only occur between a particle and external fluid surrounding it but also between its neighbour particles. The latter phenomenon is described by means of inter-particle conductances in upstream (G_u) and downstream (G_d) direction, respectively. Hence:

$$-A''\,\lambda''_{eff}\left(\frac{\partial T'_s}{\partial r}\right)_{r-} = A''\,\zeta_h\,\alpha''\left[T''_s - T_f\right] + G_u[T''_s - T''_u] + G_d[T''_s - T''_d] \quad . \tag{5.10}$$

The conductances as well as the surface temperatures of the neighbour particles in upstream und downstream direction (T''_u and T''_d) are determined as described in subsection 3.2.2. The latter two terms on the right-hand side of Eq.(5.10) are the second major difference between this RPM and the one established by Wurzenberger et al. [19]. In that previous study effective heat conductivities were used for description of inter-particle heat transfer which is inconsistent with the RPM approach as outlined in section 3.2.

In many applications, however, the phenomenon of inter-particle heat transfer is negligible. It is only relevant at high temperatures, where radiation comes into play, or at very low Reynolds numbers, i.e. stagnant gas.

In both boundary conditions (Eqs.(5.9) and (5.10)) intra-particle ($\varrho''_{f,i}, Y'_{f,i}, T''_s, T'_s$) as well as reactor quantities ($\varrho_{f,i}, T_f$) appear. Thus, these two equations represent the interconnection between intra-particle and reactor model.

5.1.3 Transport coefficients

The molecular transport coefficients (diffusivity D_i , heat conductivity λ_i , dynamic viscosity η_i) of each gaseous component i are determined by kinetic theory of gases. Real gas effects are included by considering intermolecular potentials of the Lennard-Jones-6-12 type. The relations are outlined in [61]. The empirical mixing rules for these quantities are also taken from [61].

5.1.4 Reaction kinetics

The pyrolysis of a fixed bed of wood particles will be the most complex process which will be used as an evaluation of the RPM concept in this work (see Section 5.7.4). There are numerous reactions schemes for wood pyrolysis that have been proposed in the past. A comprehensive overview can be found in [63]. Both Wilmes [22] and Wolfinger [63] were able to demonstrate that the model of independent parallel reactions is appropriate. According to this model wood is directly converted into char and gaseous compounds (CO_2, CO, H_2, H_2O, CH_4, and tar) without intermediate products. For each gaseous component i there are several devolatilization reactions j of the form

$$\text{WOOD} \quad \rightarrow \quad \text{GAS COMPONENT } i$$

considered. The driving forces for the reactions are written in terms of maximum conversion $X_{\max,ij}$ and current conversion X_{ij}:

$$\dot{r}_{ij} = k_{0,j} \, \exp\Big[-\frac{E_{A,j}}{\tilde{R}T}\Big] \, (X_{\max,ij} - X_{ij})^{n_j} \quad , \tag{5.11}$$

with

$$X_{ij} \equiv \frac{\text{mass of volatile species } i \text{ generated by reaction } j}{\text{initial mass of water-free particle}} \quad , \tag{5.12}$$

and

$$\dot{r}_{(sol|f),i} = \sum_{j=1}^{N_r} \dot{r}_{ij} \quad . \tag{5.13}$$

The pre-exponential factors $k_{0,j}$, activation energies $E_{A,j}$, and maximum conversions $X_{\max,ij}$ for the 23 reactions have been evaluated by fitting to experimental data. The

latter have been observed by TGA measurements at a linear heating rate of 5 K/min by Wolfinger [63]. Wilmes [22] demonstrated that this kinetic model allows accurate prediction of thermal conversion of a single wood particle, at least under the conditions that Wilmes applied in the simulation. Therefore, these parameters are also used in this work.

The mass of the unpyrolysed wood is given by:

$$m_{wood} = m_{wood}^{init}\left(1 - \sum_{j=1}^{N_r}\sum_{i=1}^{N_i} X_{ij}\right) \quad , \tag{5.14}$$

whereas the mass of char generated by pyrolysis can be determined by:

$$m_{char} = m_{wood}^{init}\left(1 - \sum_{j=1}^{N_r}\sum_{i=1}^{N_i} X_{max,ij}\right)\sum_{j=1}^{N_r}\sum_{i=1}^{N_i} X_{ij} \quad . \tag{5.15}$$

Unfortunately, it is not stated in [63], at what temperature intervall the experiments had been conducted. Thus, the range of validity of this model remains uncertain. This issue will become relevant later on.

In principle it is possible that oxygen containing species which are generated during pyrolysis (i.e. H_2O , CO , and CO_2) act as oxidizing agents in gasification reactions. To examine this possibility gasification reactions were considered in preliminary test calculations. For the kinetics the scheme recently developed by Mermoud et al. [64] was applied. It turned out that the impact of the gasification reactions is negligible. The temperatures in the experiments (< 250 °C) that are subject of the simulations in this work are way too low for gasification reactions to become important. The latter are significant at temperatures larger than 800 °C. Due to the same reason (low temperature) homogeneous reactions can be neglected as well.

5.1.5 Evaporation rate

The rate of evaporation $\dot{r}'_{liq|f}$ can be modeled in three different ways. The first possibility is to assume that phase equlibrium between liquid and water vapour is reached quasi-instantaneously. The evaporation rate is, therefore, modeled as:

$$\dot{r}'_{liq|f} = k_{liq|f}\,(\varrho^{eq}_{H_2O} - \varrho'_{H_2O}) \quad , \tag{5.16}$$

with

$$\varrho^{eq}_{H_2O} = \frac{p^{eq}}{(\tilde{R}/\tilde{M}_{H_2O})\,T} \quad . \tag{5.17}$$

To allow instantaneous equilibrium, the rate constant $k_{liq|f}$ has to be very large. The determination of this value is addressed in Appendix B.

A second possible model is to treat evaporation as a heterogeneous reaction, as has been suggested by Chan et al. [65]. They fitted experimental data to the following rate equation:

$$\dot{r}'_{liq|f} = A_{liq|f} \exp\left[-\frac{E_{liq|f}}{RT}\right] \varrho'_{H_2O} \quad . \tag{5.18}$$

It means that the more water vapour in the gas phase, the larger the evaporation rate. This definition of the driving force is not meaningful. Therefore, this rate equation will not be taken into consideration in this work.

A third possibility is the constant evaporation temperature model. In this case it is postulated that no water is evaporated below the evaporation temperature. Furthermore it is assumed that any temperature increase above the evaporation temperature ($T_{evap} \approx 373$ K at 1 bar) is consumed by evaporation. Hence:

$$\begin{aligned} \dot{r}'_{liq|f} &= \frac{(T - T_{evap})\, \varrho_s c_{p,s}}{\Delta h_{liq|f}\, \Delta t} \qquad \text{if} \qquad T \geqq T_{evap} \quad , \\ \dot{r}'_{liq|f} &= 0 \qquad\qquad\quad \text{if} \qquad T < T_{evap} \quad . \end{aligned} \tag{5.19}$$

If this model for water evaporation is used, the system of differential-algebraic equation becomes stiff. The LIMEX solver, which is used in this study, should be able to overcome this problem, since it is claimed by the authors of that solver [49, 50], that it can be applied to stiff problems.

For an evaluation of the RPM the single-particle model (Eqs.(5.1-5.10)) can be applied to heating-up, drying, pyrolysis, gasification, and homogeneous oxidation, respectively. While the first three sub-processes can be solved numerically quite fast, the latter two sub-processes are extremely time consuming. The simulation of heating-up, drying, and pyrolysis of a single particle on a single CPU (Apple G5) takes several hours. If gasification and homogeneous reactions are taken into account, then the simulation will last a few days. Again, this is true for solving only one particle model. In a RPM-simulation several single-particle models are to be solved.

Therefore, the three processes heating-up, drying, and pyrolysis of wood particles in a fixed bed reactor will be examined. These processes are sufficiently complex to evaluate the RPM approach at reasonable computational cost. In principle, also gasification and combustion can be simulated with RPM, but for that purpose the program code should be further developed in order to perform parallel calculations on several CPUs.

5.2 The reactor model

5.2.1 Balance equations

The differential balances of total mass, species mass, momentum, and energy of the fluid as used in this study have been derived in chapter 3 and are summarized below. The double prime ($''$) refers to the value at the particle surface.

Continuity:

$$\frac{\partial \varrho_f}{\partial t} = -\frac{\partial(\varrho_f\, w)}{\partial z} + s\,\frac{1-\varepsilon_f}{\varepsilon_f}\,(\varrho_f'' v_f'') \quad . \tag{5.20}$$

Mass balance of species i:

$$\frac{\partial \varrho_{f,i}}{\partial t} = -\frac{\partial(\varrho_{f,i} w)}{\partial z} + \frac{\partial}{\partial z}\left(\varrho_f\, D_z\,\frac{\partial Y_{f,i}}{\partial z}\right) + s\,\frac{1-\varepsilon_f}{\varepsilon_f}\left(\varrho_{f,i}''\, v_f'' + \zeta_i \beta_i''[\varrho_{f,i}'' - \varrho_{f,i}]\right) + \dot{r}_{f,i} \quad . \tag{5.21}$$

Momentum balance:

$$\frac{\partial(\varrho_f\, w_z)}{\partial t} = -\frac{\partial(\varrho_f\, w_z^2)}{\partial z} - \frac{\partial p}{\partial z} - f_1 w_z - \varepsilon_f f_2 w_z^2 \quad . \tag{5.22}$$

Partial differential equation for the fluid temperature derived from the energy balance:

$$\begin{aligned} \varrho_f\, c_{p,f}\,\frac{\partial T_f}{\partial t} = &-\varrho_f\, c_{p,f}\, w\,\frac{\partial T_f}{\partial z} + \frac{\partial}{\partial z}\left(\Lambda_z \frac{\partial T_f}{\partial z}\right) + \\ &- \alpha_W \frac{2}{\varepsilon_f\, R}\,(T_f - T_W) - \sum_{k=1}^{N_r}\left(\Delta_R \tilde{H}_k\right)\tilde{\dot{r}}_k + \\ &- s\,\frac{1-\varepsilon_f}{\varepsilon_f}\Big[(\dot{c}_p'' + \zeta_h\,\alpha'')\,(T_f - T_s'')\Big] \quad . \end{aligned} \tag{5.23}$$

The major difference in the description of the gas phase in the PBR as opposed to the RPM by Wurzenberger et al. [19] refers to the momentum balance. While it is treated un-steadily in this study, Wurzenberger et al. solved the momentum balance for steady-state which is another simplifying approximation.

5.2.2 Boundary conditions

Boundary conditions at reactor inlet and outlet have to be specified. In Tab. 5.1 these boundary conditions are summarized.

Table 5.1: *Boundary conditions as used in this study*

quantitiy	inlet	outlet
partial density	$\varrho_{f,i}(t,0) = \varrho_{f,i}^{in}(t)$	$\frac{\partial \varrho_{f,i}}{\partial z} = 0$
velocity	$w(t,0) = w^{in}(t)$	$\frac{\partial w}{\partial z} = 0$
temperature	$T_f(t,0) = T_f^{in}(t)$	$\frac{\partial T_f}{\partial z} = 0$
pressure	$\frac{\partial p}{\partial z} = 0$	$p(t,0) = p^{out}(t)$

5.2.3 Transport coefficients

The relations used for the transport coefficients of mass, momentum and energy in the packed bed are listed in Tab. 5.2.

Table 5.2: *Relations for transport coefficients as used in this study*

coefficient	relation	reference
axial mass dispersion coefficient	$D_z = \frac{1}{2}\, w\, d_s$	[56]
mass transfer coefficient (particle-fluid)	$\beta_i'' = \left(\frac{3.72}{Re^{2/3}} + \frac{1.06}{30+Re^{1/3}}\right)\mathrm{Re}\ \mathrm{Sc}^{1/3}\cdot$ $\cdot\frac{(0.12+\varepsilon_f)(1+\varepsilon_f)}{\varepsilon_f}\frac{D_{f,i}}{d_s}$	[57]
Stefan correction for mass transfer	$\zeta_i = \frac{v''/\beta_i''}{\exp(v''/\beta_i'')-1}$	[24]
coefficient of Ergun's equation	$f_1 = 150\ \frac{(1-\varepsilon_f)^2}{\varepsilon_f^3}\ \frac{\eta_f}{d_s^2}$	[25]
coefficient of Ergun's equation	$f_2 = 1.75\ \frac{(1-\varepsilon_f)}{\varepsilon_f^3}\ \frac{\varrho_f}{d_s}$	[25]
axial heat dispersion coefficient	$\Lambda_z = \varrho_f\, c_{p,f} D_z$	[10]
Stefan correction for heat transfer	$\zeta_h = \frac{\dot{c}_{p,s}/\alpha''}{\exp(\dot{c}_{p,s}/\alpha'')-1}$	[24]

Not listed in the above table are the relations for the heat transfer coefficients at the reactor wall α_W and at the particle's surface α''. The heat transfer between wall and fluid in a fixed bed has been reviewed recently by Wen and Ding [58]. They compared measured Nusselt numbers with published correlations. In Fig. 5.1 (taken from [58]) this comparison is depicted.

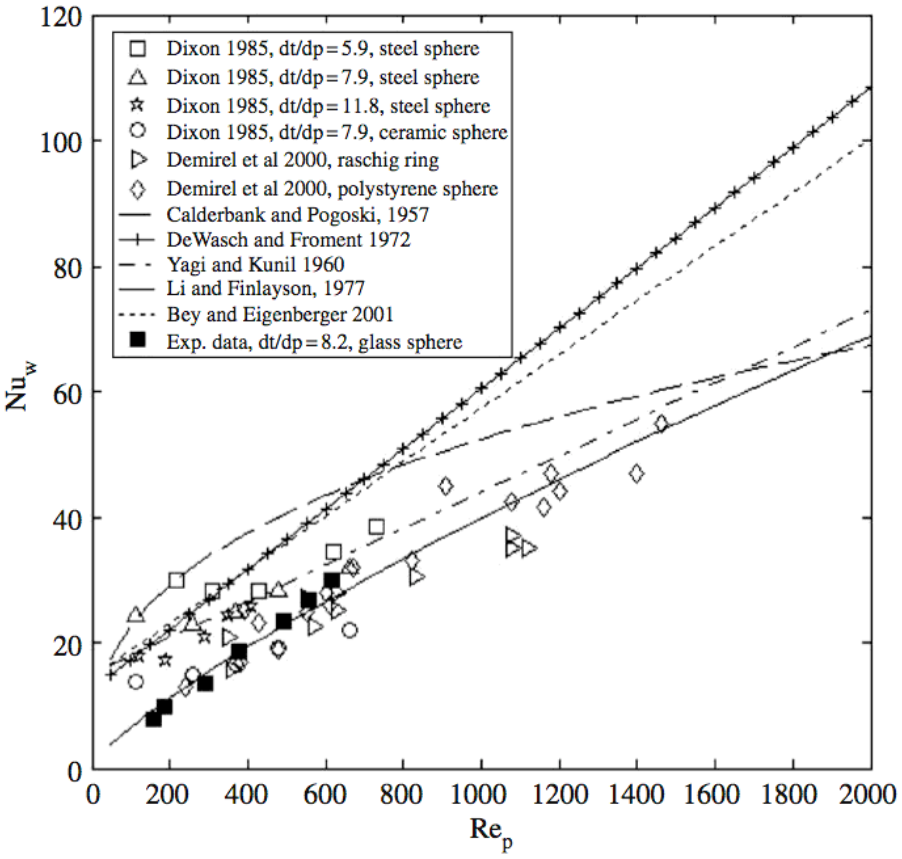

Figure 5.1: *Comparison of the measured Nusselt number at the wall of a fixed bed reactor with published correlations [58].*

It can be seen in Fig. 5.1 that the smaller the particle Reynolds number Re_p the more scattered the experimental values of Nu_W. At $\mathrm{Re}_p = 200$, for instance, the results vary by a factor of three. In the experiments which will be used for the RPM evaluation $\mathrm{Re}_p \approx 50$. To take the uncertainty of Nu_W into consideration, the two relations by Yagi and Kunii [59] as well as by Li and Finlayson [60] will be applied. The former is considered as an upper bound while the latter is considered as a lower bound of the wall-to-fluid Nusselt number.

A similar scattering was reported for the particle-to-fluid Nusselt number by Schröder [52]. These measurements were conducted in the same reactor and under very similar conditions, in which the experiments were made, that will be used for evaluation (see Section 5.4). The results are depicted in Fig. 5.2 (taken from [52]).

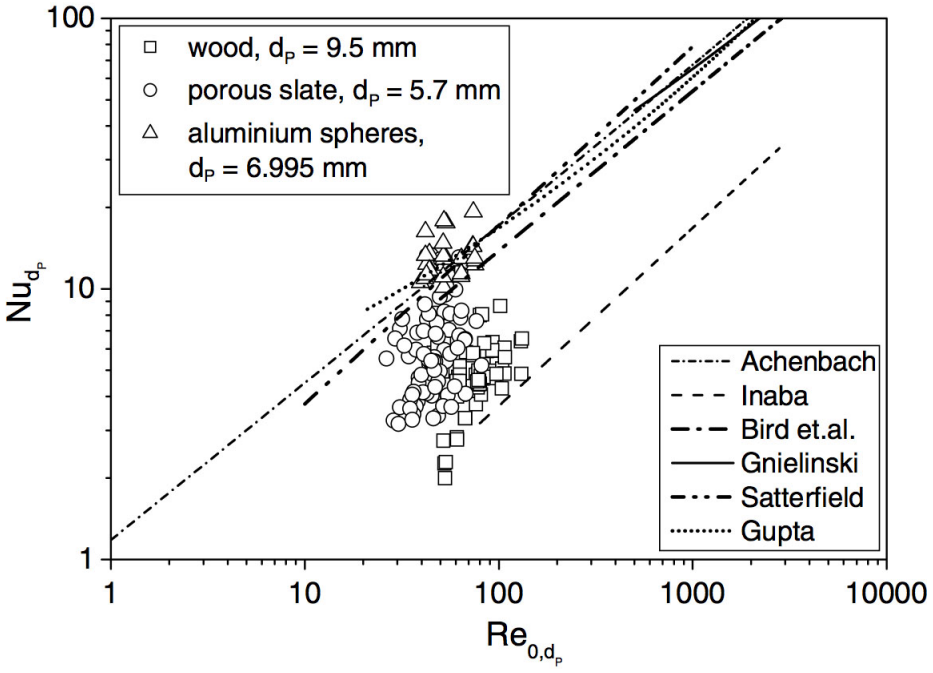

Figure 5.2: *Comparison of the measured Nusselt number at a particle in a fixed bed reactor with published correlations [52].*

It can be concluded from this figure that for $\mathrm{Re}_p \approx 50$ values between 2 and 6 have been obtained for Nu'' of wood particles whereas for porous slate the values ranged from 3 to 10.

In light of these uncertainties it seems reasonable to define two parameter sets. Set "low" can be regarded as a lower bound for heat transfer, whereas set "high" is an upper bound for heat transfer. The sets are summarized in Table 5.3.

Table 5.3: *Definition of parameter sets for heat transfer*

bed material	quantity	set "low"	set "high"
wood	Nu_W	0.17 $\mathrm{Re}_p^{0.79}$ [60]	(15+0.029 Re_p) [59]
wood	Nu''	2 [52]	6 [52]
porous slate	Nu_W	0.17 $\mathrm{Re}_p^{0.79}$ [60]	(15+0.029 Re_p) [59]
porous slate	Nu''	3 [52]	10 [52]

The molecular transport coefficients (diffusivity D_i , heat conductivity λ_i , dynamic viscosity η_i) of each gaseous component i are determined as mentioned in Subsection 5.1.3.

5.2.4 Thermodynamic properties

The heat capacities of the gaseous components $c_{p,i}$ are determined by polynomial fittings to experimental data. The same is true for the heat of water evaporation.

The heat of pyrolysis can be both exothermic and endothermic, depending on the conditions. Rath et al. [62] have investigated this topic. They reported wide variations of the heat of pyrolysis. It turned out that it can be correlated to the final char yield. Since this quantity is not known beforehand, this relation can not be applied in numerical simulations. For now the heat of pyrolysis will be set to zero. But it will be discussed again in Subsection 5.7.4.

5.3 Numerical algorithm

In the algorithm established by Jakobsen et al. [66, 67] the PDEs are discretized by finite volumes. A uniform staggered grid is used. Additionally, the concept of operator splitting is applied. It means that the change of a quantity during time step Δt can be determined by the sum of particular changes due to relevant phenomena if Δt is sufficiently small. For example: The change of the fluid temperature during Δt in a certain volume element can be calculated by summing up the changes due to convection, dispersion, chemical reactions, heat transfer between particles and fluid, and heat transfer between reactor wall and fluid, respectively. In principle, these contributions can be evaluated simultaneously. But it is much easier to do it by operator splitting.

One integration step in time is comprised of the following steps:

1. simultaneous solution of the single-particle models,
2. solution of momentum balance with constant density,
3. integration of energy and species mass balances,
4. density update due to changes in temperature and composition by equation of state,
5. density update due to solution of continuity equation,
6. partial density update due to changes in temperature, pressure, and composition.

This scheme has been implemented with first-order accuracy in time. Velocity and pressure fields are integrated with an explicit first-order Euler scheme, while all other fields are integrated by an implicit first-order Euler scheme.

For a much more comprehensive description of the numerical solution algorithm the reader is referred to [66] and [67].

The time step size for the reactor part of the RPM is chosen such that converged results can be obtained. One example of a convergence test is given in Appendix C. The same holds for the number of grid points in the particle domain (see Appendix D). The step size for the intra-particle model is automatically adapted by the LIMEX algorithm. The number of representative intra-particle models N_{par}, that are solved simultaneously, was chosen such that $N_{par} \cdot d_s \approx H$ which is the largest reasonable number.

5.4 The test facility

A sketch of the test reactor is depicted in Fig. 5.3. A detailed description is given in [68]. Here, only a brief characterization is presented.

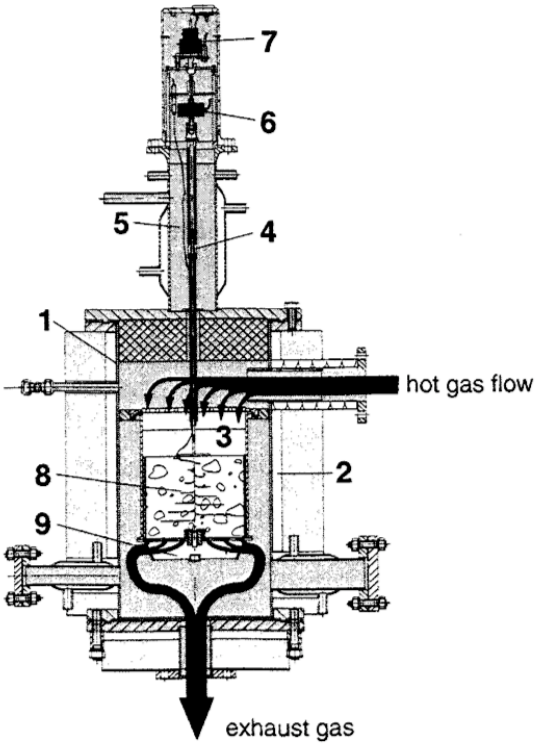

Figure 5.3: *Sketch of the test facility PANTHA, (1) steel containment, (2) electric heater, (3) reaction tube, (4) lifting rod and potentiometer, (5) cold instrumentation compartment, (6) load cell, (7) lifting motor, (8) thermocouples, (9) tub.*

The reaction tube (3) is cylindrical with radius $R = 0.125$ m and height $H = 0.210$ m. It is placed in a steel containment (1) which is heated electrically (2) to compensate heat transfer between reactor and ambient. The hot gas enters the reaction tube from

the top and passes a porous plate before entering the packed bed in order to achieve plug flow at the entrance of the bed. At the bottom of the reaction tube is a tub that collects unevaporated liquid. A lifting rod (4) connects the tube to a load cell (6) which is part of the cold instrumentation compartment (5).

Twenty k-type thermocouples (8) are positioned along the axis and the diameter of the packed bed. The thermocouples are spaced uniformly within the packed bed. One thermocouple is placed shortly above the surface of the packed to measure the temperature of the entering hot gas flow. This temperature will be referred to as "gas inlet" in the following.

While the fuel bed is heated the reaction tube rests on a metal seat. In order to record mass losses the gas flow is turned off and the reaction tube is lifted by a motor (7). The mass of the reaction tube is detected for approximately two minutes by the load cell (6). Afterwards , the reaction tube is reinstalled in its previous position and the gas flow is turned on again.

5.5 Evaluation, Part 1: Heating-up

In order to evaluate the heat transfer section of the RPM the heating-up of a packed bed of porous slate spheres by a hot air flow is simulated and compared to experimental data as observed by Peters, Schröder, and Bruch [69]. The properties of the packed bed consisting of porous slate are summarized in Table 5.4.

Table 5.4: *Properties of the packed bed with porous slate particles*

property	unit	value
bed height	mm	190
bed void fraction	-	0.52
particle diameter	mm	12.6
particle density	kg/m^3	1440
particle conductivity	W/(m K)	0.16
particle heat capacity	kJ/(kg K)	$0.104429\ T^{0.3487729}$

An air mass flow of 16 kg/h was applied in the experiments. For compensation of heat losses to the surrounding the reactor walls were heated. Unfortunately, no data (as, for instance, initial temperature and heating rate) were published on this particular point. As a first guess it will be assumed that the reactor wall is a perfect insulator, which means that there is no heat transfer across the wall. Set "high" is used for heat transfer. The results are presented in Fig. 5.4 on the next page.

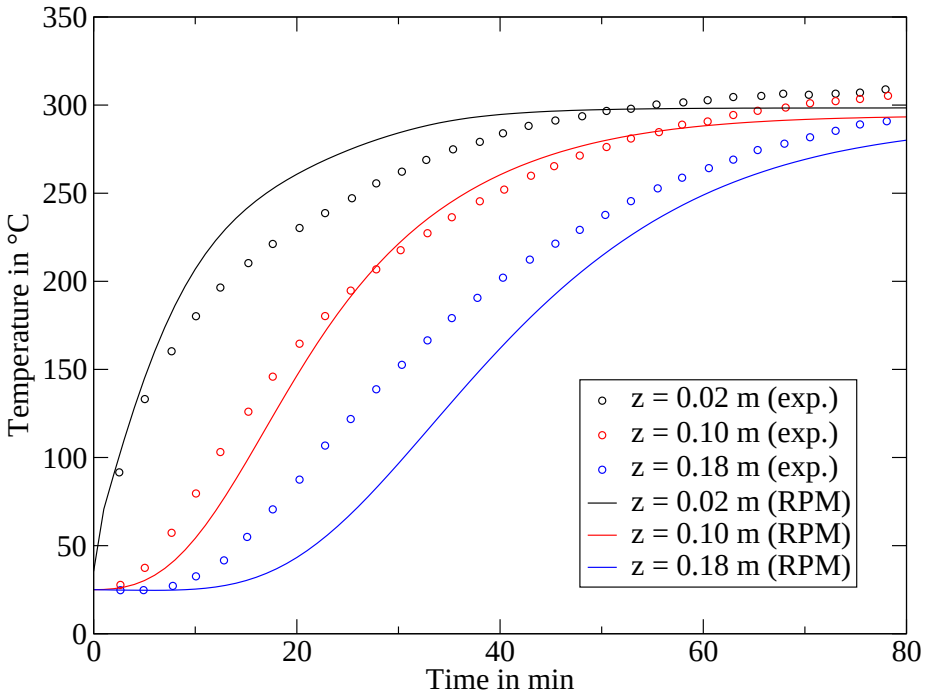

Figure 5.4: *Gas temperatures at three different axial positions during heating-up of a packed bed of porous slate spheres, comparison between experiment (dots) and simulation (lines), adiabatic walls.*

The gas temperature predicted by the simulation is in good agreement with the experiment only near the inlet (z = 0.02 m) . In the vicinity of the outlet (z = 0.18 m) the predicted gas temperature differs by more than 75 K from the experiment. The underprediction the of gas temperature increases with z, although the heat transfer parameter set "high" was applied. The impact of the reactor wall (if there is any) also increases with z. It can, thus, be supposed that the reactor wall was most probably not adiabatic in the experiments.

Due to its large heat capacity, the reactor was probably pre-heated before the hot gas flow was turned on. In [52] also the gas temperature below the packed bed is reported, which is initially about 125 °C, indicating that part of the test facility was pre-heated. Therefore, it will be assumed in a second guess that the reactor wall has a constant temperature throughout the entire experiment which is set equal to the steady-state gas inlet temperature (300 °C). Additionally, the two sets of heat transfer parameters as listed in Tab. 5.3 have been applied. The results are depicted in Fig. 5.5.

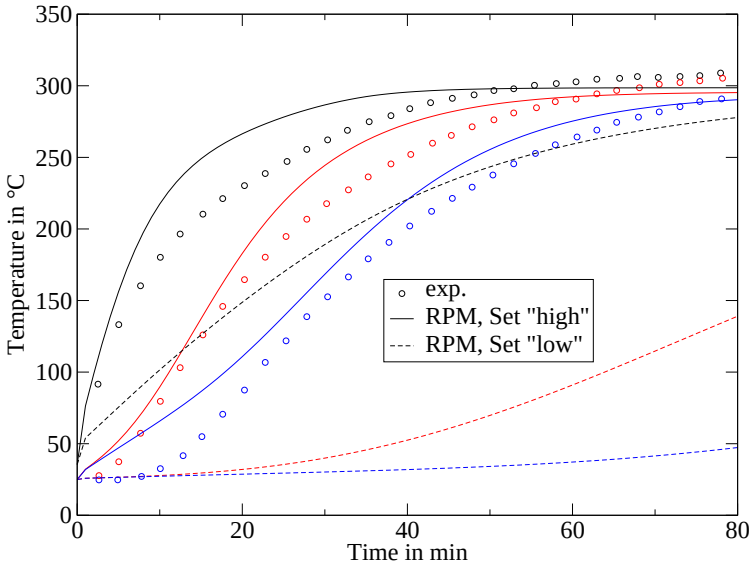

Figure 5.5: *Gas temperatures at three axial positions during heating-up of a packed bed of porous slate spheres, comparison between experiment (dots) and simulation (lines), constant wall temperature.*

While the parameter set "high" leads to a slight overestimation of the fluid temperature, the parameter set "low" severely underpredicts the temperature. It is clear, that lowering the "high" heat transfer parameters will lead to better agreement between simulation and experiment. But that would be nothing but curve fitting.

Let us focus on the predictions obtained with Set "high" which are much closer to experiment than Set "low". The results are plotted as axial fields for three different times in Fig. 5.6.

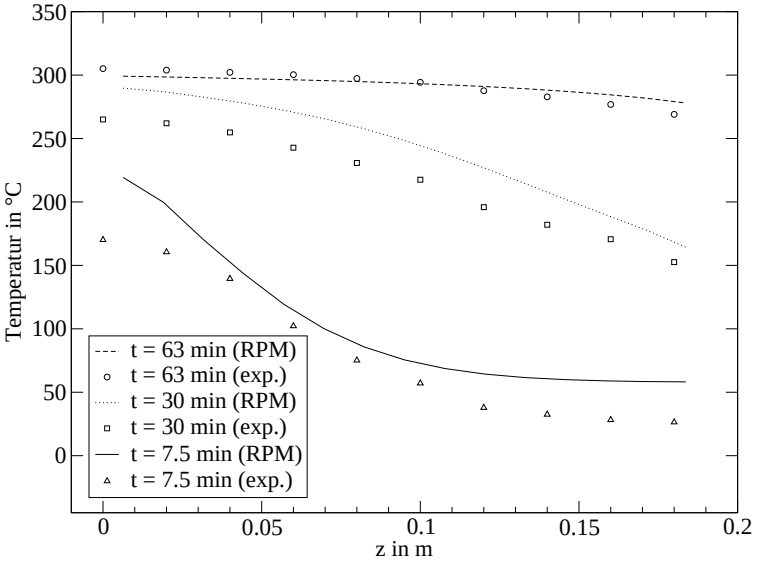

Figure 5.6: *Axial gas temperature fields at three different times during heating-up of a packed bed of porous slate spheres, comparison between experiment (dots) and simulation (lines), constant wall temperature, set "high".*

It can be observed from both Fig. 5.5 and 5.6 that near the exit of the packed bed the predicted gas temperature is initially significantly larger than in the experiment. This can be attributed - in part - to the one-dimensional nature of the reactor model. The heat transfer between reactor wall and gas leads to an increase of the gas temperature over the entire cross section without any delay. In reality, however, the lateral heat transfer is not infinitely fast. This means, that the gas temperature, which was measured in the middle of the cross section of the reactor, is initially not affected by the reactor wall. As soon as the heating front reaches the outlet of the packed bed, the axial convective heat transfer dominates the wall-to-fluid heat transfer. Since axial heat convection is covered by the reactor model - as opposed to lateral heat transfer - the initial discrepancy between simulation and experiment decreases as soon as the heating front has reached position z.

Another reason for this overprediction in the early stage of the experiment may be the assumption that the wall has an initial temperature of 300 °C (as mentioned above). This may be not true. It is possible that the reactor wall is preheated to an initial temperature which is somewhat below 300 °C and further heated during the experiment to its final value.

For times larger than 60 minutes the gas temperature is predicted too low as compared to experiment. This seems to be inconsistent with the earlier statement saying that the applied heat transfer relations are an upper limit. Why are the experimental temperatures still larger than the ones predicted by the simulation? This may be due to the reactor wall temperature, which was set to 300 °C in the simulation. It is possible that the wall was heated to more than 300 °C throughout the experiment. In [52] it has been reported that in one case the wall temperature exceeded the steady-state gas inlet temperature by more than 60 K. This would result in an underprediction of the gas temperature by the RPM as it can be observed for $t > 60$ min from Figs. 5.5 and 5.6.

In Fig. 5.7 the necessity of intra-particle modeling is illustrated. The temperature field of the representative particle in the first finite volume is depicted for different times.

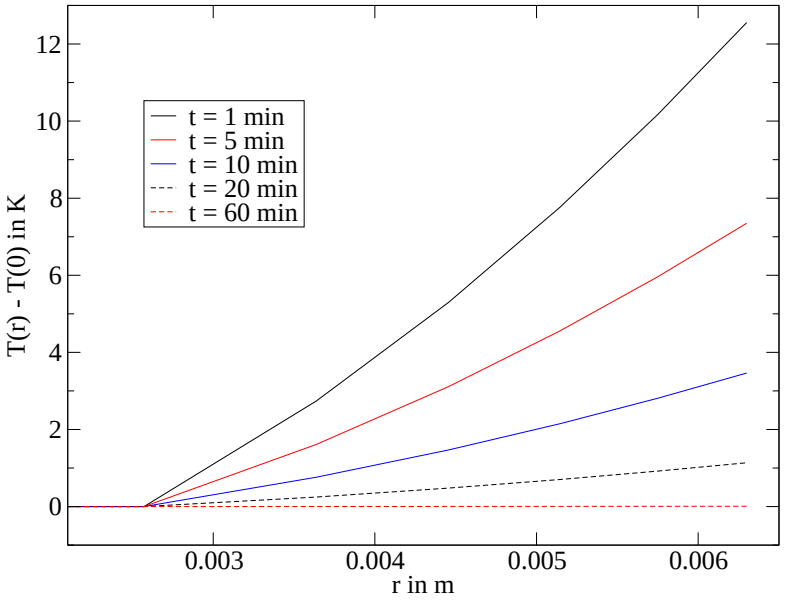

Figure 5.7: *Intra-particle temperature fields at six different times during heating-up of a packed bed of porous slate spheres, the temperatures are plotted relative to the temperature at the center of the particle*

Temperature differences of more than 10 K are obtained between particle surface and center. In presence of chemical reactions, which are often very temperature sensitive, it becomes necessary to do intra-particle modeling also in a fixed-bed reactor simulation. Again, it should be noted, that this is true only for large particles, where significant intra-particle temperature gradients are to be expected.

From the comparison of experimental data with simulation results as presented in this subsection it can be concluded that it is possible to model transient heat transfer within packed beds of thermally thick particles within the RPM framework with good accuracy. The first stage of evaluation can, thus, be considered as successful.

5.6 Evaluation, Part 2: Drying

Experiments on drying of beech wood particles in a packed-bed reactor have been conducted by Peters, Schröder, and Bruch [69]. The properties of the beech wood packed bed are summarized in Tab. 5.5.

Table 5.5: *Properties of the packed bed with beech wood particles for the drying experiments*

property	unit	value
bed height	mm	190
bed void fraction	-	0.43
initial moisture content	wt.%	10
particle diameter	mm	12.4
particle density	kg/m^3	750
particle conductivity	W/(m K)	0.16
particle heat capacity	kJ/(kg K)	1.112 + 0.00485 (T -273.15 K)

A hot nitrogen flow (16 kg/h) was used for the drying experiments. For the heat transfer in the fixed bed the parameter set "high" (see Tab. 5.3) was applied. The moisture loss of the entire packed bed was monitored as a function of time. These experimental values are plotted in Fig. 5.8 together with simulation results using different models for the evaporation rate.

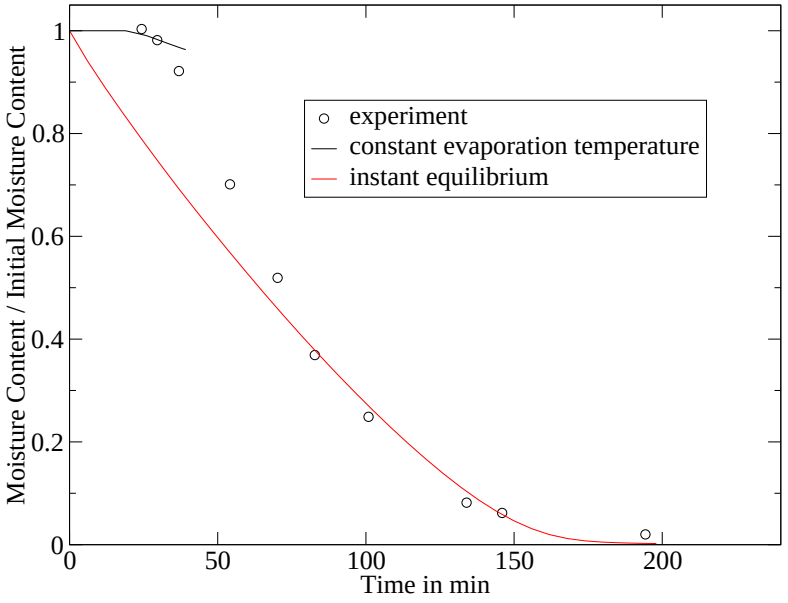

Figure 5.8: *Loss of moisture during drying of a packed bed of beech wood particles.*

If the model of constant evaporation temperature (Eq. (5.19)) is applied, then the DAE system becomes stiff. The LIMEX solver is in principle able to still solve the DAE system but the time step gets so small that it would take months to integrate over the entire intervall of 200 minutes. Therefore, the calculations have been stopped at approximately 40 minutes as indicated in Fig. 5.8.

The model of instant equilibrium (Eq. (5.16)) requires some test calculations to evaluate the rate constant. The results of the these tests are summarized in App. B. For the rate constant a value of $k_{liq|f} = 100/\mathrm{s}$ is used in the simulations.

It can be observed from Fig. 5.8 that for $t > 50$ min the agreement between experiment and simulation is quite good. In the experiments it was observed that no drying occured for $t < 25$ min. In this time intervall the instant equilibrium model already predicts a significant evaporation rate. In the intermediate time intervall (25 min $< t <$ 50 min) the evaporation rate was larger in the experiment than in the simulation.

Thus, it can be concluded that the onset of evaporation is predicted better by the constant evaporation temperature model than by the instant equilibrium model. In an attempt to improve the latter, a combination of the two models is suggested: The rate of evaporation is set to zero if $T < T_{evap}$, otherwise Eq. 5.16 applies. This leads to the same problem as encountered in case of the constant evaporation temperature model: stiffness. To overcome that problem, the discontinuity is "smeared out" with a Fermi function, i.e.:

$$\dot{r}'_{liq|f} = k_{liq|f}\ (\varrho^{eq}_{H_2O} - \varrho'_{H_2O}) \left(1 - \frac{1}{1 + \exp\left[\frac{T - T_{evap}}{2}\right]}\right) \quad . \tag{5.24}$$

A plot of the Fermi function in Eq. 5.24 is printed in Fig. 5.9.

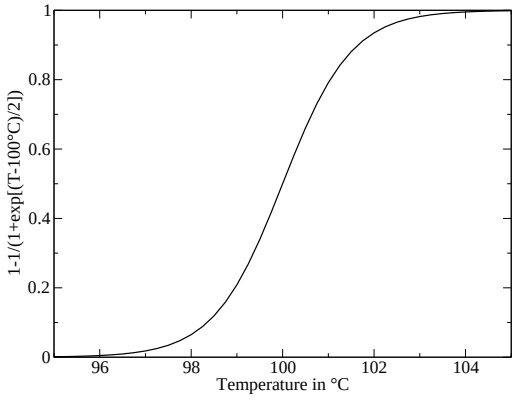

Figure 5.9: *The Fermi function as used in the modified instant equilibrium model.*

The impact on the simulation results by modifying the instant equilibrium model (Eq. 5.24) is illustrated in Fig. 5.10.

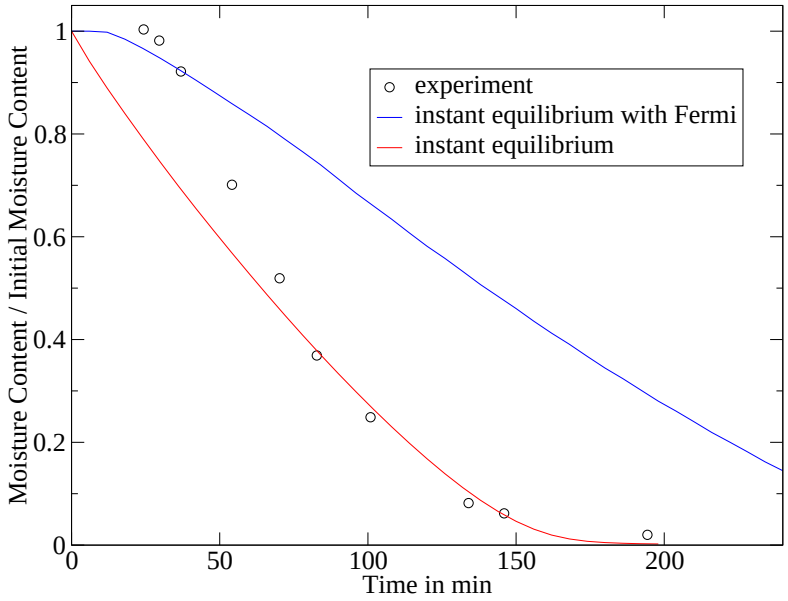

Figure 5.10: *Loss of moisture during drying of a packed bed of beech wood particles.*

Clearly, the onset of evaporation is shifted by introducing the Fermi term. But the rate of evaporation is too low in the modified model. Hence, it can be concluded that merging the two evaporation models outlined in Subsection 5.1.5 as suggested in Eq. (5.24) does not lead to an improved description of the drying in a fixed bed.

To allow further qualitative reasoning, axial profiles of the water content in the interstitial gas phase and the liquid volume fraction in the center of the particles are plotted in Fig. 5.11. The progress of the drying front through the reactor is clearly illustrated.

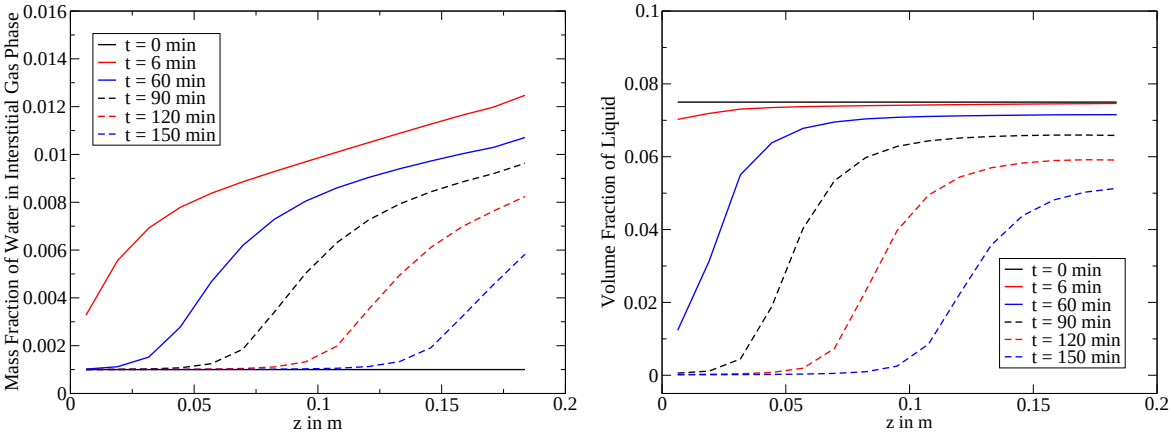

Figure 5.11: *Axial profiles of the mass fraction of water in the interstitial gas phase (left) and of the liquid volume fraction at the center of the particles (right) at different times.*

Likewise, the drying of a single particle in the middle of the fixed bed can be illustrated by plotting the same quantities as in Fig. 5.11. This is depicted in Fig. 5.12.

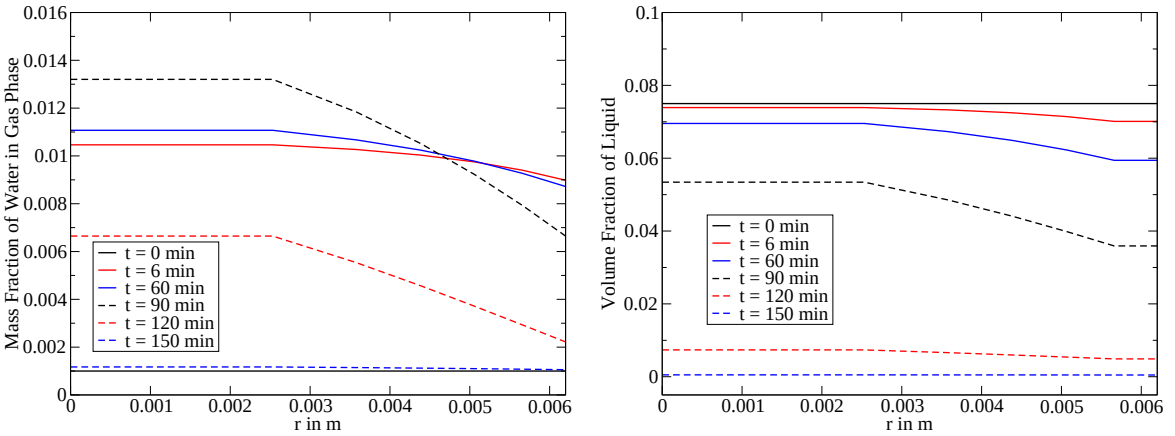

Figure 5.12: *Intra-particle radial profiles of the mass fraction of water in the gas phase (left) and of the liquid volume fraction (right) at different times.*

The particle is heated from the surrounding fluid. Thus, the evaporation rate is smaller in the center than at the outer regions of the particle. Therefore the liquid volume fraction is lower near the surface than at the center. The same is true for the water content in the gas phase of the particle. This is due to mass transfer from particle to interstitial fluid. Inside the particle the water vapour diffuses towards the external surface.

As a conclusion of the quantitative and qualitative considerations in this subsection it can be noted that the drying of a fixed bed can be described properly by the RPM approach.

5.7 Evaluation, Part 3: Pyrolysis

5.7.1 Introduction to pyrolysis

The need for renewable energies has caused numerous scientific activities in the field of thermal conversion of biomass in the last decade. The potential of biomass to substitute natural gas, oil, and coal as primary energy sources is rather limited in countries with high population density. But in countries with lower population density and huge natural biomass resources - as, for instance, in Scandinavia and Austria - biomass may play a major role as primary energy source in the future. The swedish government has announced that by 2020 the country plans to be independent from oil imports primarily by use of bioenergy. This means that gasification of biomass will become a technique of major importance in these countries since it is much more advantageous as compared to simply burning the biomass.

But also in Germany there are remarkable activities in bioenergy. The German Federal Ministry for the Environment, Nature Conservation and Nuclear Safety announced in it's latest environmental report (www.bmu.de/files/pdfs/allgemein/application/pdf/umweltbericht_2006.pdf) that the government seeks to increase the biomass fraction of the primary energy consumption significantly in the middle-term. Biogas (generated by biological conversion of biomass) has become very attractive for German farmers. More than 2700 biogas facilities have been installed in recent years (German Biogas Association, www.biogas.org). A very ambitious bioenergy concept has been developed at the Research Center Karlsruhe. It is called BIOLIQ (biomass to liquid). The basic idea is to utilize the large amount of agricultural waste (mainly straw) by converting it in small, decentral pyrolysis-units into a pyrolysis slurry (oil + char) which has a much higher energy density. That slurry is transported to a few central plants where it is converted to synthesis gas. The latter is then used for Fischer-Tropsch synthesis to give a liquid fuel. A demonstration plant of the BIOLIQ process will be constructed in China, a country of enormous potential for bioenergy.

It can, thus, be concluded that pyrolysis of biomass is most probably becoming a more and more important process when it comes to substituting conventional primary energy sources with biomass. And, hence, modeling this process is a prominent task for science.

The pyrolysis of wood actually comprises three major processes which occur consecutively in small particles: heating-up, drying (if wet material is used), and devolatilization. This is also true for gasification. The difference between pyrolysis and gasification is the atmosphere. In the former case the atmosphere is inert while in the latter case oxygen is present (e.g. in the form of O_2, CO_2, H_2O). In particles with diameter in the cm range these three basic steps can occur simultaneously.

5.7.2 Existing models for thermal conversion of biomass in packed bed reactors

There are four outstanding groups that have been working for several years on modeling thermal conversion of biomass in PBRs. The types of models developed by these groups will be outlined in the following along with fields of applications.

Thunman and Leckner (Department of Energy Conversion, Chalmers University of Technology, Gothenburg, Sweden) established a single-particle model for Eulerian calculations [70]. In a subsequent work they modeled fixed-bed combustion of biofuels with a heterogeneous, quasi continuous model [71]. While energy and species mass balances were treated as transient, the momentum was postulated to be constant in time. For the source terms in the energy and species mass balances they used relations derived from their single-particle model. This approach was also applied in another work, where they examined the effect of particle size and density on fuel combustion in PBRs [7].

Di Blasi (Dipartimento di Ingegneria Chimica, Universita degli Studi di Napoli Frederico II, Naples, Italy) and co-workers have conducted several studies on fast pyrolysis of wood [72–74]. But they also examined slow pyrolysis by experiment [75] and modeling [76]. The PBR model they established is heterogeneous and quasi-continuous. The intra-particle processes are accounted for by applying modified reaction rates according to the shrinking core approximation.

A model which is very similar to the one developed by Di Blasi et al. was established by Yang et al. (Sheffield University Waste Incineration Centre, Department of Chemical and Process Engineering, Sheffield University, Sheffield, United Kingdom). This group not only investigated slow pyrolysis of waste [77], but also gasification of biomass [78,79] and combustion of biomass [80–83].

The three abovementioned modeling approaches have in common that they treat the solid phase quasi-continuously. This is equivalent to assuming a homogeneous intra-particle temperature field at every time which is only approximately true for thermally thin particles. For thermally thick particles it is more appropriate to use a non-continuous description of the solid phase as has been outlined by Thunman and Leckner [7]. This can be done by DPM or RPM (see Chapter 2).

While Peters (former member of the Research Center Karlsruhe, Karlsruhe, Germany) et al. modeled combustion [15,55] and pyrolysis [54] in a PBR with DPM, Wurzenberger et al. (Institut fuer Apparatebau, Mechanische Verfahrenstechnik und Feuerungstechnik, Technische Universitaet Graz, Graz, Austria) were the only group - so far - that modeled thermal conversion of biomass with a RPM [19]. But the reactor model they established was not evaluated by comparison of experimental results with simulation

results. In other words: until now it has never been investigated if the RPM is able to describe heat transfer and reactive processes in a PBR appropriately. One objective of this work is to prove this.

The RPM in this work differs from the previous model by Wurzenberger et al. in the treatment of the momentum balance (see section 5.2) as well as in the formulation of the boundary condition for the energy balance of the single-particle model (see Section 5.1.

5.7.3 Preliminary remarks on the experiments

Detailed experimental data for fixed-bed pyrolysis of beech wood particles were presented by Schröder [53]. Pyrolysis experiments were conducted at temperatures ranging from 245 to 525 °C. Since the effects of pyrolysis (change in gas and solid composition, change of bed mass) are the more significant the larger the pyrolysis temperature, it is advantageous to use the experimental data obtained at 525 °C. But that is, unfortunately, not possible, because at these temperatures it was obtained that the bed height sinks by roughly 50 %. Although it is in principle possible to model a shrinking bed height also with RPM (some remarks on that topic are presented in Chapter 7), it is required that the single-particle model is able to predict a shrinking particle diameter. The particle model developed by Wilmes [22] is not able to do that (yet). Therefore, for now the pyrolysis experiments at 245 °C will be considered as benchmarks for the RPM evaluation. The bed height decreased in these experiments by less than 10 %. As mentioned earlier, the disadvantage is that at 245 °C the devolatilization reactions are very slow.

The procedure of the experiments was quite similar to the heating-up and drying experiments. For illustrative purposes the transient temperature development during a pyrolysis experiment is shown in Fig. 5.13 (taken from [53]).

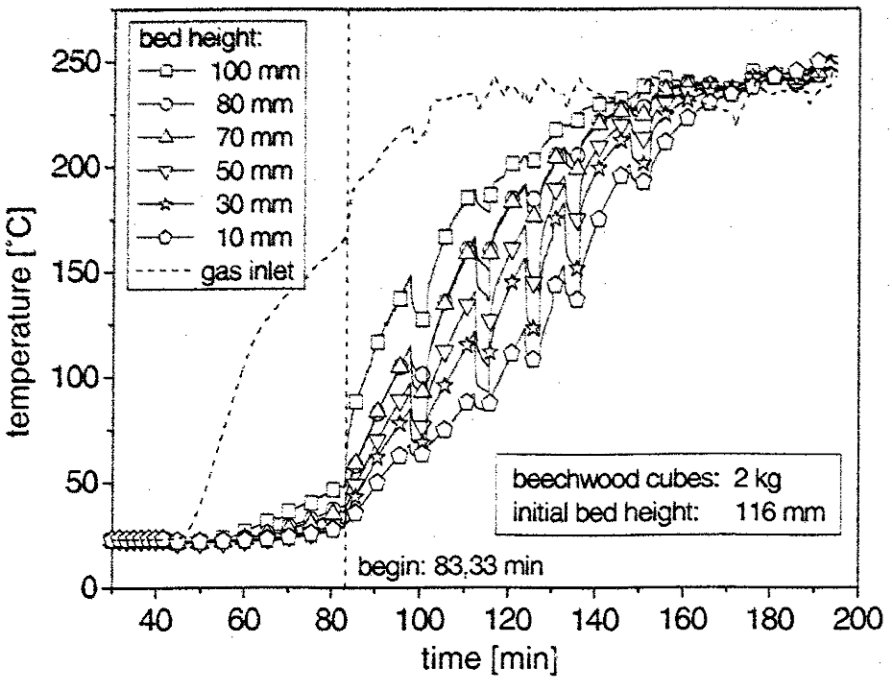

Figure 5.13: *Typical temperature evolution in a fixed bed during pyrolysis.*

It can clearly be observed that roughly 20 minutes before the start of the experiment (i.e. before the hot nitrogen flow is switched on) the reactor has been pre-heated. The resulting temperature field at 83.33 min is the initial temperature field in the simulation.

It is obvious, that during pre-heating some water is evaporated. This means that the initial moisture content of 7.2 wt% (dry basis) is decreased. But it can unfortunately not be determined what moisture the wood had at 83.33 minutes. This issue will be addressed in the next subsection.

In intervalls of approximately 15 minutes the bed temperature decreases. That is because the bed mass was weighed at these times. To do this, the nitrogen flow (16 kg/h) was switched off for 2 minutes.

Other relevant parameters of the pyrolysis experiments are summarized in Tab. 5.6.

Table 5.6: *Properties of the packed bed with beech wood particles for the pyrolysis experiments.*

property	unit	value
bed height	mm	116
bed void fraction	-	0.43
particle diameter	mm	10.0
initial moisture	wt% (dry basis)	7.2
initial particle density	kg/m^3	665

During pyrolysis wood is converted to gaseous components (including tar) and char. Thus, in contrast to simulation of heat transfer and drying, there are two different solid species (namely wood and char) which have to be considered. The thermal properties of the two solid components are taken from [63] and listed in Tab. 5.7.

Table 5.7: *Thermal properties of wood and char.*

property	unit	wood	char
thermal conductivity	W/(m K)	$0.439\left(1+\frac{T-273.15\mathrm{K}}{1155.6\mathrm{K}}\right)$	$0.087\sqrt{T/\mathrm{K}}$
heat capacity	J/(kg K)	$1113.68+\frac{T-273.15\mathrm{K}}{0.2059\mathrm{K}}$	$420+2.09\frac{T}{\mathrm{K}}-0.000685\left(\frac{T}{\mathrm{K}}\right)^2$

The effective thermal conductivity - depending on the composition of the solid as well as on the humidity of the particle - is calculated according to [63]. For the heat transfer coefficients set "high" (please refer to Tab. 5.3) is used.

5.7.4 Simulation results

Schröder [53] recorded transient temperature profiles along the reactor axis. In a first attempt the initial moisture content of 7.2 wt% (dry basis) as reported in [53] shall be used in the simulation. The heat transfer parameter set "high" is applied in combination with a constant wall temperature of 245 °C. Additionally the weighing intervalls are not considered, i.e. the nitrogen flow is not interrupted. Thus, the heat transfer should be better than in experiment. Additionally, the evaporation rate in Eq. (5.24) is used. Therefore, the computed temperature field can be considered as an upper bound. The results obtained are depicted in Fig. 5.14 along with experimental data.

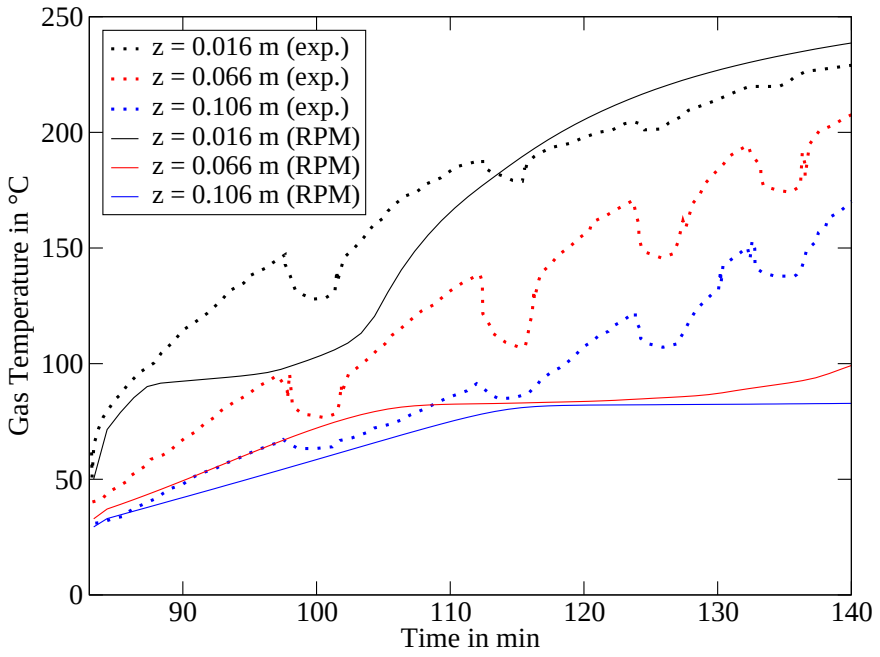

Figure 5.14: *Temperature development during pyrolysis as predicted by numerical simulation (solid) compared to experimental data (dotted), initial moisture of 7.2 wt.% (dry basis)*

Since the actual initial moisture content can not be reproduced, the case of a totally dry bed is considered in the next simulation. Also the nitrogen flow interruptions are included. All other parameters remain unchanged. Results are plotted in Fig. 5.15.

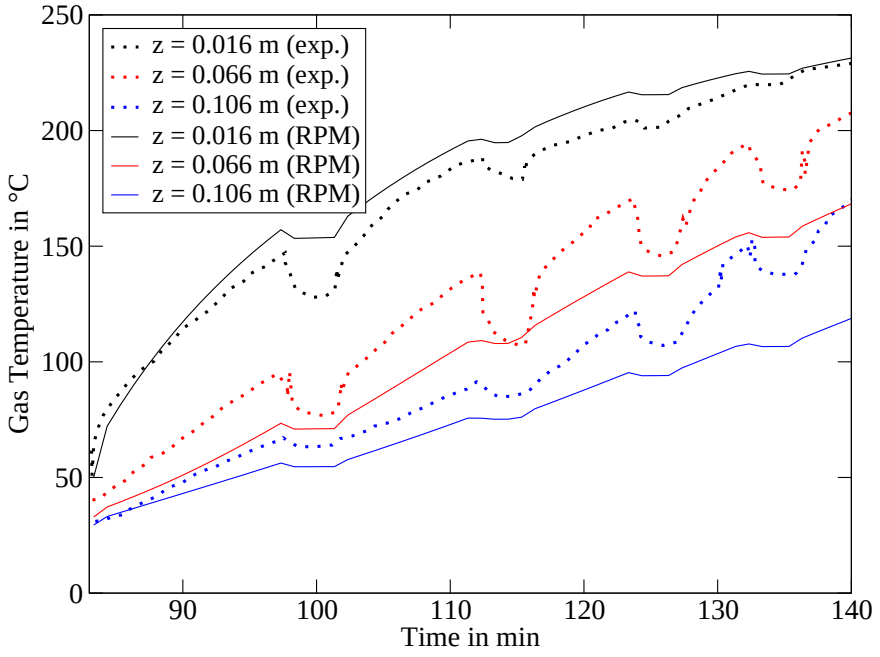

Figure 5.15: *Temperature development during pyrolysis as predicted by numerical simulation (solid) compared to experimental data (dotted), dry wood*

The agreement between simulation and experiment is much better for the dry bed (Fig. 5.15) than for the wet bed (Fig. 5.14). Thus, it can be concluded that most probably the wood particles had been dry at the beginning of the pyrolysis experiment. For a further discussion the axial temperature profiles are plotted for three different times in Fig. 5.16.

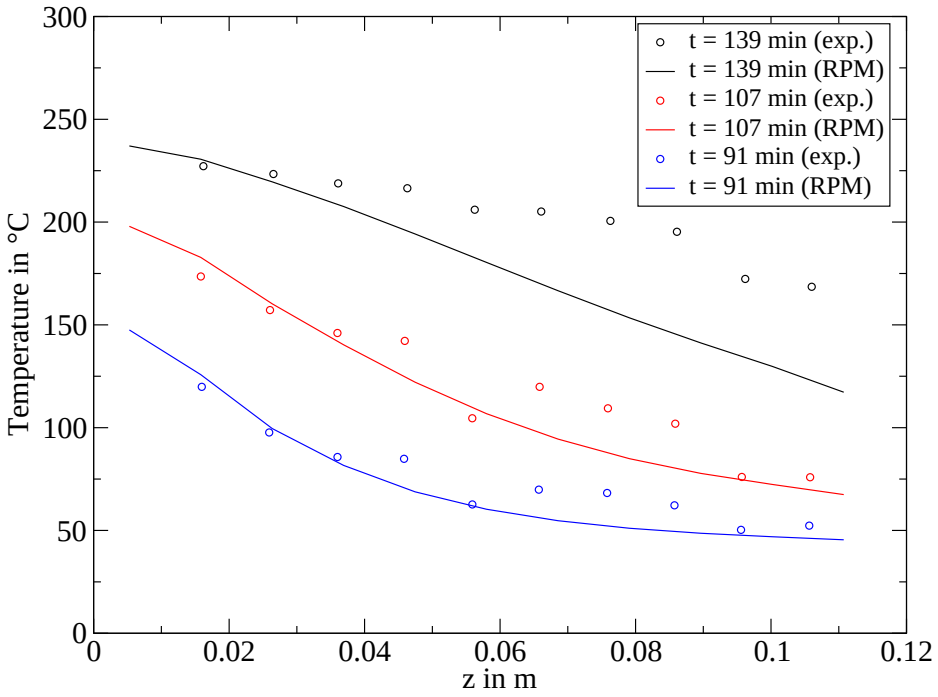

Figure 5.16: *Axial temperature profiles during pyrolysis at three different times, comparison between numerical simulation (lines) and experimental data (dots)*

Near the inlet of the fixed bed the agreement between experiment and simulation is good. But the longer the time, the more significant the disagreement for the region $z > 0.04$ m. Although the heat transfer parameters used in this calculation can be considered as an upper bound, the predicted temperature is lower than observed in experiment. After 140 minutes the difference amounts to roughly 50 K.

One possible reason for the discrepancy is the initial temperature field in the bed. The latter has been estimated from Fig. 5.13. But these temperatures were measured close to the symmetry axis if the reactor. Since the reactor wall was pre-heated before the start of the experiment, it can be expected that the regions close to the reactor wall had a temperature which was somewhat larger than the ones reported in Fig. 5.13. Since the effective conductivity of a fixed bed at stagnant flow is rather low it is indeed possible that the temperatures in the eccentric regions of the vessel differ significantly from the temperature at the center axis of the reactor. In other words: the average temperature over the cross-section of the reactor is certainly larger than the temperatures published in [53].

But this can not be the only reason, because a lower initial temperature of the particles would lead to a higher driving force for fluid-to-particle heat transfer and, hence, the temperature difference between experiment and simulation should decrease over time. But instead, it increases.

Another reason can be anticipated from Fig. 5.13. It can be observed that for t > 160 min the measured gas temperature in the center of the fixed bed exceeds the inlet gas temperature. Additionally, the temperature still increases slightly in that time intervall. This means, that the reactor wall temperature is most probably larger than the inlet gas temperature (245 °C). In the simulation, however, the reactor wall temperature was set to 245 °C. In fact, a larger wall temperature would lead to an increasing disagreement between simulation and experiment with time, similar to what is shown in Fig. 5.16.

Another quantitative measure for an evaluation is the overall mass loss of the fixed bed with time. The latter is shown in Fig. 5.17.

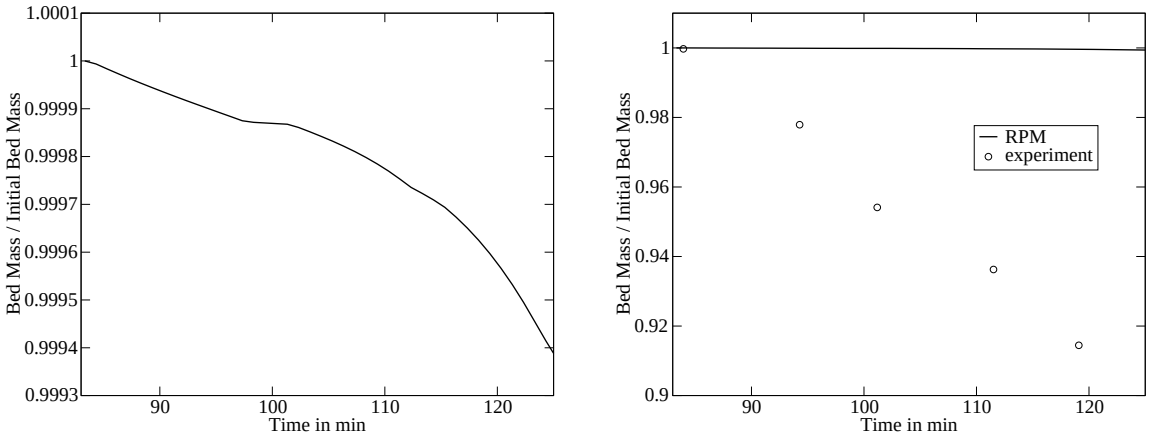

Figure 5.17: *Overall mass los of the bed during pyrolysis, comparison between simulation (line) and experiment (dots) plotted on two different scales*

Clearly, the mass loss during pyrolysis according to the simulation is two orders of magnitude lower than in experiment. In test calculations of fixed bed pyrolysis at 525 °C the mass loss as predicted by the RPM simulation was quite close to the experimental values. Although these numerical results are not reliable due to not considering shrinking particle diameter, the order of magnitude of mass loss shoult not be affected by that shortcoming. These results are in accordance with earlier findings of Wilmes [22] and Wolfinger [63], who both applied temperatures larger than 250 °C. Hence, these three studies indicate that the kinetic coefficients of Eq. (5.11) may be not applicable to temperatures below 250 °C.

Due to the very low reaction rates the extend of the reaction is very small. Hence, the reaction enthalpy does not have a significant impact.

Since quantitative evaluation is obviously problematic in this case, qualitative considerations have to be taken into account. The CO_2 mass fraction in the interstitial gas can be regarded as an indicator for the extend of pyrolysis. The char mass fraction in the solid phase, on the other hand, is an indicator in the particle domain. Both quantities are plotted in the subsequent diagrams.

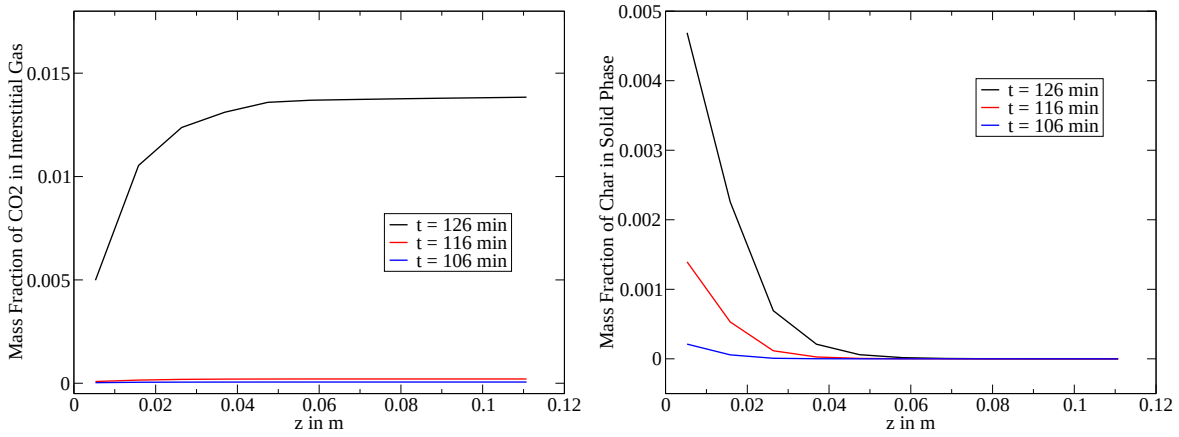

Figure 5.18: *Axial profiles of the mass fraction of CO_2 in the interstitial gas phase (left) and of the char mass fraction at the center of the particles (right) at three characteristic times.*

It has been stated earlier, that at temperatures as low as 245 °C the pyrolysis reaction rate is rather small. Therefore, it is not surprising that both CO_2 content in the interstitial gas and char content in the solid phase are very small. But also at these low concentrations, the general trends can be observed for a qualitative evaluation.

During pyrolysis the CO_2 mass fraction increases downstream until the part of the reactor is reached, where no pyrolysis occurs. In these parts of the reactor the CO_2 diffuses into the particle, if no intra-particle CO_2 is present. But since the concentrations are very low, the driving force for mass transfer from fluid to particle is small, too. Therefore, the CO_2 content in the interstitial gas phase is not significantly affected by fluid to particle mass transfer.

The char mass fraction in the particles decreases down the reactor axis. The latter corresponds to the temperature field. The higher the temperature, the faster the pyrolysis reactions (see Fig. 5.16).

Likewise, the pyrolysis of a single particle at the inlet of the fixed bed can be illustrated by plotting the same quantities as in Fig. 5.18. This is depicted in Fig. 5.19.

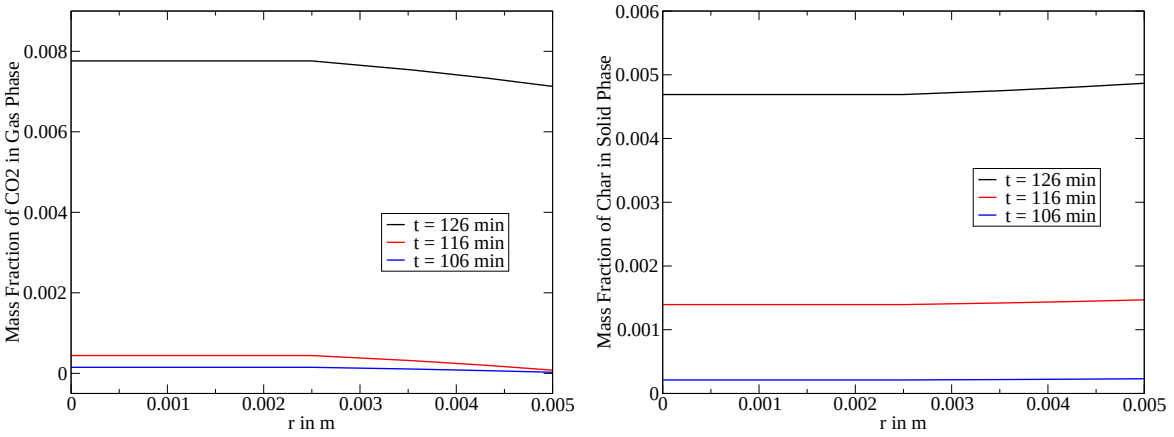

Figure 5.19: *Intra-particle radial profiles of the mass fraction of CO_2 in the gas phase (left) and of the char mass fraction in the solid phase (right) at three different times.*

The particle is heated from the surrounding fluid. Thus, the devolatilization rate is smaller in the center than at the outer regions of the particle. Therefore the char mass fraction is larger near the surface than at the center. The opposite is true for the CO_2 mass fraction in the gas phase of the particle. This is due to mass transfer from particle to interstitial fluid. Inside the particle the CO_2 diffuses towards the external surface.

The qualitative considerations regarding the devolatilization reactions and the resulting mass transfer processes show that RPM performs well.

5.8 Conclusion

In this chapter the RPM concept was evaluated. Experimental results for heating-up, drying, and pyrolysis of fixed beds were used as a benchmark. The single-particle model established by Wilmes [22] is used for that purpose.

It could be shown that the heat transfer in packed beds can be well described by RPM. However, the wide range of possible values for heat transfer coefficients (particle to fluid as well as wall to fluid) and the unknown reactor wall temperature do not allow an accurate evaluation.

The mass loss during drying of wood particles can also be successfully modeled by RPM. A shortcoming is that in the initial stage of drying the evaporation rate according to the instant equilibrium model is too large. A modification of the latter model by introducing a Fermi-like term leads to improved prediction of evaporation onset. But the evaporation rate after the onset is significantly lower than observed in experiment.

The mass loss during pyrolysis is not well predicted by the simulation. The quantitative discrepancies between simulation and experiment can be attributed in part to invalid kinetic parameters. However, the qualitative trends in the reactor and the particle domain can be considered as successfully evaluated.

Chapter 6

Summary

Several detailed single-particle models for thermal conversion of biomass have been established in recent years. With the Representative Particle Model (RPM) it is possible to integrate such a single-particle model into a packed-bed reactor model. This is helpful for packed beds with large particle sizes, where significant intra-particle gradients occur. Examples for such processes are pyrolysis, gasification, and combustion of solid biomass particles.

The major objectives of this work have been the establishment, development, and evaluation of the RPM approach in PBR modeling.

The basic idea behind this approach is that instead of modeling each individual particle in a packed-bed reactor, which would be computationally very expensive, only a limited number of particles are described in detail. These particular particles are considered as being representative for a finite volume element of the reactor.

A detailed derivation of the governing differential balance equations has been outlined. Special emphasis was put on the boundary conditions of the single-particle model. The phenomenon of inter-particle heat transfer was modeled in a consistent manner for the first time. Another improvement as compared to previous works was the implementation of the transient momentum balance. Most commonly, the steady-state momentum balance is applied to transient processes.

Furthermore, it was investigated under which conditions the RPM may help to improve the description of transient heat transfer in heterogeneous media. To do that, the history term for heat transfer between neighbour particles has been derived. It has been shown that the history term can be interpreted as a correction term. It corrects the error of applying heat transfer coefficients (as well as effective thermal conductivites) to transient processes. These quantities are valid for steady state processes only and must be corrected if they are applied to transient processes. The latter can be done by considering the history term, which is readily possible within the RPM framework. It

could be concluded that the history term can be neglected in most cases of transient heat transfer in gas-solid packed beds. It can not be neglected if the heat flux is very large ($\dot{q} > 10^6$ W/m^2), as is the case in laser pulse heatings. In liquid-solid packed beds the history term is always significant.

For the first time the RPM concept was evaluated. Experimental results for heating-up, drying, and pyrolysis of fixed beds were used as a benchmark. The single-particle model established by Wilmes [22] was applied in this study. It could be shown that the heat transfer and drying in packed beds can be well described by RPM. The mass loss during pyrolysis is not well predicted by the simulation. The quantitative discrepancies between simulation and experiment can be attributed in part to invalid kinetic parameters. However, it can be concluded that the qualitative trends in the reactor and the particle domain can be considered as successfully evaluated.

Chapter 7

Outlook

The most important feature that should be included in the RPM is the shrinkage of the bed height. Once, a single-particle model is available that includes particle shrinkage, a method has to be established, that accounts for decreasing bed height due to shrinking particle diameter. First attempts have shown that it is not sufficient to simply increase the void fraction ε_f (to unity) in a finite volume of the reactor, because this introduces a discontinuity which can not be handled by the poisson solver. It is suggested, that regriding is applied to the reactor grid after each global time step. Thereby the problems of the poisson solver are circumvented. The bed height is evaluated after each time step. And the axial step length Δz is adapted to the new height (or length) of the fixed bed. The void fraction within this domain remains constant. With this modification it should be possible to improve the simulation of fixed bed pyrolysis significantly, since temperature ranges can be addressed for which the reaction kinetics introduced in Subsection 5.1.4 are more appropriate.

The extension to a two-dimensional reactor grid would be extremely costly as far as the computational effort is concerned. One simulation run of the pyrolysis outlined in Subsection 5.7.4 takes approximately three weeks on a single CPU (apple G5). In this case 15 single-particle models had to be solved simultaneously. A lateral grid with only 5 gridpoints would increase this time to roughly three months. Therefore it is necessary to examine if the single-particle model can be parametrized somehow. But this is a very comprehensive task for a transient process.

Prominent processes that are already included in the single-particle model are gasification and combustion. Thus, fixed-bed gasification or combustion can readily be modeled and numerically simulated once the bed shrinkage is included in the RPM. However, these processes occur at significantly higher temperatures than pyrolysis. That means that homogeneous reactions (both in the particle as well as in the reactor domain) can not be neglected anymore, as has been done in this study. Including these homogeneous reactions also increases the computational effort significantly.

Therefore the following road map is suggested to further develop the RPM at hand:

1. include particle shrinkage in single-particle model,
2. include bed shrinkage in the RPM,
3. simulate pyrolysis at 525 °C for evaluation,
4. parameterize the single-particle model and/or,
5. parallelize the RPM code to enhance computational speed,
6. simulate gasification and/or combustion in fixed beds,
7. extend the RPM model to two dimensions.

A promising appllication that can be modeled with RPM already at it's current stage is smouldering and self-ignition in piles of biomass. This work is currently under way.

Appendix A

Dimensionless energy balance of a particle in the topmost layer

For a particle in the topmost layer a term including the external heat flux $\dot{q}$ has to be added to the energy balance as written in Eq. (4.21). Substituting the temperature and the time by the dimensionless variables as defined in section 4.5 leads to the following equation:

$$\begin{aligned}\frac{2}{3\beta(2-\gamma)}\frac{\mathrm{d}T_1^*}{\mathrm{d}t^*} = \quad & (T_2^* - T_1^*) + \frac{1}{(2-\gamma)}\,\frac{\dot{q}\,d_s}{\lambda_f(T_0 - T_{1,\infty})} + \dots \\ & + 2\int_0^{t^*}\sum_{n=1}^{\infty}\exp\left[-\left(\frac{n\pi}{\gamma}\right)^2(t^*-\tau^*)\right]\left((-1)^n\frac{\mathrm{d}T_2^*}{\mathrm{d}\tau^*} - \frac{\mathrm{d}T_1^*}{\mathrm{d}\tau^*}\right)\mathrm{d}\tau^*.\end{aligned} \tag{A.1}$$

For $t \to \infty$ this balance reduces to:

$$0 = (T_{2,\infty}^* - T_{1,\infty}^*) + \frac{1}{(2-\gamma)}\,\frac{\dot{q}\,d_s}{\lambda_f(T_0 - T_{1,\infty})} \quad . \tag{A.2}$$

For the case of constant properties of solid and fluid phase the temperature field in the particle chain is linear at steady state, which is why:

$$\frac{T_{2,\infty}^* - T_{1,\infty}^*}{d_s} = \frac{T_{N,\infty}^* - T_{1,\infty}^*}{(N-1)\,d_s} = -\frac{1}{(N-1)\,d_s} \quad . \tag{A.3}$$

With this relation and since $T_{N,\infty} = T_0$ Eq. (A.2) can be rewritten as:

$$0 = -\frac{1}{(N-1)} + \frac{1}{(2-\gamma)}\,\frac{\dot{q}\,d_s}{\lambda_f(T_0 - T_{1,\infty})} \quad . \tag{A.4}$$

Solving this equation for $\dot{q}$ yields:

$$\dot{q} = \left(\frac{2-\gamma}{N-1}\right)\frac{\lambda_f(T_0 - T_{1,\infty})}{d_s} \quad . \tag{A.5}$$

Substituting $\dot{q}$ in Eq. (A.2) with Eq. (A.5) yields Eq. (4.35).

Appendix B

Convergence with respect to the evaporation rate constant

The rate constant in the instant equilibrium model ($k_{liq|f}$ in Eq. (5.16)) has to be chosen such that quasi-instantaneous evaporation is possible. The rate constant is large enough if further increase does not influence the simulation results. The calculated moisture loss for different values of the parameter $k_{liq|f}$ are depicted in Fig. B.1.

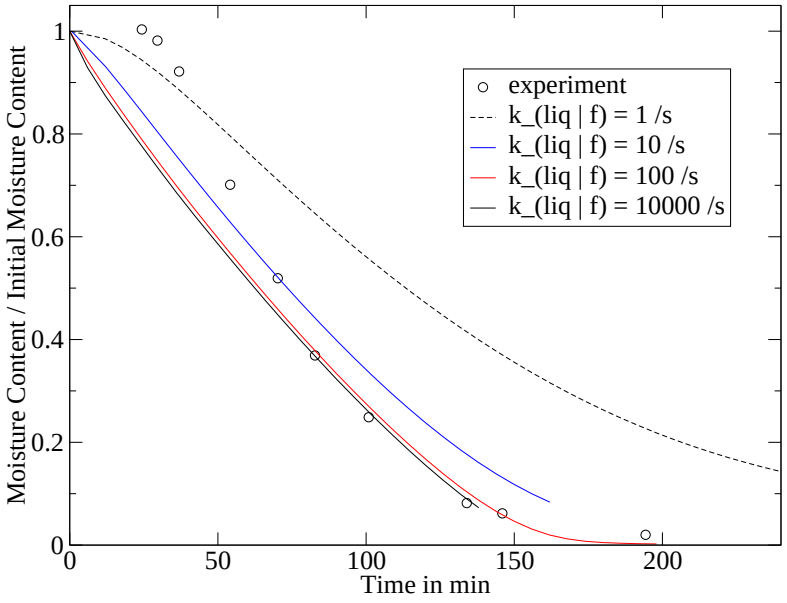

Figure B.1: *Calculated moisture loss during drying of wood particles for different evaporation rate constants.*

It can be concluded that $k_{liq|f} = 100/\mathrm{s}$ gives converged results.

Appendix C

Convergence with respect to time step Δt

The global time step Δt has to be chosen such that further decrease does not influence the simulation results. The calculated temperature developments in a fixed bed for two different Δt are depicted in Fig. C.1.

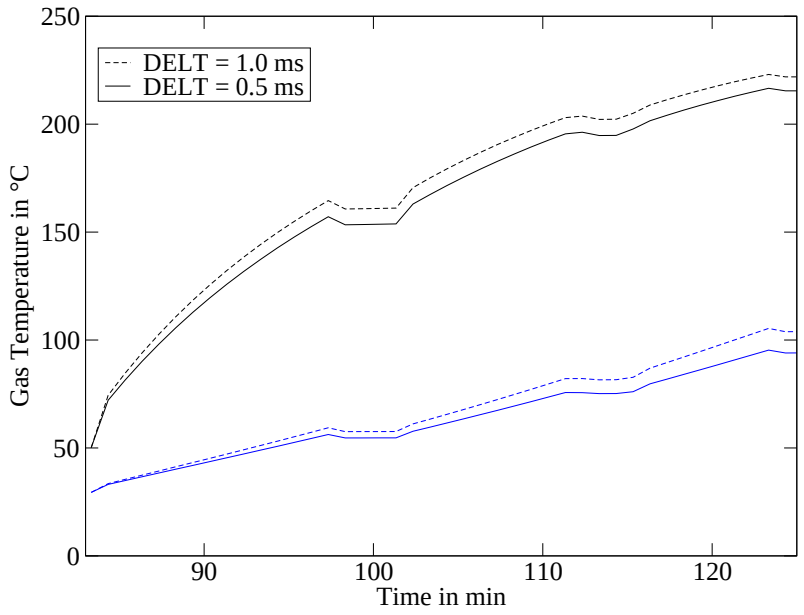

Figure C.1: *Calculated temperature development at two axial positions in the fixed bed under pyrolysis conditions for two different global time step sizes.*

Decreasing the time step size from 1 ms to 0.5 ms leads to a change in temperature of only a few K. A further decrease leads to even less temperature change. In light of the uncertainties related to heat transfer coefficients and wall temperature, this convergence is totally sufficient. Therefore a time step size of $\Delta t = 0.5$ ms is adopted in this case.

Appendix D

Convergence with respect to the intra-particle grid

The influence of the number of intra-particle grid points (NGP) on the simulation results has also to be examined. The calculated temperature developments in a fixed bed for two different NGP are depicted in Fig. D.1.

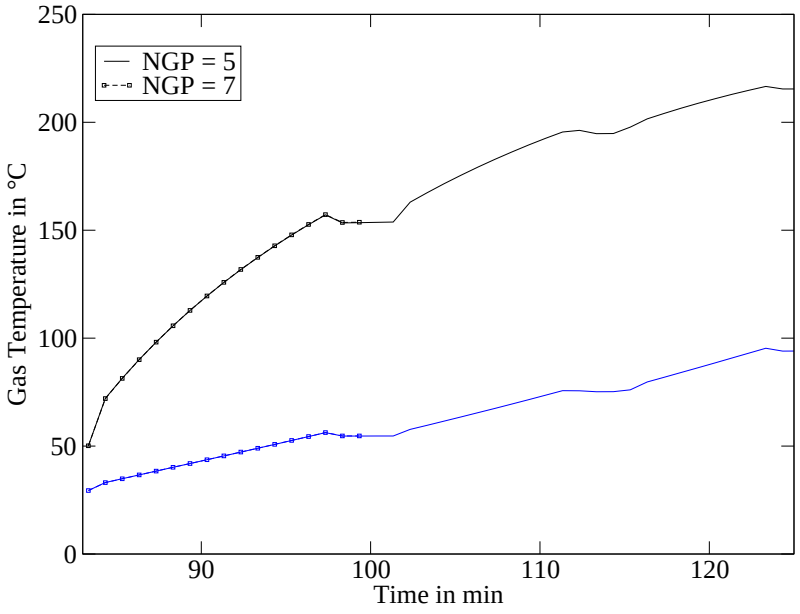

Figure D.1: *Calculated temperature development at two axial positions in the fixed bed under pyrolysis conditions for two different numbers of intra-particle grid points*

Obviously, choosing five or seven grid points for the particle grid does not affect the calculated temperature development. Therefore NGP = 5 was chosen in this case.

Nomenclature

Latin symbols		
a	thermal diffusivity	[m^2/s]
A	surface, area	[m^2]
A	pre-exponential factor	[1/s]
A_R	cross-sectional area of the reactor	[m^2]
c	molar density, concentration	[mol/m^3]
c_p	mass specific heat capacity at constant pressure	[J/(kg K)]
$\dot{c}_p$	heat capacity flux as defined in Eq.(3.72)	[$W/(m^2$ s)]
c_v	mass specific heat capacity at constant volume	[J/(kg K)]
C	coefficient as defined in Eq.(4.25)	[-]
d	diameter	[m]
D	diffusivity, dispersion coefficient	[m^2/s]
E	activation energy	[J/mol]
f_{HT}	history term	[W]
f_1	coefficient of the Ergun equation	[$kg/(m^3s^2)$]
f_2	coefficient of the Ergun equation	[$kg/(m^4)$]
F	Force	[N]
g	specific gravity	[m/s^2]
G	conductance	[W/K]
h	roughness	[m]
H	height / length of the fixed bed	[m]
$\Delta_R\tilde{H}$	reaction enthalpy	[J/mol]
j	diffusion / dispersion flux density	[$kg/(m^2$ s)]
J	diffusion / dispersion flux	[kg/s]
k	integer index	[-]
k	evaporation rate constant	[1/s]

K	permeability	[m^2]
L	distance between two parallel planes	[m]
m	mass	[kg]
$\dot{m}$	convective mass flux density	[kg/(m^2 s)]
$\dot{M}$	convective mass flux	[kg/s]
$\tilde{M}$	molar mass	[kg/mol]
n	integer index	[-]
$\underline{n}$	normal vector of a surface	[-]
N	number of particle layers	[-]
N_i	number of species	[-]
N_k	number of species	[-]
N_{par}	number of representative particles	[-]
N_r	number of reactions	[-]
N_s	number of particles in the control volume	[-]
p	pressure	[Pa]
$\dot{q}$	heat flux density	[W/m^2]
$\dot{Q}$	heat flux	[W]
r	radial coordinate	[m]
$\dot{r}$	sink/source of mass per unit volume	[kg/(m^3 s)]
$\tilde{\dot{r}}$	molar sink/source per unit volume	[mol/(m^3 s)]
$\vec{r}$	position vector	[$\vec{m}$]
R	inner radius of the cylindric reactor	[m]
$\tilde{R}$	universal gas constant	[J/(mol K)]
s	volume specific external surface of the particles	[1/m]
S	external particle surface area	[m^2]
t	time	[s]
T	temperature	[K]
$\tilde{T}$	artificial temperature	[K]
u	generic quantity	
u	mass specific inner energy	[J/kg]
$\dot{u}$	flux density of inner energy	[J/(m^2 s)]
v	intra-particle velocity	[m/s]
V	volume	[m^3]

∂V	edge of volume / surface	[m^2]
w	velocity in axial direction of the reactor	[m/s]
x	spacial coordinate	[m]
X	conversion	[-]
y	generic quantity	
Y	mass fraction	[-]
z	axial coordinate	[m]

Greek symbols

α	heat transfer coefficient	[W/(m^2 K)]
β_i	mass transfer coefficient of species i	[m/s]
γ	geometric parameter	[-]
$\underline{\underline{\delta}}$	unit matrix	[-]
ε	volume fraction (of solid, liquid or gaseous phase)	[-]
ζ	Stefan correction	[-]
η	dynamic viscosity	[Pa s]
θ	angle	[rad]
ϑ	dimensionless temperature difference	[-]
Λ	thermal dispersion coefficient	[W/(m K)]
ν	stoichiometric coefficient	[-]
ϱ	density	[kg/m^3]
ρ	specific absorbed radiation	[W/kg]
τ	(lag) time	[s]
$\underline{\underline{\tau}}$	stress tensor	[N/m^2]
ϕ	mass specific volumetric force	[m/s^2]
χ	ratio of volumetric heat capacities (fluid/solid)	[-]
Ω	mean free path	[m]

Subscripts

0	initial value
eff	effective value
c	pertains to inter-particle heat transfer by contact conduction
d	pertains to downstream
f	pertains to fluid
$f\|f$	pertains to homogeneous reactions in the gas phase
h	pertains to hollow sphere

i	pertains to the inner zone of inter-particle heat transfer
i	pertains to species with index i
j	pertains to neighbour particle j
j	pertains to dispersion
k	pertains to species with index k
liq	pertains to liquid phase of a porous particle
$liq\|f$	pertains to evaporation / condensation
max	maximum value
o	pertains to the outer zone of inter-particle heat transfer
q	pertains to heat flux
r	pertains to radiation
ref	reference value
R	pertains to reactor
s	pertains to particle
sol	pertains to solid phase of a porous particle
$sol\|f$	pertains to heterogeneous reactions
$sol\|sol$	pertains to homogeneous reactions in the solid phase
sj	pertains to transfer between particle (s) and its neighbour (j)
sf	pertains to the external interface of particle and fluid
T	pertains to temperature gradient
u	pertains to upstream
w	pertains to convection
W	pertains to reactor wall
z	pertains to axial direction
Δs	pertains to temperature step change at the particle's surface
Δj	pertains to temperature step change at the surface of the j-th neighbour particle
λ	pertains to heat conduction
∞	at large distance from particle

Superscripts

$*$	dimensionless quantity
$'$	intra-particle quantity
$''$	quantity at the external particle surface
eq	quantity at phase equilibrium / saturation
in	quantity at the reactor inlet
out	quantity at the reactor outlet

Bibliography

[1] Hammer, M. J.: *Water and Wastewater Technology.* 2nd ed. New York : John Wiley and Sons, 1986

[2] Heermann, C.: *Pyrolysis and Gasification of waste: A worldwide technology and business review.* 1st ed. Juniper Consultancy Services Ltd., 2001

[3] Knoef, H. (Hrsg.): *Handbook Biomass Gasification.* 1st ed. Enschede : BTG biomass technology group, 2005

[4] Adler, R.: State of the art of the simulation of heterogeneous gas catalytic reaction processes in fixed bed tubular reactors - Part 1. In: *Chemie Ingenieur Technik* 72 (2000), Nr. 6, S. 555–564

[5] Adler, R.: State of the art of the simulation of heterogeneous gas catalytic reaction processes in fixed bed tubular reactors - Part 2. In: *Chemie Ingenieur Technik* 72 (2000), Nr. 7, S. 688–699

[6] Hofmann, H.: Progress in the Modeling of Fixed-Bed Reactors. In: *Chemie Ingenieur Technik* 51 (1979), Nr. 4, S. 257–265

[7] Thunman, H. ; Leckner, B.: Influence of size and density of fuel on combustion in a packed bed. In: *Proceedings of the Combustion Institute* 30 (2005), S. 2939–2946. – Part 2

[8] Westerterp, R. ; Bos, R. ; Wijngaarden, R. ; Kusters, W. ; Martens, A.: Selective hydrogenation of acetylene in an ethylene stream in an adiabatic reactor. In: *Chemical Engineering and Technology* 25 (2002), Nr. 5, S. 529–539

[9] Levec, J. ; Carbonell, R. G.: Longitudinal and Lateral Thermal Dispersion in Packed-Beds .2. Comparison between Theory and Experiment. In: *AIChE Journal* 31 (1985), Nr. 4, S. 591–602

[10] Tsotsas, E.: Wärmeleitung und Dispersion in durchströmten Schüttungen (in German). In: VDI-GVC (Hrsg.): *VDI-Wärmeatlas*. 10th. Berlin Heidelberg : Springer-Verlag, 2006, S. Mh1–Mh15

[11] Slavin, A. J. ; Arcas, V. ; Greenhalgh, C. A. ; Irvine, E. R. ; Marshall, D. B.: Theoretical model for the thermal conductivity of a packed bed of solid spheroids in the presence of a static gas, with no adjustable parameters except at low pressure and temperature. In: *International Journal of Heat and Mass Transfer* 45 (2002), Nr. 20, S. 4151–4161

[12] Zehner, P. ; Schlünder, E.U.: Influence of Thermal-Radiation and of Pressure on Heat-Transfer in Packings through Which No Fluid Is Flowing. In: *Chemie Ingenieur Technik* 44 (1972), Nr. 23, S. 1303–1308

[13] Zehner, P. ; Schlünder, E.U.: Thermal Conductivity of Packings at Moderate Temperatures. In: *Chemie Ingenieur Technik* 42 (1970), Nr. 14, S. 933–941

[14] Kruggel-Emden, H. ; Wirtz, S. ; Simsek, E. ; Scherer, V.: Simultane Beschreibung von Material- und Wärmetransport in bewegten Schüttungen mittels Diskreter Elemente Simulation. In: *22. Flammentag*, VDI, Dusseldorf, 2005

[15] Bruch, C. ; Peters, B. ; Nussbaumer, T.: Modelling wood combustion under fixed bed conditions. In: *Fuel* 82 (2003), Nr. 6, S. 729–738

[16] Sheikholeslami, R. ; Watkinson, A. P.: Transient heat transfer in a fixed bed of slab-shaped and spherical particles with intraparticle conduction. In: *Canadian Journal of Chemical Engineering* 76 (1998), Nr. 1, S. 141–147

[17] JalalzadehAzar, A. A. ; Steele, W. G. ; Adebiyi, G. A.: Heat transfer in a high-temperature packed bed thermal energy storage system - Roles of radiation and intraparticle conduction. In: *Journal of Energy Resources Technology-Transactions of the ASME* 118 (1996), Nr. 1, S. 50–57

[18] Handley, D. ; Heggs, P. J.: Effect of Thermal Conductivity of Packing Material on Transient Heat Transfer in a Fixed Bed. In: *International Journal of Heat and Mass Transfer* 12 (1969), Nr. 5, S. 549–570

[19] Wurzenberger, J. C. ; Wallner, S. ; Raupenstrauch, H. ; Khinast, J. G.: Thermal conversion of biomass: Comprehensive reactor and particle modeling. In: *AIChE Journal* 48 (2002), Nr. 10, S. 2398–2411

[20] Bauer, M.: *Theoretische und Experimentelle Untersuchungen zum Wärmetransport in gasdurchströmten Festbettreaktoren.* Dissertation. Halle (Saale) : Martin-Luther-Universität Halle-Wittenberg, 2001

[21] Reuter, K. ; Stampfl, C. ; Scheffler, M.: Ab initio atomistic thermodynamics and statistical mechanics of surface properties and functions. In: Yip, S. (Hrsg.): *Handbook of Materials Modeling.* Dordrecht : Springer, 2005, S. 149–194

[22] Wilmes, B.: *Modeling and simulation of the gasification of a spherical wood particle (in German)*, Berlin University of Technology, Dissertation, 2007

[23] Müller, I.: *Thermodynamics.* 1st ed. Boston London Melbourne : Pitman, 1985

[24] Bird, R. B. ; Stewart, W. E. ; Lightfoot, E. N.: *Transport Phenomena.* 2nd ed. New York : Wiley, 2002

[25] Ergun, S.: Fluid Flow through Packed Columns. In: *Chemical Engineering Progress* 48 (1952), Nr. 2, S. 89–94

[26] Chejne, F. ; Hernandez, J. P. ; Florez, W. F. ; Hill, A. F. J.: Modelling and simulation of time-dependent coal combustion processes in stacks. In: *Fuel* 79 (2000), Nr. 8, S. 987–997

[27] Gay, M. ; Michaelides, E. E.: Effect of the history term on the transient energy equation for a sphere. In: *International Journal of Heat and Mass Transfer* 46 (2003), Nr. 9, S. 1575–1586

[28] Coimbra, C. F. M. ; Rangel, R. H.: Unsteady heat transfer in the harmonic heating of a dilute suspension of small particles. In: *International Journal of Heat and Mass Transfer* 43 (2000), Nr. 18, S. 3305–3316

[29] Coimbra, C. F. M. ; Edwards, D. K. ; Rangel, R. H.: Heat transfer in a homogeneous suspension including radiation and history effects. In: *Journal of Thermophysics and Heat Transfer* 12 (1998), Nr. 3, S. 304–312

[30] Feng, Z. G. ; Michaelides, E. E.: Unsteady heat and mass transfer from a spheroid. In: *AIChE Journal* 43 (1997), Nr. 3, S. 609–614

[31] Michaelides, E. E. ; Feng, Z. G.: Heat-Transfer from a Rigid Sphere in a Nonuniform Flow and Temperature-Field. In: *International Journal of Heat and Mass Transfer* 37 (1994), Nr. 14, S. 2069–2076

[32] Nnanna, A. G. A. ; Haji-Sheikh, A. ; Harris, K. T.: Experimental study of non-fourier thermal response in porous media. In: *Journal of Porous Media* 8 (2005), Nr. 1, S. 31–44

[33] Roetzel, W. ; Putra, N. ; Das, S. K.: Experiment and analysis for non-Fourier conduction in materials with non-homogeneous inner structure. In: *International Journal of Thermal Sciences* 42 (2003), Nr. 6, S. 541–552

[34] Jiang, F. M. ; Liu, D. Y. ; Zhou, J. H.: Non-Fourier heat conduction phenomena in porous material heated by microsecond laser pulse. In: *Microscale Thermophysical Engineering* 6 (2002), Nr. 4, S. 331–346

[35] Mitra, K. ; Kumar, S. ; Vedavarz, A. ; Moallemi, M. K.: Experimental-Evidence of Hyperbolic Heat-Conduction in Processed Meat. In: *Journal of Heat Transfer-Transactions of the ASME* 117 (1995), Nr. 3, S. 568–573

[36] Kaminski, W.: Hyperbolic Heat-Conduction Equation for Materials with a Non-homogeneous Inner Structure. In: *Journal of Heat Transfer-Transactions of the Asme* 112 (1990), Nr. 3, S. 555–560

[37] Tzou, D. Y.: *Macro- to Microscale Heat Transfer: The Lagging Behaviour*. 1st ed. Washington, D.C. : Taylor and Francis, 1997

[38] Vadasz, P.: Heat conduction in nanofluid suspensions. In: *Journal of Heat Transfer-Transactions of the ASME* 128 (2006), Nr. 5, S. 465–477

[39] Antaki, P. J.: New interpretation of non-Fourier heat conduction in processed meat. In: *Journal of Heat Transfer-Transactions of the ASME* 127 (2005), Nr. 2, S. 189–193

[40] Cattaneo, C.: Sur Une Forme De Lequation De La Chaleur Eliminant Le Paradoxe Dune Propagation Instantanee. In: *Comptes Rendus Hebdomadaires Des Seances De L Academie Des Sciences* 247 (1958), Nr. 4, S. 431–433

[41] Vernotte, P.: Les Paradoxes De La Theorie Continue De Lequation De La Chaleur. In: *Comptes Rendus Hebdomadaires Des Seances De L Academie Des Sciences* 246 (1958), Nr. 22, S. 3154–3155

[42] Grassmann, A. ; Peters, F.: Experimental investigation of heat conduction in wet sand. In: *Heat and Mass Transfer* 35 (1999), Nr. 4, S. 289–294

[43] Herwig, H. ; Beckert, K.: Experimental evidence about the controversy concerning Fourier or non-fourier heat conduction in materials with a nonhomogeneous inner structure. In: *Heat and Mass Transfer* 36 (2000), Nr. 5, S. 387–392

[44] Troadec, J. P. ; Dodds, J. A.: Global geometrical description of homogeneous hard sphere packings. In: Bideau, D. (Hrsg.) ; Hansen, A. (Hrsg.): *Disorder and Granular Media*. Amsterdam : North-Holland, 1993, S. 133–163

[45] Slavin, A. J. ; Londry, F. A. ; Harrison, J.: A new model for the effective thermal conductivity of packed beds of solid spheroids: alumina in helium between 100 and 500 degrees C. In: *International Journal of Heat and Mass Transfer* 43 (2000), Nr. 12, S. 2059–2073

[46] Leonhard, W.: *Einführung in die Regelungstechnik*. 6th ed. Braunschweig : Vieweg, 1992

[47] Carslaw, H. S. ; Jaeger, J. C.: *Conduction of Heat in Solids*. 2nd ed. Oxford : Oxford University Press, 1959

[48] Ehrig, R. ; Nowak, U. ; Oeverdieck, L ; Deuflhard, P.: Advanced extrapolation methods for large scale differential algebraic problems. In: Bungartz, H.-J. (Hrsg.) ; Durst, F. (Hrsg.) ; Zenger, C. (Hrsg.): *High Performance Scientific and Engineering Computing*. Berlin : Springer, 1999, S. 233–244

[49] Deuflhard, P. ; Hairer, E. ; Zugck, J.: One-Step and Extrapolation Methods for Differential-Algebraic Systems. In: *Numerische Mathematik* 51 (1987), Nr. 5, S. 501–516

[50] Deuflhard, P.: Recent Progress in Extrapolation Methods for Ordinary Differential-Equations. In: *Siam Review* 27 (1985), Nr. 4, S. 505–535

[51] Polesek-Karczewska, S.: Effective thermal conductivity of packed beds of spheres in transient heat transfer. In: *Heat and Mass Transfer* 39 (2003), Nr. 5-6, S. 375–380

[52] Schröder, E. ; Class, A. ; Krebs, L.: Measurements of heat transfer between particles and gas in packed beds at low to medium Reynolds numbers. In: *Experimental Thermal and Fluid Science* 30 (2006), Nr. 6, S. 545–558

[53] Schröder, E.: Experiments on the pyrolysis of large beechwood particles in fixed beds. In: *Journal of Analytical and Applied Pyrolysis* 71 (2004), Nr. 2, S. 669–694

[54] Peters, B. ; Bruch, C.: Drying and pyrolysis of wood particles: experiments and simulation. In: *Journal of Analytical and Applied Pyrolysis* 70 (2003), Nr. 2, S. 233–250

[55] Peters, B.: Measurements and application of a discrete particle model (DPM) to simulate combustion of a packed bed of individual fuel particles. In: *Combustion and Flame* 131 (2002), Nr. 1-2, S. 132–146

[56] Aris, R. ; Amundson, N. R.: Some Remarks on Longitudinal Mixing or Diffusion in Fixed Beds. In: *Aiche Journal* 3 (1957), Nr. 2, S. 280–282

[57] Kraume, M. *Verfahrenstechnik I (in German).* 2000 2000

[58] Wen, D. S. ; Ding, Y. L.: Heat transfer of gas flow through a packed bed. In: *Chemical Engineering Science* 61 (2006), Nr. 11, S. 3532–3542

[59] Yagi, S. ; Kunii, D.: Studies on Heat Transfer near Wall Surface in Packed Beds. In: *AIChE Journal* 6 (1960), Nr. 1, S. 97–104

[60] Li, C. ; Finlayson, B. A.: Heat-Transfer in Packed-Beds - Re-Evaluation. In: *Chemical Engineering Science* 32 (1977), Nr. 9, S. 1055–1066

[61] Warnatz, J. ; Maas, U. ; Dibble, R. W.: *Combustion.* 2nd ed. Berlin Heidelberg New York : Springer, 1999

[62] Rath, J. ; Wolfinger, M. G. ; Steiner, G. ; Krammer, G. ; Barontini, F. ; Cozzani, V.: Heat of wood pyrolysis. In: *Fuel* 82 (2003), Nr. 1, S. 81–91

[63] Wolfinger, M. G.: *Modellierung der thermischen Umsetzung nicht-isothermer Holzpartikel in inerter und reaktiver Atmosphäre (in German)*, TU Graz, Dissertation, 2001

[64] Mermoud, F. ; Golfier, F. ; Salvador, S. ; Van de Steene, L. ; Dirion, J. L.: Experimental and numerical study of steam gasification of a single charcoal particle. In: *Combustion and Flame* 145 (2006), Nr. 1-2, S. 59–79

[65] Chan, W. C. R. ; Kelbon, M. ; Krieger, B. B.: Modeling and Experimental-Verification of Physical and Chemical Processes During Pyrolysis of a Large Biomass Particle. In: *Fuel* 64 (1985), Nr. 11, S. 1505–1513

[66] Lindborg, H. ; Eide, V. ; Unger, S. ; Henriksen, S. T. ; Jakobsen, H. A.: Parallelization and performance optimization of a dynamic PDE fixed bed reactor

model for practical applications. In: *Computers and Chemical Engineering* 28 (2004), Nr. 9, S. 1585–1597

[67] Jakobsen, H. A. ; Lindborg, H. ; Handeland, V.: A numerical study of the interactions between viscous flow, transport and kinetics in fixed bed reactors. In: *Computers and Chemical Engineering* 26 (2002), Nr. 3, S. 333–357

[68] Schröder, E.: Entwurf einer Anlage zur Pyrolyse eines Modellbrennstoffs. In: Krebs, L. (Hrsg.) ; Peters, B. (Hrsg.): *Experimente und Modellierung zur heterogenen und homogenen Verbrennung.* Karlsruhe : Forschungszentrum Karlsruhe, 1998, S. 127–133

[69] Peters, B. ; Schroder, E. ; Bruch, C.: Measurements and particle resolved modelling of the thermo- and fluid dynamics of a packed bed. In: *Journal of Analytical and Applied Pyrolysis* 70 (2003), Nr. 2, S. 211–231

[70] Thunman, H. ; Leckner, B. ; Niklasson, F. ; Johnsson, F.: Combustion of wood particles - A particle model for Eulerian calculations. In: *Combustion and Flame* 129 (2002), Nr. 1-2, S. 30–46

[71] Thunman, H. ; Leckner, B.: Co-current and counter-current fixed bed combustion of biofuel - a comparison. In: *Fuel* 82 (2003), Nr. 3, S. 275–283

[72] Di Blasi, C. ; Signorelli, G. ; Portoricco, G.: Countercurrent fixed-bed gasification of biomass at laboratory scale. In: *Industrial and Engineering Chemistry Research* 38 (1999), Nr. 7, S. 2571–2581

[73] Di Blasi, C. ; Branca, C.: Kinetics of primary product formation from wood pyrolysis. In: *Industrial and Engineering Chemistry Research* 40 (2001), Nr. 23, S. 5547–5556

[74] Di Blasi, C.: Modeling intra- and extra-particle processes of wood fast pyrolysis. In: *Aiche Journal* 48 (2002), Nr. 10, S. 2386–2397

[75] Di Blasi, C. ; Signorelli, G. ; Di Russo, C. ; Rea, G.: Product distribution from pyrolysis of wood and agricultural residues. In: *Industrial and Engineering Chemistry Research* 38 (1999), Nr. 6, S. 2216–2224

[76] Di Blasi, C.: Modeling wood gasification in a countercurrent fixed-bed reactor. In: *Aiche Journal* 50 (2004), Nr. 9, S. 2306–2319

[77] Yang, Y. B. ; Phan, A. N. ; Ryu, C. ; Sharifi, V. N. ; Swithenbank, J.: Mathematical modelling of slow pyrolysis of segregated solid wastes in a packed-bed pyrolyser. In: *Fuel* 86 (2007), S. 169–180

[78] Yang, W. H. ; Ponzio, A. ; Lucas, C. ; Blaslak, W.: Performance analysis of a fixed-bed biomass gasifier using high-temperature air. In: *Fuel Processing Technology* 87 (2006), Nr. 3, S. 235–245

[79] Yang, Y. B. ; Ryu, C. ; Sharifi, V. N. ; Swithenbank, J.: Effect of model and operating parameters on air gasification of char. In: *Energy and Fuels* 20 (2006), Nr. 4, S. 1698–1708

[80] Ryu, C. ; Yang, Y. B. ; Khor, A. ; Yates, N. E. ; Sharifi, V. N. ; Swithenbank, J.: Effect of fuel properties on biomass combustion: Part I. Experiments - fuel type, equivalence ratio and particle size. In: *Fuel* 85 (2006), Nr. 7-8, S. 1039–1046

[81] Yang, Y. B. ; Ryu, C. ; Khor, A. ; Yates, N. E. ; Sharifi, V. N. ; Swithenbank, J.: Effect of fuel properties on biomass combustion. Part II. Modelling approach - identification of the controlling factors. In: *Fuel* 84 (2005), Nr. 16, S. 2116–2130

[82] Yang, Y. B. ; Ryu, C. ; Khor, A. ; Sharifi, V. N. ; Swithenbank, J.: Fuel size effect on pinewood combustion in a packed bed. In: *Fuel* 84 (2005), Nr. 16, S. 2026–2038

[83] Yang, W. ; Ryu, C. ; Choi, S.: Unsteady one-dimensional model for a bed combustion of solid fuels. In: *Proceedings of the Institution of Mechanical Engineers Part a-Journal of Power and Energy* 218 (2004), Nr. A8, S. 589–598

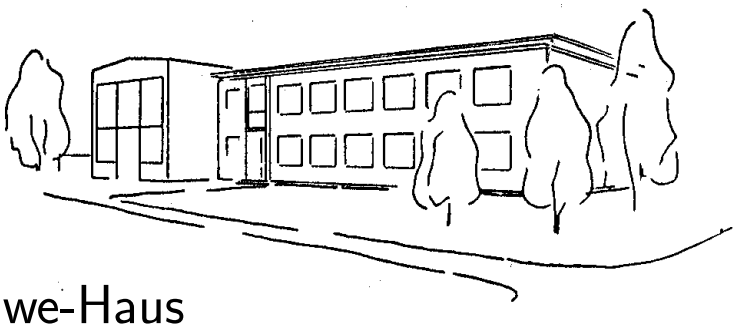

MITTEILUNGEN

aus dem Rudolf-Drawe-Haus

der Technischen Universität Berlin

[**739**] Jörg Langohr: Zur Oxidativen Kopplung von Methan
Dissertation (2003)

[**740**] Nils Paust: Implementierung eines Ascheablagerungsmodells in den kommerziellen CFD-code $FLUENT^{TM}$
Diplomarbeit (2004)

[**741**] Nikolas Rommeiss: Zur Verwendung von Bindemitteln in der Pelletproduktion
Diplomarbeit (2004)

[**742**] Armin Muggli: Genehmigungsvorbereitende Untersuchungen zu einem Holzheizwerk unter Berücksichtigung von Brennstoff und Emissionen
Diplomarbeit (2004)

[**743**] Sebastian Matera: On reactive diffusive flows in porous media with regard to gasification of biomass
Studienarbeit (2005)

[**744**] Yunfei Kuo: Effekte der spezifischen Oberfläche von Li/MgO-Katalysatoren bei der oxidativen Kopplung von Methan
Dissertation (2005)

[**745**] Ireen Kamprad, Jan Knodel: Entwicklung einer Online-Analytik für PAK im Produktgas der Biomassevergasung
Projektarbeit (2005)

[**746**] Kicki Klevmar: Kinetic Parameter Estimation for the Pyrolysis of Coal
Studienarbeit (2005)

[**747**] Jochen Grünig: Modellierung und Simulation der Oberflächenreaktionen bei der Vergasung von Holzkohle
Studienarbeit (2005)

[**748**] Nadine Mireille Tchuendem: F"order- und Dosierverhalten sowie Brennstoffcharakterisierung holzartiger Biomasse f"ur eine Wirbelschicht-Vergaseranlage
Diplomarbeit (2005)

[**749**] Ines Braune: Ganzheitliche Systemanalyse in der Energieversorgung
Studienarbeit (2006)

[**750**] Axel Funke: Implementierung einer Richtlinie zur Messung vom Teergehalt in Produktgasen der Biomassevergasung
Diplomarbeit (2006)

[**751**] Kicki Klevmar: Numerical Modelling and Simulation of Thermal Deactivation in 3D of Automotive Three-Way Catalytic Converters
Diplomarbeit (2006)

[**752**] Stephan Gerber: Implementierung eines Euler-Lagrange-Verfahrens zur Modellierung einer inerten Fluid-Feststoff-Str"omung
Diplomarbeit (2006)

[**753**] Max Lautenbach: Messung der Feinstaubemissionen bei Biomassefeuerungen und Bestimmung der Partikeldichte
Diplomarbeit (2006)

[**754**] Tibor Dalenburg: Theoretische Grundlagen des Projektmanagements und praktische Umsetzung im Rahmen der "'International Engineering Summer School (IESS)"' der TU Berlin
Diplomarbeit (2006)

[**755**] Stephan Gerber: Implementierung und Test einer Vier-Wege-Kopplung zur Berechnung dichter inerter Partikelströmungen
Diplomarbeit (2006)

[**756**] Kapu Srinivasa Reddy: Thermodynamic Analysis of Transfer Hydrogenation
Masterarbeit (2006)

[**757**] Anja Morosky: Aerodynamic Design, Parametric Studies and Optimisation of a Gasturbine Combustor Adopting CFD
Diplomarbeit (2006)

[**758**] Andrea Dziubek: Condensation in an inclined tube with a small diameter - Modelling, analysis and numerical simulation of a moving boundary problem with phase change and surface tension
Dissertation (2006)

[**759**] Peter Kasten: Entwicklung eines Prüfstands für Porenbrenner-Prototypen
Studienarbeit (2007)

[**760**] Maria Gaggl: Untersuchungen zur Abtrennung von Wasserstoff aus Gasgemischen mit mikroporösen Membranen aus Beton
Diplomarbeit (2007)

[**761**] Felix Nelles: Simulationsgestützte Untersuchung des Feinstaubverhaltens in einer Biomassefeuerung
Diplomarbeit (2007)

[**762**] Matija Bogdanić: Simulation von Autoabgasanlagen
Dissertation (2007)

[**763**] Nico Zobel: The Representative Particle Model
Dissertation (2007)